This is to certify that the

dissertation entitled

Structure and Dynamics of Layered Molecular Assemblies

presented by

Jennifer Conrad Horne

has been accepted towards fulfillment
of the requirements for

Ph.D. degree in Chemistry

Gary J. Blanchard
Major professor

Date August 14, 1998

DATE DUE	DATE DUE	DATE DUE
AUG 3 0 2003		

STRUCTURE AND DYNAMICS OF LAYERED MOLECULAR ASSEMBLIES

By

Jennifer Conrad Horne

A DISSERTATION

Submitted to
Michigan State University
in partial fulfillment of the requirements
for the degree of

DOCTOR OF PHILOSOPHY

Department of Chemistry

1998

ABSTRACT

STRUCTURE AND DYNAMICS OF LAYERED MOLECULAR ASSEMBLIES

By

Jennifer Conrad Horne

This dissertation focuses on the goal of understanding and controlling layered material properties from a molecular perspective. With this understanding, materials can be synthetically tailored to exhibit predetermined bulk properties. This investigation describes the optical response of a family of metal-phosphonate (MP) monolayers and multilayers, materials that are potentially useful because the films are easy to synthesize and are chemically and thermally stable. MP films have shown potential in a variety of chemical sensing and optical applications, and in this dissertation, the suitability of MP films for optical information storage is explored. For this application, the extent of photonic energy transport within and between optically active layers is an important factor in determining the stability and specificity of optical modifications made to a material. Intralayer and interlayer energy transport processes can be studied selectively in MP films because the composition, and thus the properties, of each layer are controlled synthetically. It was determined by fluorescence relaxation dynamics in conjunction with atomic force microscopy (AFM) that the substrate and layer morphologies are key factors in determining the layer optical and physical properties. The initial MP layers in a multilayer are structurally heterogeneous, characterized by randomly distributed islands that are ~ 50 Å in diameter. The population dynamics measured for these layers are non-exponential, chromophore concentration-independent, and identical for two different

chromophores. The data is explained in the context of an excitation hopping model in a system where the surface is characterized by islands of aggregated chromophores as well as non-aggregated monomers. Within a MP monolayer, the dynamics are dominated by intra-island excitation hopping. Förster (dipolar) energy transfer between the energetically overlapped chromophores does not play a significant role in determining the relaxation dynamics of these systems, as the islands are separated by distances greater than the critical distance required for this process. Investigation of the interlayer energy transfer behavior revealed that transport between adjacent chromophore layers is precluded by the spatial modulation of the dielectric response of the MP film. These results are important for understanding the morphological, structural, and optical properties that will be useful for the incorporation of layered organic materials in future technologies.

In Memory of Dziadzi

ACKNOWLEDGMENTS

I could not fully appreciate until now how fortunate I was to have had Gary Blanchard as my research as my research advisor. I learned a great deal from him about science, the professional world and life, (and how to have a smart-aleck comment about everything). He is a mentor in every sense of the word. I would also like to thank Alice Deckert, my research advisor at Holy Cross, for her support and encouragement through the years. I can only hope to have the same positive effect on everyone I meet. My committee members also deserve recognition: Marcos Dantus, Merlin Breuning, Jeff Ledford, and especially Greg Baker, who, along with his group, helped me through the organic syntheses for the materials used in this dissertation.

Best of luck to the Blanchard group members, past and present, and the many other acquaintances I have made at MSU. Two group members who deserve special recognition are Selezion Hambir and Dave Karpovich, for their generous help in the lab, and for always having a word of encouragement (unless Dave thought I deserved something a little more sarcastic). I also want to thank Greg Noonan for the interesting times in the house on Cornell Ave. Thanks for letting me borrow your dog sometimes. Also, summer would have been incredibly boring without all of the softball teams I have been a part of, especially the '94 Lansing Grass Stains.

My family, especially my brothers, were real troopers for driving the twelve hours to come out for visits. And finally, I would like to acknowledge Al Schwartz, my best friend. Thanks for all the love and support - I'll return the favor soon. Here's to taking chances!

TABLE OF CONTENTS

LIST OF TABLES

LIST OF FIGURES

Chapter 1

Introduction

Molecular assemblies first captured the attention of scientists decades ago. In 1917, Irving Langmuir first studied the behavior of amphiphilic molecules at the air-water interface[1], and Katharine Blodgett later introduced the technology of depositing the monomolecular layers on substrates.[2] Since then, organized molecular assemblies have found use in numerous chemical and physical applications. This class of interfacial materials has characteristically well defined structures of controlled composition and, with a small amount of material, they offer a widely tunable range of chemical, electrical, and optical properties.

Langmuir-Blodgett (LB) films were the first examples of multilayer films with highly ordered layers and controlled layer-by-layer growth.[2] These films have been used in a wide range of studies, from optical properties of chromophores to ordered polymerizations on a substrate.[3] However, because of the delicate nature of the van der Waals forces linking each layer and the inherent difficulty in pre-assembling the molecules for transfer of each layer, LB films have become limited to mostly fundamental studies of layered assemblies and their properties.

The next step in the development of this field was the discovery of self-assembling materials, which, in contrast to LB layers, did not have to be pre-assembled and were more chemically stable. The first detailed examinations of self-assembled monolayers were published by Allara and Nuzzo in 1985.[4] Their studies showed that certain molecules would chemisorb to a compatible substrate *in situ*, with crystalline-like

order within the layer. There are many possible combinations of molecules and substrates that can be used to make self-assembled monolayers (SAMs): thiols on gold,[5] carboxylates on aluminum[4] or silver,[6] and silanes on glass[7]. These systems have been investigated widely, particularly the thiol/gold system, and much is known about their formation, structure, and properties. Despite the extensive discussion in the literature on the potential utility of alkanethiol-gold SAMs,[8] recent work has demonstrated that these assemblies are labile[9,10] and sensitive to ozone-mediated oxidative degradation.[11,12] While there is still much to explore with monolayer systems, the opportunity to form complex, interfacial structures with this chemistry is limited unless specially functionalized molecules are used in the formation of the initial layer.

In the last fifteen years, some of the focus has shifted to developing materials for covalent multilayer growth. The buildup of multiple, discrete layers using thiol and disulfide chemistry has not been investigated until recently,[13] and there is much to be learned about these systems. Silane chemistry has been used for covalent multilayer growth,[7] but this chemistry can be difficult to control and it is susceptible to unwanted polymerization reactions, precluding the ability to create uniform, layered interfaces. Metal-phosphonate (MP) organic multilayer structures have been investigated extensively,[14-30] and, like self-assembling monolayers, show potential for use in practical applications such as surface modification,[31-34] electronic device,[35-37] nonlinear optics,[16,25,26] and molecular recognition applications.[38-43] Phosphonic acids form strong, sparingly soluble complexes with metal ions, giving them significant advantages over many self-assembled monolayer systems. MP structures are comparable to SAMs in ease of synthesis, which generally involves immersion of the functionalized substrate into

a solution of the appropriate (α,ω)-organobisphosphonate. Because there are two separately deposited components required to build a layer, spontaneous multilayer growth is precluded. MP multilayers are versatile in a chemical sense because the identity of individual layers can be controlled selectively as the structure is assembled and, in this way, chemical potential or optical properties can be built into the system in three dimensions rather than two. Like other systems that exhibit mesoscopic organization, metal phosphonate structures have been used successfully in many studies, including optical second harmonic generation,[24,25] artificial photosynthesis,[44] and light harvesting.[45]

One application for which three dimensional, layer-by-layer control of multilayer structure could potentially be useful is in optical information storage.[46] Present-day storage devices use a single layer medium, and the addition of a useful third dimension could enhance the storage density of a given volume of the surface. The use of MP multilayers with chemically and optically distinct layers could be the foundation for such a three-dimensional structure, but there are aspects of this scheme that could serve to limit the utility of these materials for information storage. The density of optical information that can be stored within a single molecular layer is limited, and the spatial resolution or "bit size" available with optical approaches is determined by the diffraction limit for the optics used and the wavelengths of reading and writing light. The ability to store information in a material optically depends on making a specific, stable modification to the optical response of a given layer of the material.

The chemical change associated with writing or erasing, while still under investigation, will likely be a *cis-trans* isomerization. Regardless of the means used to

create a molecular "bit", the writing process will necessarily be mediated by an excited electronic state to achieve the necessary spatial selectivity and contrast. During conversion from one logical state to another, the chromophore will be excited, probably to its S_1 state, and dissipative processes from the first excited singlet state can, in principle, serve to limit the conversion efficiency or definition of the written spot. The conformational change must be an activated process with a sufficiently high barrier to ensure that the operation is irreversible under ambient dark conditions. The presence of other optically active constituents within the same layer or in neighboring layers creates the possibility of intra- or inter-layer energy exchange processes, which serve to place limits on the utility of these materials for information storage applications. Because of the requisite electronic excitation and the proximity of chromophores to one another, the issue of excitation transport must be considered in detail for these systems.

The focus of this dissertation is to understand the energy migration and excited state population dynamics that occur within an optically active film. By using simple chromophores that don't "switch", we can observe these processes without complications associated with large scale chromophore isomerization. The investigation of MP materials that show potential for optical switching is underway in our lab. In this dissertation, we use oligothiophenes as chromophores because they are relatively well understood and form ordered layers due to their rigid structure.[24] We chose 2,2'-bithiophene-5,5'-diylbis-(phosphonic acid) (BDP) and 2,2':5',2'':5'',2'''-quaterthiophene-5,5'''-diylbis(phosphonic acid) (QDP) because the BDP emission band overlaps the QDP absorption band, as shown in Figure 1.1. The spectral overlap of the two chromophores is useful for evaluating excitation transport in MP multilayers, as we explain in Chapter 6

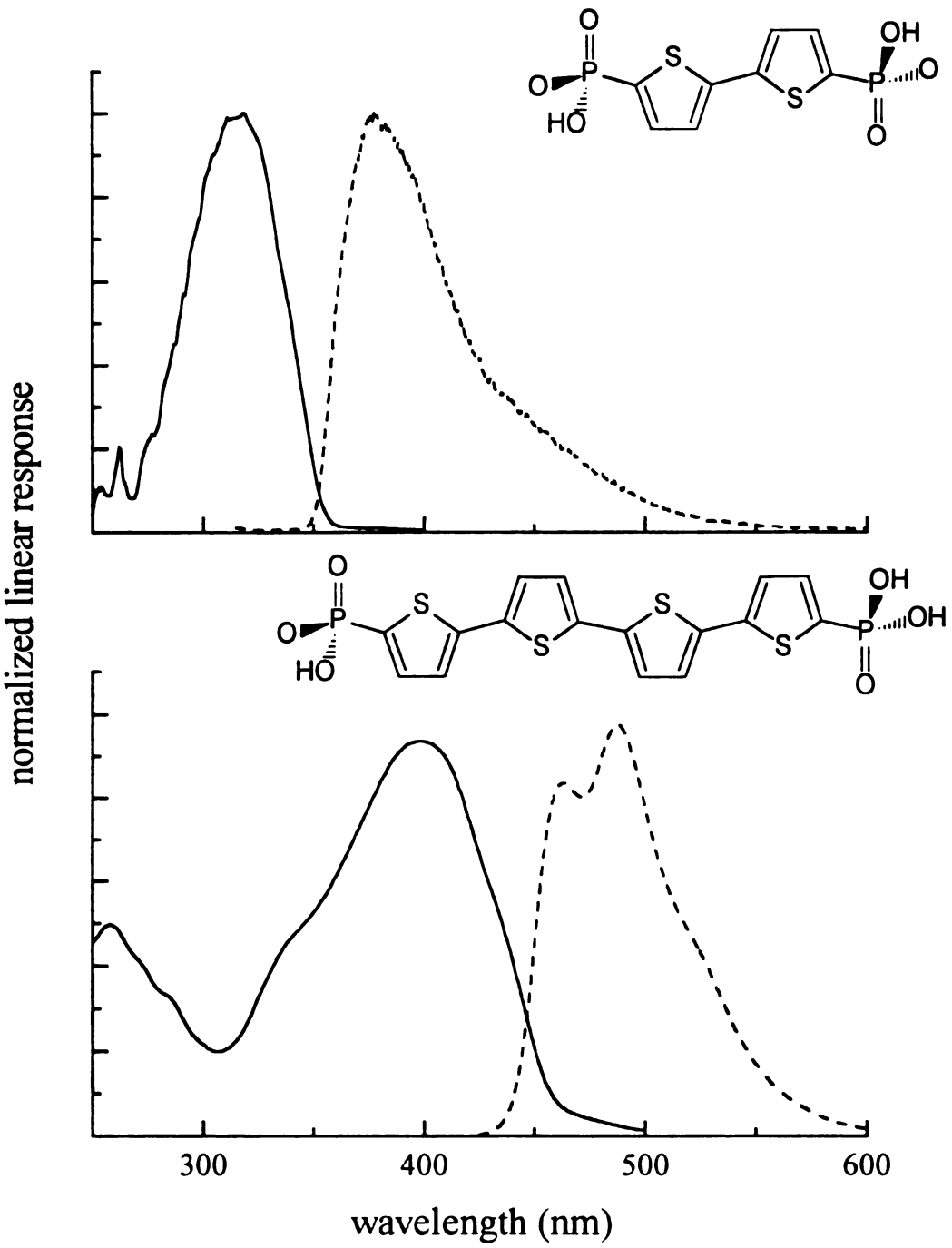

Figure 1.1 Structures and absorbance (——) and emission (- - -) spectra (10^{-5} M solutions) for 2,2'-bithiophene-5,5'-diylbis-(phosphonic acid) (top) and 2,2':5',2":5",2"'-quaterthiophene-5,5"'-diylbis(phosphonic acid) (bottom). Note the spectral overlap between BDP emission and QDP absorption. Emission spectra have been normalized to the absorption spectra for clarity of presentation.

in the context of Förster energy transfer. These chromophores can photoisomerize via ring rotation and this property is of value in understanding their dynamical response in layered assemblies.

This dissertation describes a systematic study of the structure and dynamics of a family of optically active self-assembled MP monolayers and multilayers. The microscopic structure, optical properties, and effects of local environment are all important factors for determining the feasibility of using these materials in practical devices. Chapter 2 describes the synthesis of the organobisphosphonate compounds and preliminary characterization of the growth of multilayer films. Chapter 3 is a study of related oligothiophenes in solution. Isomerization barriers measured in both ground state and excited state gave us a baseline understanding of the conformational behavior of the chromophores in films. Chapters 4 and 5 detail the characterization of each of the two chromophores individually in MP monolayers. It is here that we first realize indications of structural inhomogeneity in the layer. Chapter 5 also demonstrates the substrate-dependence of the motional dynamics of the chromophores in a layer. Other optical properties are not affected. Chapters 6 and 7 are investigations of the intra- and interlayer population dynamics of mixed monolayers and multilayer structures, respectively. We find two factors that profoundly influence the energy transport dynamics in MP films. The morphology of the substrate and the MP layer, in which islands of chromophore are predominant, precludes intralayer energy transfer from donor to acceptor chromophores, but facilitates excitation transport within an island of aggregated chromophore. In multilayer structures, interlayer transport is not observed. The spatial modulation of the dielectric response between the metal-phosphonate and organic portions of the layers

serves to screen the dipolar coupling between chromophores in adjacent layers. Both the structure and the dynamics components of this dissertation contribute to a broader understanding of MP films that will be useful for further study of the feasibility of using these materials in more applied areas.

1.1 Literature Cited

1. Langmuir, I. *J. Am. Chem. Soc.* **1917**, *39*, 1848.

2. Blodgett, K. B. *J. Am. Chem. Soc.* **1935**, *57*, 1007.

3. Ulman, A. *Introduction to Thin Organic Films: From Langmuir-Blodgett to Self-Assembly* Academic Press: Boston, 1991.

4. (a) Allara, D. L.; Nuzzo, R. G. *Langmuir* **1985**, *1*, 45. (b) Allara, D. L.; Nuzzo, R. G. *Langmuir* **1985**, *1*, 45.

5. (a) Nuzzo, R. G.; Dubois, L. H.; Allara, D. L. *J. Am. Chem. Soc.* **1990**, *112*, 558. (b) Ulman, A. *Chem. Rev.* **1996**, *96*, 1533.

6. (a) Smith, E. L.; Porter, M. D. *J. Phys. Chem.* **1993**, *97*, 8032. (b) Canning, N. D. S.; Madix, R. J. *J. Phys. Chem.* **1984**, *88*, 2437.

7. (a) Gun, J.; Iscovici, R.; Sagiv, J. *J. Colloid Interface Sci.* **1984**, *101*, 201. (b) Maoz, R.; Sagiv, J. *J. Colloid Interface Sci.* **1984**, *100*, 465. (c) Maoz, R.; Sagiv, J. *Thin Solid Films* **1985**, *132*, 135.

8. Xia, Y.; Whitesides, G. M. *Angew. Chem. Int. Ed.*, **1998**, *37*, 551.

9. Karpovich, D. S.; Blanchard, G. J. *Langmuir* **1994**, *10*, 3315.

10. Schessler, H. M.; Karpovich, D. S.; Blanchard, G. J. *J. Am. Chem. Soc.* **1996**, *118*, 9645.

11. Zhang, Y.; Terrill, R. H.; Tanzer, T. A.; Bohn, P. W. *J. Am. Chem. Soc.*, **1998**, *120*, 2654.

12. Norrod, K. L.; Rowlen, K. L. *J. Am. Chem. Soc.*, **1998**, *120*, 2656.

13. Kohli, P.; Harris, J. J.; Blanchard, G. J. *J. Am. Chem. Soc.*, in review.

14. Hong, H.-G.; Sackett, D. D.; Mallouk, T. E. *Chem. Mater.* **1991**, *3*, 521.

15. Thompson, M. E. *Chem. Mater.* **1994**, *6*, 1168.

16. Katz, H. E.; Wilson, W. L.; Scheller, G. *J. Am. Chem. Soc.* **1994**, *116*, 6636.

17. Yonemoto, E. H.; Saupe, G. B.; Schmehl, R. H.; Hubig, S. M.; Riley, R. L.; Iverson, B. L.; Mallouk, T. E. *J. Am. Chem. Soc.* **1994**, *116*, 4786.

18. Katz, H. E.; Bent, S. F.; Wilson, W. L.; Schilling, M. L.; Ungashe, S. B. *J. Am. Chem. Soc.* **1994**, *116*, 6631.

19. Frey, B. L.; Hanken, D. G.; Corn, R. M. *Langmuir* **1993**, *9*, 1815.

20. Yang, H. C.; Aoki, K.; Hong, H.-G.; Sackett, D. D.; Arendt, M. F.; Yau, S.-L.; Bell, C. M.; Mallouk, T. E. *J. Am. Chem. Soc.* **1993**, *115*, 11855.

21. Vermeulen, L.; Thompson, M. E. *Nature* **1992**, *358*, 656.

22. Ungashe, S. B.; Wilson, W. L.; Katz, H. E.; Scheller, G. R.; Putvinski, T. M. *J. Am. Chem. Soc.* **1992**, *114*, 8717.

23. Cao, G.; Rabenberg, L. K.; Nunn, C. M.; Mallouk, T. M. *Chem. Mater.* **1991**, *3*, 149.

24. Katz, H. E.; Schilling, M. L.; Chidsey, C. E. D.; Putvinski, T. M.; Hutton, R. S. *Chem. Mater.* **1991**, *3*, 699.

25. Katz, H. E.; Scheller, G.; Putvinski, T. M.; Schilling, M. L.; Wilson, W. L.; Chidsey, C. E. D. *Science* **1991**, *254*, 1485.

26. Putvinski, T. M.; Schilling, M. L.; Katz, H. E.; Chidsey, C. E. D.; Mujsce, A. M.; Emerson, A. B. *Langmuir* **1990**, *6*, 1567.

27. Rong, D.; Hong, H.-G.; Kim, Y.-I.; Krueger, J. S.; Mayer, J. E.; Mallouk, T. E. *Coord. Chem. Rev.* **1990**, *97*, 237.

28. Lee, H.; Kepley, L. J.; Hong, H.-G.; Akhter, S.; Mallouk, T. E. *J. Phys. Chem.* **1988**, *92*, 2597.

29. Lee, H.; Kepley, L. J.; Hong, H.-G.; Mallouk, T. E. *J. Am. Chem. Soc.* **1988**, *110*, 618.

30. Katz, H. E. *Chem. Mater.* **1994**, *6*, 2227.

31. Dubois, L. H.; Zegarski, B. R.; Nuzzo, R. G. *J. Am. Chem. Soc.* **1990**, *112*, 570.

32. Chidsey, C. E. D.; Bertozzi, C. R.; Putvinski, T. M.; Mujsce, A. M. *J. Am. Chem. Soc.* **1990**, *112*, 4301.

33. Collard, D. M.; Fox, M. A. *Langmuir* **1991**, *7*, 1192.

34. Chidsey, C. E. D. *Science* **1991**, *251*, 919.

35. Batchelder, D. N.; Evans, S. D.; Freeman, T. L.; Haussling, L.; Ringsdorf, H.; Wolf, H. *J. Am. Chem. Soc.* **1994**, *116*, 1050.

36. Tarlov, M. J.; Burgess, D. R. F.; Gillen, G. *J. Am. Chem. Soc.* **1993**, *115*, 5305.

37. Wollman, E. W.; Kang, D.; Frisbie, C. D.; Lorkovic, I. M.; Wrighton, M. S. *J. Am. Chem. Soc.* **1994**, *116*, 4395 (1994).

38. Zak, J.; Yuan, H.; Ho, M.; Woo, L. K.; Porter, M. D. *Langmuir* **1993**, *9*, 2772.

39. Obeng, Y. S.; Laing, M. E.; Friedli, A. C.; Yang, H. C.; Wang, D.; Thulstrup, E. W.; Bard, A. J.; Michl, J. *J. Am. Chem. Soc.* **1993**, *114*, 9943.

40. Finklea, H. O.; Hanshew, D. D. *J. Am. Chem. Soc.* **1992**, *114*, 3173.

41. Sun, L.; Crooks, R. M. *Langmuir* **1993**, *9*, 1775.

42. Sun, L.; Kepley, L. J.; Crooks, R. M. *Langmuir* **1992**, *8*, 2101.

43. Spinke, J.; Liley, M.; Schmitt, F.-J.; Guder, H.-J.; Angermaier, L.; Knoll, W. *J. Chem. Phys.* **1993**, *99*, 7012.

44. (a) Vermeulen, L. A.; Snover, J. L.; Sapochak, L. S.; Thompson, M. E. *J. Am. Chem. Soc.* **1993**, *115*, 11767. (b) Snover, J. L.; Byrd, H.; Suponeva, E. P.; Vicenzi, E.; Thompson, M. E. *Chem. Mater.* **1996**, *8*, 1490.

45. Kaschak, D. M.; Mallouk, T. E. *J. Am. Chem. Soc.* **1996**, *118*, 4222.

46. (a) Feriga, B. L.; Jager, W. F.; de Lange, B. *Tetrahedron* **1993**, *49*, 8267. (b) Emmelius, M.; Pawlowski, G.; Vollmann, H. W. *Angew. Chem. Int. Ed. Engl.* **1989**, *28*, 1445.

Chapter 2

Synthesis and Characterization of Metal-Phosphonate Materials

2.1 Introduction

As materials science research becomes more focused, the materials required for study become more specialized. The organophosphonate compounds needed to build MP films are not commercially available. This Chapter summarizes the syntheses of the compounds used for the experiments reported in Chapters 4 through 7. We chose a series of oligothiophenes to use as chromophores. Oligomeric materials are useful as model compounds in many areas of chemistry, and we use the oligothiophenes here because their optical response is easily tunable by varying the length of the chain. Bithiophene (BT), terthiophene (TT) and quaterthiophene (QT) were the oligomers chosen. QT is the longest oligomer we use, because of solubility requirements and spectral limitations. The syntheses as well as the layer deposition are performed in solution phase, and the solubility of oligothiophenes longer than five rings drops drastically with increasing oligomer length. The other limiting factor regarding oligomeric materials is related to the effect of conjugation length on optical response. As the chain length is increased, there is a point at which the conjugation length can no longer increase, due to the statistical distribution of structural defects along the chain. At this point, oligomers with longer chain lengths exhibit approximately the same steady state spectra, as determined by the average conjugation length of the material. The synthesis of QT and its phosphorylation were reported by Katz, *et al.*,[1] and these procedures were modified slightly for the

syntheses reported in this chapter. In general, the oligothiophenes were derivatized to the phosphonate by lithium coupling to a phosphochloridate followed by acid hydrolysis.

We have also bisphosphonated a series of alkanes: hexane, octane, and dodecane, to serve as optically inactive components in the MP films, in order to separate the optically active components of the film. Spatial separation of chromophores can be accomplished by depositing alkane layers between oligothiophene layers, or by making mixed oligothiophene-alkane layers, thereby diluting the chromophore within the layer. The lengths of these alkanes in their all-*trans* conformations are approximately the same lengths as BT, TT, and QT, respectively, in their all-*anti* conformations. This allows us to dilute chromophore layers but maintain uniform height within a given layer. The alkane bisphosphonates were synthesized by the Michaelis-Arbuzov reaction of dibromoalkane with triethylphosphite, followed by acid hydrolysis.[2]

2.2 Experimental

Purification of Materials. All chemicals were purchased from Aldrich Chemical Co. and used as received except where noted. All tetrahydrofuran (THF) used in these syntheses was distilled over CaH_2 and sodium before use. Copper (II) chloride was dried under vacuum and treated with thionyl chloride, after which excess solvent was removed by vacuum distillation. Triethylphosphite was treated with sodium and vacuum distilled.

Synthesis of Quaterthiophene. This synthesis is shown in Figure 2.1. QT was prepared by the reaction of 20 mmol bithiophene in THF with one equivalent of *n*-butyllithium (2.5 M in hexanes) at –78 °C for 20 minutes. The mixture was transferred by canula to a second flask containing a suspension of anhydrous $CuCl_2$ (excess) in THF.

The clear yellow solution was allowed to warm slowly to room temperature, and was stirred overnight. The addition of 50 mL of 1 M HCl resulted in the formation of a yellow precipitate from a brown-green solution, which was vacuum filtered and dried (64% yield).

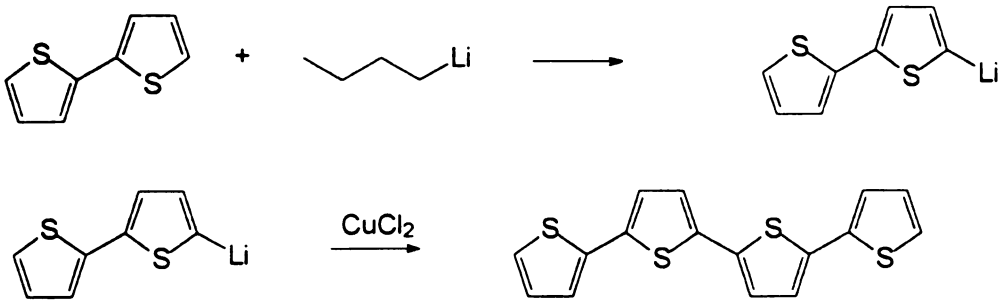

Figure 2.1 Synthetic scheme for quaterthiophene.

Phosphorylation of oligothiophenes. The procedure described below was used for phosphorylation of BT, TT, and QT. The synthesis of QDP is used as an example in the text and schematically in Figure 2.2. A solution of QT (3 mmol) in THF was cooled to –40 °C, and an excess (12.5 mmol) of *n*-BuLi (2.5 M in hexanes)was added. After stirring for 2 hours, a second solution of 12.5 mmol bis(dimethylamino) phosphochloridate and 0.625 mmol *n*-BuLi in THF was added to the first solution via canula, and the resulting solution was allowed to warm to room temperature. The reaction was stopped after three days, the product was extracted from water with ether, and the aqueous layer was extracted twice with CH_2Cl_2. The product was purified chromatograpically on silica plates (Fisher) using a mobile phase of 1:1 CH_2Cl_2 and THF. (For TT: 95:5 THF and CH_2Cl_2; for BT: 50:30:20 EtOAc; MeOH; THF) The most polar component, which was yellow, was collected in 46% yield. (For TT and BT, the component that emitted blue upon UV excitation was collected). A portion of this

tetraamide was dissolved in dioxane at 80 °C. The solution was acidified with 50 mL each of H_2O and concentrated HCl, and refluxed overnight. Upon cooling to room temperature, bright yellow QDP precipitated from solution and was collected by vacuum filtration in 55% yield. Final yields and ^{1}H NMR peaks are reported in Table 2.1.

Phosphorylation of alkanes. The same synthesis was used for all alkanes, and DDBPA is used as an example (see Figure 2.3). DDBPA was prepared by the Michaelis-Arbuzov reaction of 1,12-dibromododecane with triethylphosphite. The mixture was refluxed for 5 hours to allow evolution of ethyl bromide. Excess triethyl phosphite was removed by vacuum distillation. Concentrated HCl was added to the solution, which was then refluxed for 12 hours, and the resulting white precipitate was collected by vacuum filtration and washed with acetonitrile. Yields are reported in Table 2.1.

Table 2.1 ^{1}H NMR results (500 MHz) and final yields for bisphosphonated compounds. DMSO-d_6 was used as the solvent for all spectra.

	Compound	% Yield	^{1}H NMR peaks
oligothiophenes	BDP	10	7.3 – 7.5 ppm (m)
	TDP	11	7.2 – 7.4 ppm (m)
	QDP	21	7.3 - 7.4 ppm (m)
alkanes	HBPA	57	1.2 – 1.6 ppm (m)
	OBPA	67	1.2 – 1.5 ppm (m)
	DDBPA	68	1.2 – 1.5 ppm (m)

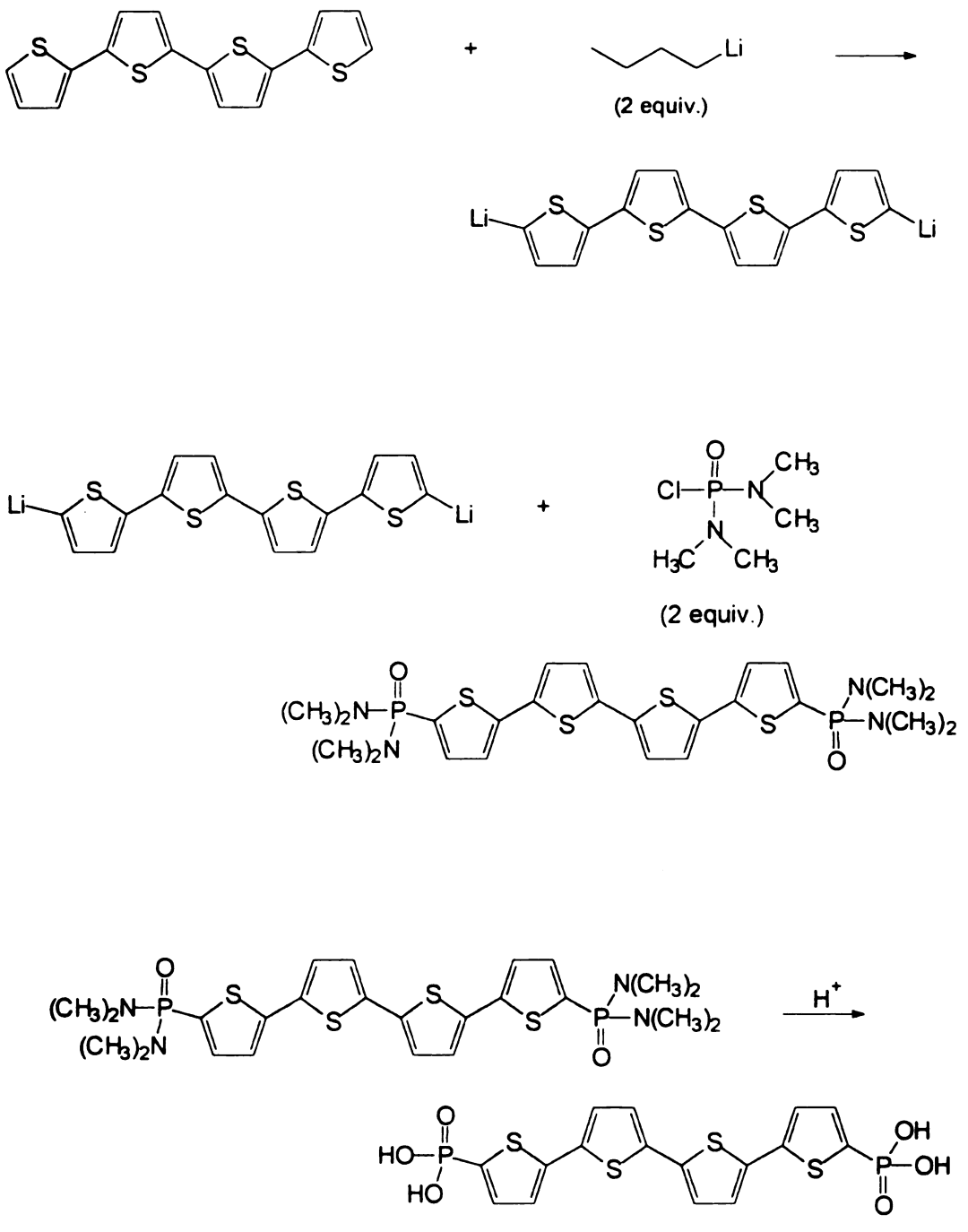

Figure 2.2 Three-step synthetic scheme for phosphorylation of quaterthiophene: (1) lithiation of QT; (2) formation of phosphamide; (3) hydrolysis to phosphonate.

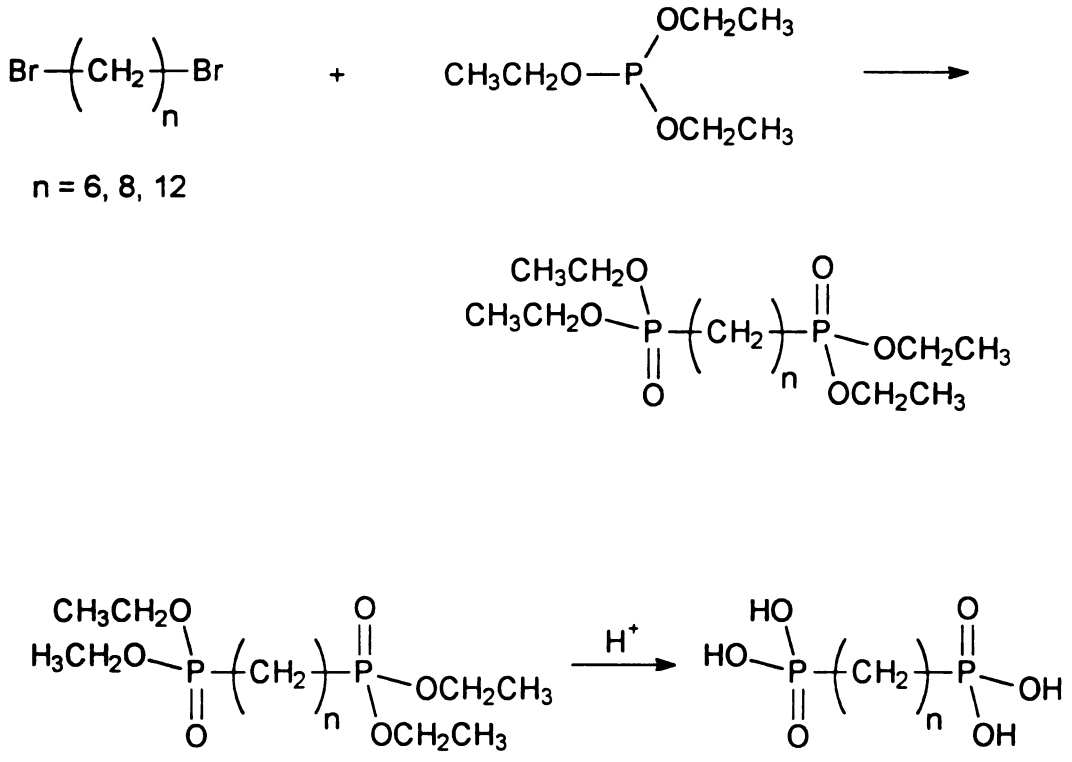

Figure 2.3 Synthetic scheme for alkane bisphosphonic acids. (1) Formation of phosphonate with triethylphosphate; (2) hydroylsis to phosphonate.

Multilayer Synthesis. Silica substrates, cut from quartz slides, or polished single crystal (100) silicon substrates were cleaned by immersion in piranha solution (1 H_2O_2:3 H_2SO_4) for 15 minutes, rinsed with distilled water, and dried under a N_2 stream. Clean substrates were used immediately. Under Ar atmosphere, 20 mL anhydrous octane was added to a roundbottom flask containing the substrate. The octane was heated to reflux, and 0.2 mL 3-(aminopropyl) triethoxysilane (Petrarch) was added. After ten minutes reaction time, the primed substrate was removed and rinsed with reagent grade *n*-hexane and then distilled water, and dried with N_2. An alternative primer layer could be deposited by overnight immersion in a 0.5% solution of (3-aminopropyl) dimethylethoxysilane in dry toluene. The amine primer layer was derivatized to the phosphonate by reaction with 100 mM $POCl_3$ and 100 mM 2,4,6-collidine in anhydrous acetonitrile under Ar for 30 minutes and rinsed with solvent grade acetonitrile. The phosphonic acid surface was zirconated overnight with a 5 mM solution of $ZrOCl_2$ in 60% EtOH/H_2O. Subsequent layers were added by sequential reaction with alkane bisphosphonate (1.25 mM in 95% EtOH, three hours at 55 °C) and zirconium (5 mM in 60% EtOH, 30 minutes) solutions, with extensive rinsing (H_2O) between each step. The pH of the solutions was maintained between 2 and 4.

Optical null ellipsometry. The thicknesses of primed substrates and monolayer samples were determined using a commercial optical null ellipsometer (Rudolph Auto-EL II) operating at 632.8 nm. Data were acquired and reduced using Rudolph software. For both primer and ZP layers, we used a value of the refractive index of $\mathbf{n} = 1.462 + 0i$ for the determination of film thickness.

Reflection-Absorption FTIR. Infrared spectra of MP films were obtained from a Nicolet Magna 550 FTIR spectrometer. The external reflection sample mount and optics used were obtained from Harrick Scientific Corp. and the polarization of the IR light was controlled using a Cambridge Physical Sciences broad band IR polarizer. The light was *p*-polarized and was incident at 70° with respect to the surface normal of the substrate. Spectral resolution was 4 cm^{-1}.

2.3 Results and Discussion

We have synthesized in moderate yield the bisphosphonates needed for the monolayer and multilayer experiments in this dissertation. Most of the loss of product in these procedures involved side-reaction of water-sensitive reagents (BuLi, phosphochloridate) with trace amounts of moisture in the reaction vessels, and the extra steps taken to ensure the purity of the compounds (chromatographic separations, recrystallizations). Mechanical losses also were more significant because of the small amounts of starting material used.

The property of interest for the chromophores in this study is that their spectra are overlapped, to allow efficient energy transfer from one to another. As illustrated in Figure 2.4, this condition applies. The spectra of the three oligothiophenes are highly overlapped. In order to distinguish between the optical responses of multiple chromophores in a given sample, the excitation wavelengths of each and the emission maximum of each must be sufficiently resolved, ideally by 50 nm or more. We note that TDP is not well resolved from either BDP or QDP. However, the emission spectra of BDP and QDP are sufficiently resolved, and the emission band of BDP and the

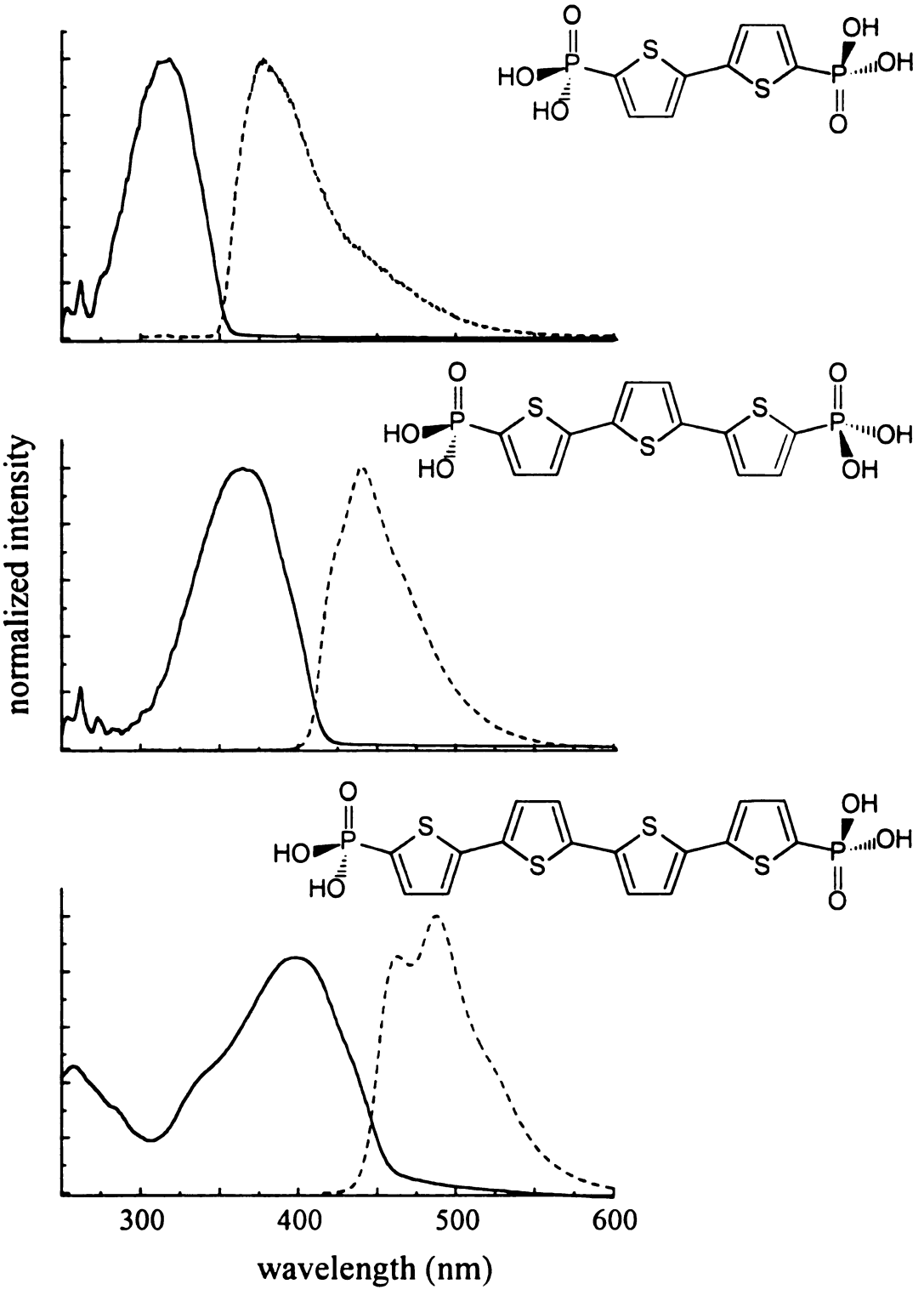

Figure 2.4 Structures and absorption (——) and emission (- - -) spectra for (top) BDP; (middle) TDP; (bottom) QDP.

absorption band of QDP are still well overlapped. Clearly, the best choice is to use BDP as the donor chromophore and QDP as the acceptor chromophore in the energy transfer experiments. We can excite a film containing both BDP and QDP at 315 nm, which is a maximum in the BDP absorbance and a minimum for QDP absorbance. Emission can be collected for BDP and QDP at 400 nm and 525 nm, respectively, without significant interference.

The alkanes synthesized for this study serve two purposes: dilution of chromophore layers and spacing of chromophore layers. The separation of chromophore layers within a film with optically inactive material is expected to be important for controlling energy transfer that occurs between layers. We can control sensitively the interlayer spacing using alkanes of various lengths. We have confirmed by absorbance (Figure 4.2) and fluorescence (not shown) that the alkane phosphonates do not have visible spectra that would potentially interfere with the chromophores. Each alkane was purposely chosen to have a length matching closely the length of a corresponding oligothiophene. We determined the lengths of the molecules using molecular modeling software (Hyperchem 4.0). The dimensions of the molecules were determined for the most extended conformations: all-*trans* for the alkanes and all-*anti* for the thiophenes. These theoretical lengths are recorded in Table 2.2.

Table 2.2 Calculated lengths of alkanes and oligothiophenes. The length is measured as the distance between the outermost oxygen atoms.

	Length (Å)		Length (Å)
HBPA	12.0	BDP	11.3
OBPA	14.5	TDP	14.9
DDBPA	19.6	QDP	18.5

We note that the calculated length for undecane-BPA (C_{11}) is 18.3 Å, which corresponds more closely to the length of QDP than C_{12} does. We chose to use DDBPA for this work because of the possibility of odd-even effects in the ordering of the layers, as has been seen in other types of monolayers. In the case of bisphosphonates, the active phosphonate groups of even-carbon chains are oriented more favorably for multilayer growth than they are on odd-carbon chains, as illustrated in Figure 2.5. Using even-carbon chains is more beneficial for the packing of individual layers and for the stability and uniform buildup of additional layers in the film.

Prior to starting the energy transfer work, we needed verification that we could reproduce the ordered MP films that others had synthesized. In this Chapter, we study the growth of individual layers and of MP multilayer films by building multilayer films of alkanes. Throughout this work we use substrates with silanol active sites, namely fused silica and single crystal silicon (100) with its native oxide layer. To anchor the film to the substrate, we treat the substrate with a short aminoalkylsilane primer. The identity of the substrate and the primer has been shown to have an effect on the optical properties of chromophore monolayers, as discussed in later chapters. However, these effects are

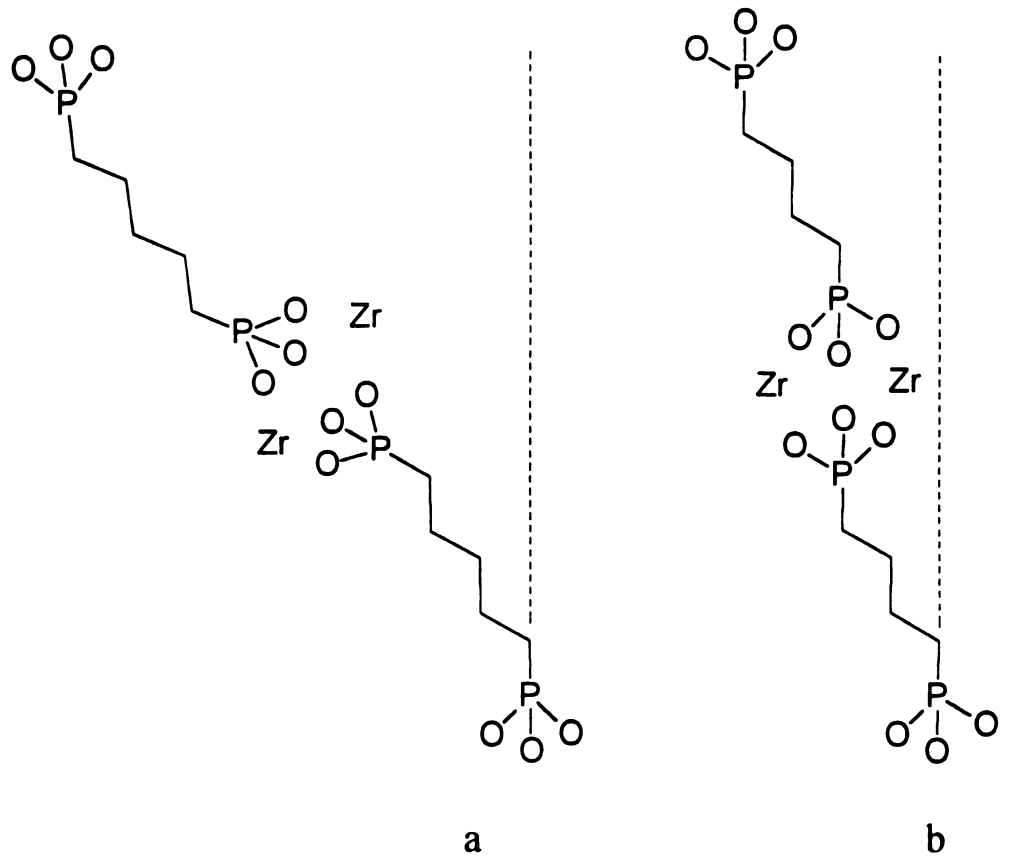

Figure 2.5 Schematic of the buildup of two zirconium-phosphonate layers of (a) odd-carbon chain and (b) even-carbon chain. The dashed lines indicate the surface normal.

not relevant in the preliminary characterization of the alkane films discussed in this Chapter.

The terminal amino groups on the surface are derivatized to aminophosphonates to provide the active sites necessary for MP growth. The next step is to deposit a layer of metal ions. MP films have been synthesized using a wide variety of metals, including Zn^{2+}, Cu^{2+}, Y^{3+}, Zr^{4+}, and Hf^{4+}.[3] Zirconium is the most common, because the structure of the ZP lattice has been studied extensively, and because the complex that Zr forms with phosphonates is one of the least soluble of the MP complexes. This property allows fast (5 minute) formation of the interlayer linkages and makes the films especially robust. Longer times are required for organophosphonate depositions to allow for the ordering of organic portion of the layer. Byrd, *et al.*[4] have demonstrated by atomic force microscopy that an alkane bisphosphonate layer is well ordered within four hours.

Part of the annealing process within a layer involves conformational relaxation of the alkanes or thiophenes. One concern associated with this process is the possibility that a bisphosphonate could form "loops," connecting both phosphonate ends to the previous layer and thus terminating layer growth at those sites. This is more of a concern for the longer alkanes. The oligothiophenes are energetically unlikely to loop to the same extent because of the sterics involved with the more bulky ring structure and the substantial electron density associated with the sulfur in each ring. We address the reproducibility of MP multilayer synthesis by monitoring the growth of films layer-by-layer.

One method we use to monitor the buildup of multilayer films is ellipsometry. In this technique, changes in polarization of a light beam are measured as it passes through a film and is reflected off the substrate. The polarization angles are directly related to the

real and imaginary parts of the refractive indices of the substrate and the film, and the thickness of the film. There are two factors that affect how we take these measurements. One is that the optical constants of the film must differ substantially from those of the substrate. If the indices are matched, the instrument is unable to distinguish the film from the substrate, resulting in meaningless film thicknesses. To eliminate this problem, we use only silicon ($\mathbf{n} = 3.858 + 0.018i$) substrates for ellipsometry and not silica ($\mathbf{n} = 1.46 + 0i$), as the estimated refractive index of MP films is $\mathbf{n} \approx 1.51 + 0i$.[5,3d] The native oxide layer on silicon has constant thickness, and is easily corrected for with the software. The other limitation is in knowing the exact indices of the film. For very thin films, (< 100 Å), n_{film} and k_{film} do not affect the polarization measurably. These parameters can be estimated from bulk measurements, but many studies have shown that these values are not necessarily accurate for the same material in films. Because of the uncertainty in n_{film} and because our films are thin (20 - 200 Å), we use $\mathbf{n} = 1.462 + 0i$, which is equivalent to that of the native oxide layer. In this case, we measure the MP film and the oxide together, and manually subtract the oxide thickness for each measurement.

Figure 2.6 shows the results from the synthesis of a ten layer MP film of DDBPA. We observe linear growth of layers with an average thickness of 19 Å. The fact that the thickness increases monotonically for all layers indicates that looping of the alkanes is not a factor in these films. If looping was occurring, we would observe a leveling-off in the ellipsometric data as more active sites were terminated. Assuming the input indices are approximately accurate, we can geometrically determine the average tilt angle of the alkanes. The theoretical length of a Zr-DDBPA layer is 3.8 Å[1] + 19 Å = 21.8 Å. This produces an average tilt angle of 30°, which agrees well with molecular tilts found for

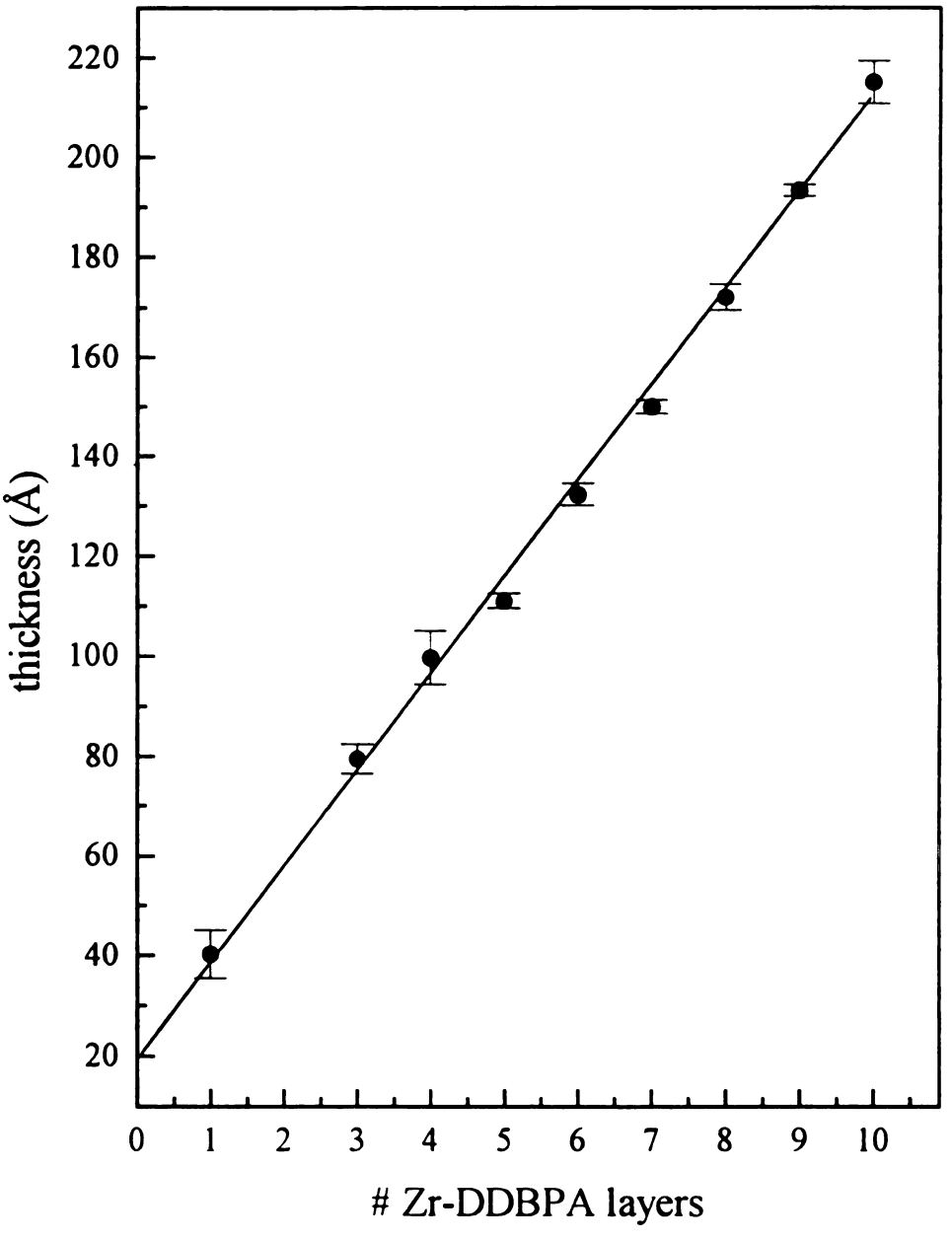

Figure 2.6 Plot of ellipsometric thickness measured for 10-layer DDBPA film and regression of data. The zero-layer thickness is that due to the native oxide layer and the primer layer.

many other layered systems.

Another technique that is especially sensitive in monitoring thin film buildup is reflection-absorption FTIR spectroscopy (RAIRS). RAIRS stands in contrast to a typical transmission experiment, where a spectrum is obtained of the film on both sides of the substrate and includes potentially large interference from the substrate, which can be on the order of 10^5 times thicker than the film itself. In the RAIRS configuration, the IR beam is reflected off the substrate at a grazing angle, typically 70 – 85°, so that the absorbance of the film is the main component of the spectrum. At grazing angle, most of the incident radiation is reflected through the film, in accordance with the Fresnel equations. The substrate still contributes to the overall spectrum, but not to as great an extent as in transmission experiments. RAIRS spectra were collected for films on both silica and silicon substrates, with similar results. The spectra for a representative DDBPA film on silica are shown in Figure 2.7.

The region of interest in these measurements is the – CH_2 stretching region. The CH_2 stretches can provide two important pieces of information about these films. One is the uniform growth of layers, as evidenced by the linear increases in peak height and area as layers are added. Another aspect is the relative order of the film overall. The peak positions of the CH_2 stretches provide a measure of the order of the alkane portions of the film. Using this criterion, many researchers have determined that the order of alkane-thiol monolayers on gold is relatively high, even superior to that of the same material in crystalline form. The peak positions for the alkane bisphosphonate layers are $\nu(CH_2)_a$ = 2925 cm^{-1} and $\nu(CH_2)_s$ = 2854 cm^{-1}. In comparison to the low frequencies measured for alkanethiols on gold ($\nu(CH_2)_a$ = 2916 cm^{-1}; $\nu(CH_2)_s$ = 2848 cm^{-1}) and bulk crystalline

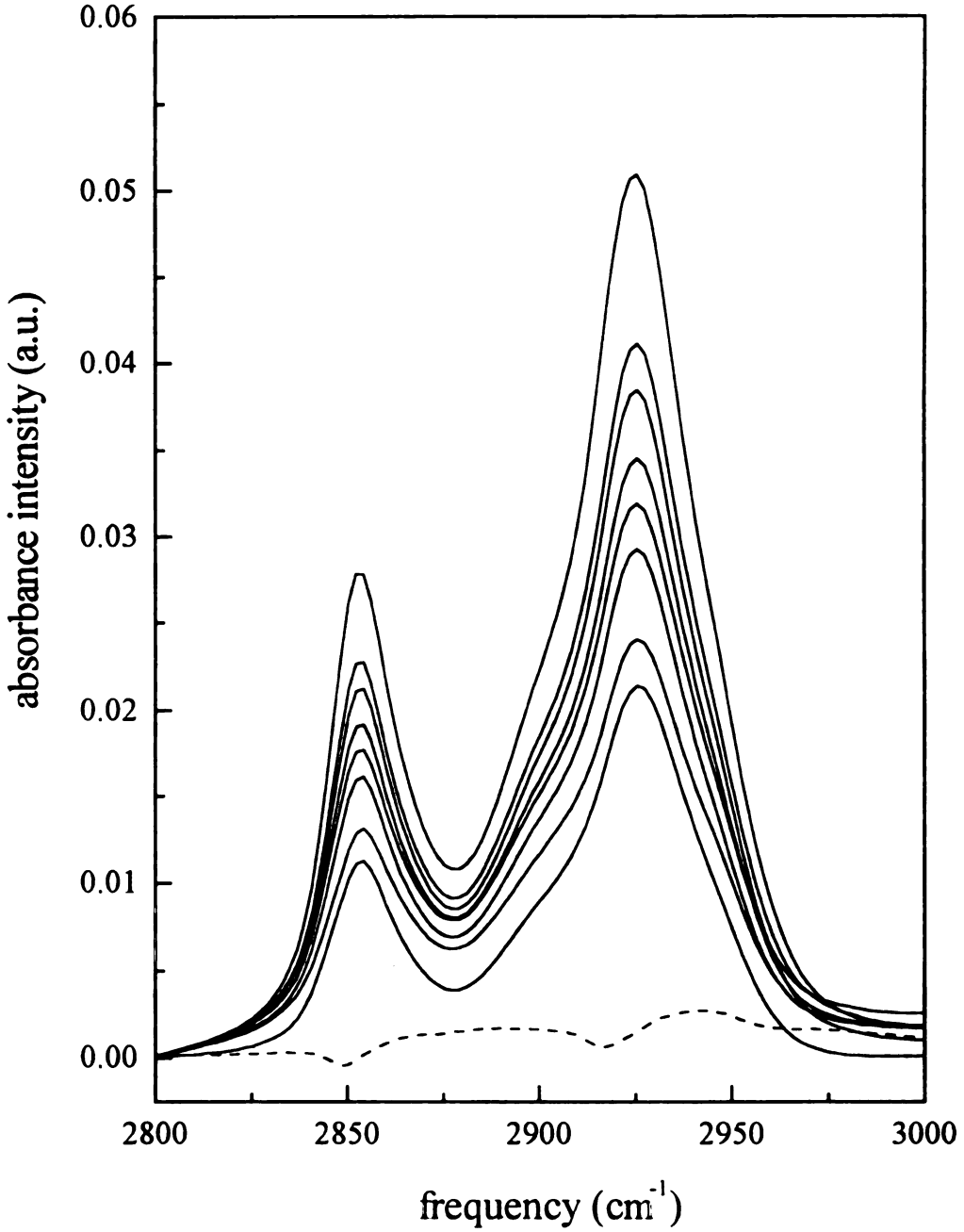

Figure 2.7 Reflection-absorption FTIR spectra measured for layers 4 – 11 of a Zr-DDBPA film on silica. The dashed line is the spectrum of the silane primer layer. Spectra were baseline corrected at 2800 cm^{-1}.

alkanes ($\nu(CH_2)_a$ = 2918 cm^{-1} and $\nu(CH_2)_s$ = 2849 cm^{-1}), the alkanes in MP films are not well-ordered. It has been proposed that the disorder in alkane MP films is due to lattice mismatch of the organic and inorganic portions of the layers. The ZP lattice produces active sites that can accommodate molecules with molecular area up to 24 $Å^2$,[6,7] which is about the size of a benzene ring. That area is much greater than that required for a simple alkane chain, allowing for a greater extent of conformational freedom within each site, and thus less overall order in each layer.

2.4 Conclusions

The compounds required for making some simple metal-phosphonate films have been synthesized. These compounds and subsequently synthesized films were characterized by ^1H NMR, ellipsometry, FTIR, and steady-state optical spectroscopy. We found that alkane bisphosphonate films grow monotonically, as evidenced by both ellipsometry and FTIR. We determined from the ellipsometric thicknesses that the average tilt angle of the alkanes in a film is 30°, which is common for self-assembled layers. The FTIR data indicate that, while the layers can be grown uniformly, there is some structural heterogeneity that decreases the average order within a layer. Between the uniform layer growth and the favorable overlap of the emission band of BDP and absorption band of QDP, these materials will be useful for future energy transport studies.

2.5 Literature Cited

1. Katz, H. E.; Schilling, M. L.; Chidsey, C. E. D.; Putvinski, T. M.; Hutton, R. S. *Chem. Mater.* **1991**, *3*, 699.

2. Bhattacharya, A. K.; Thyagarajan, G. *Chem. Rev.* **1981**, *81*, 415.

3. (a) Lee, H.; Kepley, L. J.; Hong, H.-G.; Akhter, S.; Mallouk, T. E. *J. Phys. Chem.* **1988**, *92*, 2597. (b) Akhter, S; Lee, H.; Hong, H.-G.; Mallouk, T. E.; White, J. M. *J. Vac. Sci. Technol. A* **1989**, *7*, 1608. (c) Yang, H. C.; Aoki, A.; Hong, H.-G.; Sacket, D. G.; Arendt, M. F.; Yau, S.-L.; Bell, C. M.; Mallouk, T. E. *J. Am. Chem. Soc.* **1993**, *115*, 11855. (d) Zeppenfeld, A. C.; Fiddler, S. L.; Ham, W. K.; Klopfenstein, B. J., Page, C. J. *J. Am. Chem. Soc.* **1994**, *116*, 9158.

4. Byrd, H.; Snover, J. L.; Thompson, M. E. *Langmuir* **1995**, *11*, 4449.

5. Hanken, D. G.; Corn, R. M.; *Anal. Chem.* **1995**, *67*, 3767.

6. Thompson, M. E. *Chem. Mater.* **1994**, *6*, 1168.

7. Cao, G.; Hong, H.-G.; Mallouk, T. E. *Acc. Chem. Res.* **1992**, *25*, 420.

Chapter 3

Rotational Isomerization Barriers of Thiophene Oligomers in the Ground and First Excited Electronic States. A ^{1}H NMR and Fluorescence Lifetime Investigation

Summary

We report on the isomerization dynamics of a family of substituted thiophene oligomers designed for the synthesis of soluble poly(alkylthiophene)s possessing a minimal coupling defect density. The data we report for 3',4'-dibutyl-2,2':5',2"-terthiophene, 3",4"-dibutyl-2,2':5',2":5",2"':5"', 2""-pentathiophene and 3',4',3"",4""-tetrabutyl-2,2':5',2":5",2"':5"',2"":5"",2""'-sexithiophene indicate that the ground state isomerization barrier for all of these oligomers is on the order of 8 kcal/mol, with no discernible dependence on the length of the oligomer. For oligomer isomerization in the S_1 electronic state, we find that the isomerization barrier for both the pentathiophene and sexithiophene oligomer is ~5.2 kcal/mol, slightly larger than the value we reported previously for S_1 3',4'-dibutyl-2,2:5',2"-terthiophene. Experimental data for both electronic states in these oligomers are in excellent agreement with semi-empirical calculations using the PM3 parameterization.

3.1 Introduction

This Chapter focuses on the rotational isomerization barriers of thiophene oligomers in the context of determining the intrinsic, structural limits to the synthesis of conjugated polymers possessing a minimum defect density. This is a central issue in the development of practical organic optical and electronic devices. Understanding and controlling the extent of structural disorder in a material is also critical to studies aimed at optimizing the nonlinear optical response of strongly coupled three level systems.[1,2] There are a limited number of conjugated polymers for which it is possible to synthesize crystalline materials possessing a very low structural defect density. For the majority of conjugated polymer systems, however, syntheses are by electrochemical or, less commonly, photochemical means and are often carried out in solution. For this reason, any amount of structural heterogeneity intrinsic to the monomer units will be expressed in the resulting polymer. We focus here on poly(alkylthiophene) because of the importance of this family of materials for conducting[3-8] and nonlinear optical information processing[9-13] applications.

Polythiophenes and poly(alkylthiophene)s have received a great deal of recent attention for both fundamental and practical reasons. This family of polymers has found application in the fabrication of organic light emitting diodes and for this reason, there has been a significant amount of research effort aimed at producing processable materials with a minimal density of structural defects. The first polythiophenes were synthesized from thiophene and the dominant defect in this material was from inter-ring linkages between positions α and β to the S heteroatom on adjacent thiophene rings.[14] These materials are also insoluble and, as a result, were of limited utility for device applications requiring

material processability. The next advance in the synthesis of polythiophenes was to use a 3-alkylthiophene as the monomer.[15-20] While the solubility of the resulting polymer was improved, head-to-head and tail-to-tail coupling defects contributed significantly to molecular scale disorder in the resultant material. There have been several successful attempts to minimize these coupling defects synthetically by using asymmetric monomers, and it is now possible to make poly(3-alkylthiophene)s where the inter-ring coupling is ~95% "pure", *i.e.* head-to-tail coupling.[6,21-23] An alternative approach to such syntheses is to use oligomeric forms of thiophenes where head-to-tail coupling defects are precluded for structural reasons. Recent work by Wang *et al.*[5] has shown this to be a successful approach, yielding corresponding polymer material that exhibits conductivities higher than those reported for poly(thiophene)s synthesized from 3-alkylthiophene monomers. Even with the development of synthetic routes aimed at minimizing the extent of inter-ring coupling defects, rotational isomerization between individual thiophene rings in oligomeric and polymeric thiophenes can give rise to a different class of structural defects. For this reason it is important to consider the intrinsic inter-ring isomerization characteristics of thiophene oligomers and to understand how the energetics of isomerization in this family of oligomers are affected by oligomer length. We have examined the rotational isomerization characteristics of three substituted thiophene oligomers in order to address these questions. In previous work in the Blanchard group[4] it was indicated that the ground state isomerization barrier of 3',4'-dibutyl-2,2':5',2"-terthiophene (DBTT) was ~20 kcal/mol based on variable temperature ^{1}H NMR measurements. Further investigation of this system with a higher field (500 MHz) NMR spectrometer has revealed that the data reported previously were limited in resolution, causing the estimate of the isomerization

barrier to be too large. The data we report here possess the resolution required to establish the ground state isomerization barrier of DBTT, and two larger oligomers, to be ~8 kcal/mol. Measurements of the excited state isomerization characteristics of thiophene oligomers indicate this energy to be ~5.2 kcal/mol for both the substituted pentathiophene and sexithiophene compounds. In an earlier report the isomerization energy determined for the substituted terthiophene oligomer was 4.2 ± 0.4 kcal/mol.[4] We discuss below the means used to acquire the experimental data, the form and temperature dependence of the ^{1}H NMR data and the way in which we relate the NMR chemical shift results to the dynamical response of the molecule, and the viscosity-dependence of the fluorescence lifetime data for the pentathiophene and sexithiophene oligomers. In addition, we present semi-empirical calculations[24-28] for these molecules using the PM3 parameterization. The PM3 parameterization offers a significant improvement over the AM1 parameterization for these oligomers. The calculated predictions are in excellent agreement with experimental data.

3.2 Experimental

Chemicals. The thiophene oligomers used in this study were provided by Prof. E. LeGoff. A brief summary of the syntheses follows. 3',4'-Dibutyl-2,2':5',2"-terthiophene (DBTT), was synthesized according to a published procedure.[23] To synthesize the 3",4"-dibutyl-2,2':5',2":5",2"':5"', 2""-pentathiophene oligomer (DBPtT), DBTT was dibrominated at the α positions of the terminal thiophene rings using tetramethyl ammonium tribromide and subsequently coupled on both ends to thiophene magnesium

bromide in the presence of a catalyst. The 3',4',3"",4""-tetrabutyl-2,2':5',2":5",2"':5"',2"":5"",2""':5""',2""'-sexithiophene oligomer (TBSxT) was synthesized by coupling two equivalents of DBTT which had been treated sequentially with *n*-butyl lithium and copper chloride. A detailed description of these oligothiophenes has been reported elsewhere.[29] For the fluorescence lifetime measurements, all solvents were purchased from the Aldrich Chemical Company as either reagent grade or spectroscopic grade and were used without further purification. For the ^{1}H NMR measurements, d_8-toluene (99.6 atom% D) was purchased from Isotech, Inc. and used as received.

Steady State Optical Spectroscopy. The absorption spectra of DBPtT and TBSxT were measured using a Hitachi U-4001 UV-visible spectrophotometer. The emission spectra for these oligomers were determined using a Hitachi F-4500 fluorescence spectrophotometer. These data were used to determine the appropriate excitation and observation wavelengths for the fluorescence lifetime measurements.

NMR Spectroscopy. ^{1}H NMR spectra of DBTT, DBPtT, and TBSxT in d_8-toluene, referenced to tetramethylsilane (TMS), were measured using a 500 MHz Varian (VXR-500) NMR spectrometer. The temperature of the samples was controlled with an FTS Systems air-jet and temperature control unit, and was varied between -40°C and +90°C for DBPtT and TBSxT measurements and between -40°C and +105°C for DBTT measurements. Uncertainty in the sample temperature was determined to be 0.5°C.

Time Correlated Single Photon Counting Spectroscopy. The spectrometer we used for the fluorescence lifetime measurements of the oligomers DBPtT and TBSxT is shown schematically in Figure 3.1. A mode-locked CW Nd:YAG laser (Quantronix 416) produces ~ 11 W average power at 1064 nm, with 100 ps pulses at 80 MHz. An angle-

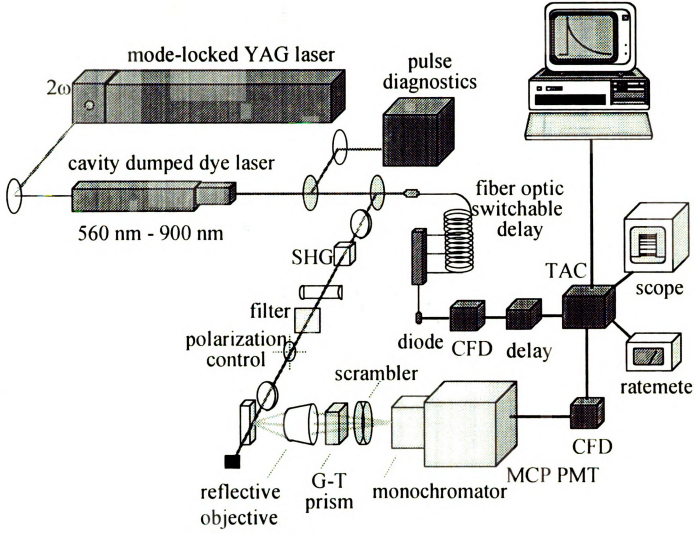

Figure 3.1 Time correlated single photon counting spectrometer

tuned Type II KTP crystal is used to frequency double the pulse train to 532 nm (~ 750 mW). The 532 nm light excites a cavity-dumped, synchronously pumped dye laser (Coherent 702-2) which is dumped at a repetition rate of 4 MHz, producing ~ 5 ps pulses. The output from the dye laser is divided using a 90/10 beam splitter into two paths: 90% of the light is used to excite the sample, and 10% is used for the reference. The beam sent to the sample is frequency doubled with a Type I $LiIO_3$ crystal. The fundamental is separated from the second harmonic using color filters, and the excitation polarization is controlled using a fused silica half-wave rhomb. (CVI) Emission from the sample is collected at 90° with respect to the incident light, and the polarization of the emission is selected using a Glan-Taylor prism. The reflective microscope objective shown in Figure 3.1 is used for low-signal samples, such as the monolayers in the following Chapters. The polarization of this light is subsequently scrambled, and collection wavelengths are selected using a subtractive double monochromator. (American Holographic DB-10) The detection electronics have been described in detail previously,[4] and we briefly review them here. The signal from the detector (MCP-PMT, Hammamatsu R2809U-07) is sent to a constant fraction discriminator (CFD, Tennelec TC454), where it is processed and sent to the time-to-amplitude converter (TAC, Tennelec TC864), which we operate in reverse mode. The reference consists of the remainder of the divided dye laser beam (10%), which is sent through a fiber optic delay line, where we control the time offset between signal and reference channels. The TAC output counts are observed using an oscilloscope (Tektronix 2230) and are sent to a multichannel analyzer (MCA, Tennelec PCA-II) for collection. DBPtT was excited at 390 nm (LDS 751, Exciton), and TBSxT was excited at 406 nm (LDS 821, Exciton). Fluorescence was collected at 54.7° with

respect to the polarization of the excitation pulse at the wavelengths indicated in Table 3.1. A representative fluorescence lifetime scan, together with the instrumental response function (typically ~ 35 ps FWHM) is shown in Figure 3.2.

Table 3.1 Excitation and emission wavelengths used for TCSPC measurements.

	DBPtT		TBSxT	
solvent	λ_{exc} (nm)	λ_{em} (10 nm bandwidth)	λ_{exc} (nm)	λ_{em} (10 nm bandwidth)
methanol	390	481	406	504
1-butanol	390	484	406	507
1-heptanol	390	485	406	508
1-decanol	390	485	406	508

Data Analysis. The lifetimes we report here are derived from data deconvoluted from the instrumental response function using software written by Snyder and Demas.[30] The lifetimes we report are averages and standard deviations of at least twelve individual determinations for each solvent.

Calculations. Semiempirical calculations[24-28] were performed using Hyperchem® Release 4.0 on an IBM compatible PC (Gateway 2000 486-66V). The PM3 parameterization, used for these calculations, is a modification of the AM1 parameterization that treats molecules containing polar heteroatoms, such as sulfur, more accurately than previous parameterizations. The calculation strategy for the three oligomers was to perform an initial optimization of the structures using a molecular mechanics routine (MM+)[31] followed by a geometry optimization at the semiempirical

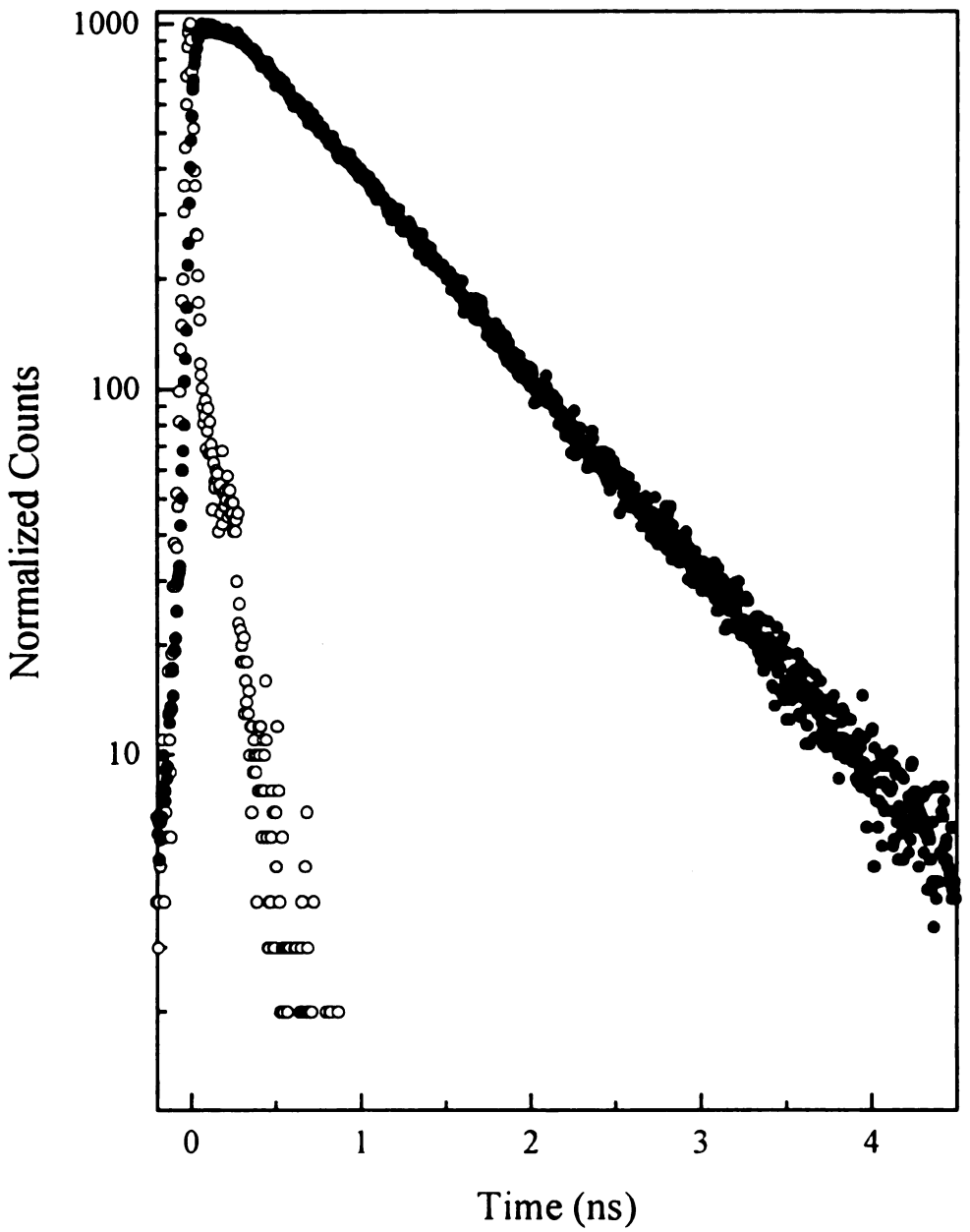

Figure 3.2 Example of excited state population decay (●) for TBSxT in n-butanol. The instrument response (O) time is ~ 35 ps.

level using an SCF algorithm. Semiempirical optimization was performed until the lowest energy conformation for each molecule was attained. Heats of formation and electronic charges of individual protons and carbons were calculated for the geometrically optimized molecules.

3.3 Results and Discussion

The primary focus of this paper is to obtain information on the isomerization characteristics of the thiophene oligomers DBTT, DBPtT and TBSxT (Figure 3.3), in both their ground and first excited singlet electronic states. The motivation for this work is to understand the intrinsic limits to conformational disorder in polymers synthesized from these oligomers and, based on this information, determine whether there is a preferred synthetic strategy for alkylated thiophene polymers. Because the measurement strategy for the isomerization of a molecule in its ground state differs significantly from that for excited state measurements, we will treat measurements of rotational isomerization in these two states separately.

Ground State Measurements. Representative ^{1}H NMR spectra are shown for each of the three oligomers in Figures 3.4 – 3.6. The proton assignments are as indicated in Figure 3.3. The chemical shift of each proton exhibits a unique temperature dependence, from 0.0001 - 0.002 ppm/K, as shown for a series of DBTT spectra in Figure 3.7. Analogous protons on different oligomers exhibit almost identical temperature dependencies. Measurements of proton resonances that appear furthest downfield were limited, due to the presence of solvent peaks in the same chemical shift range. In a previous examination of DBTT in the Blanchard group, it was observed, using a 300 MHz

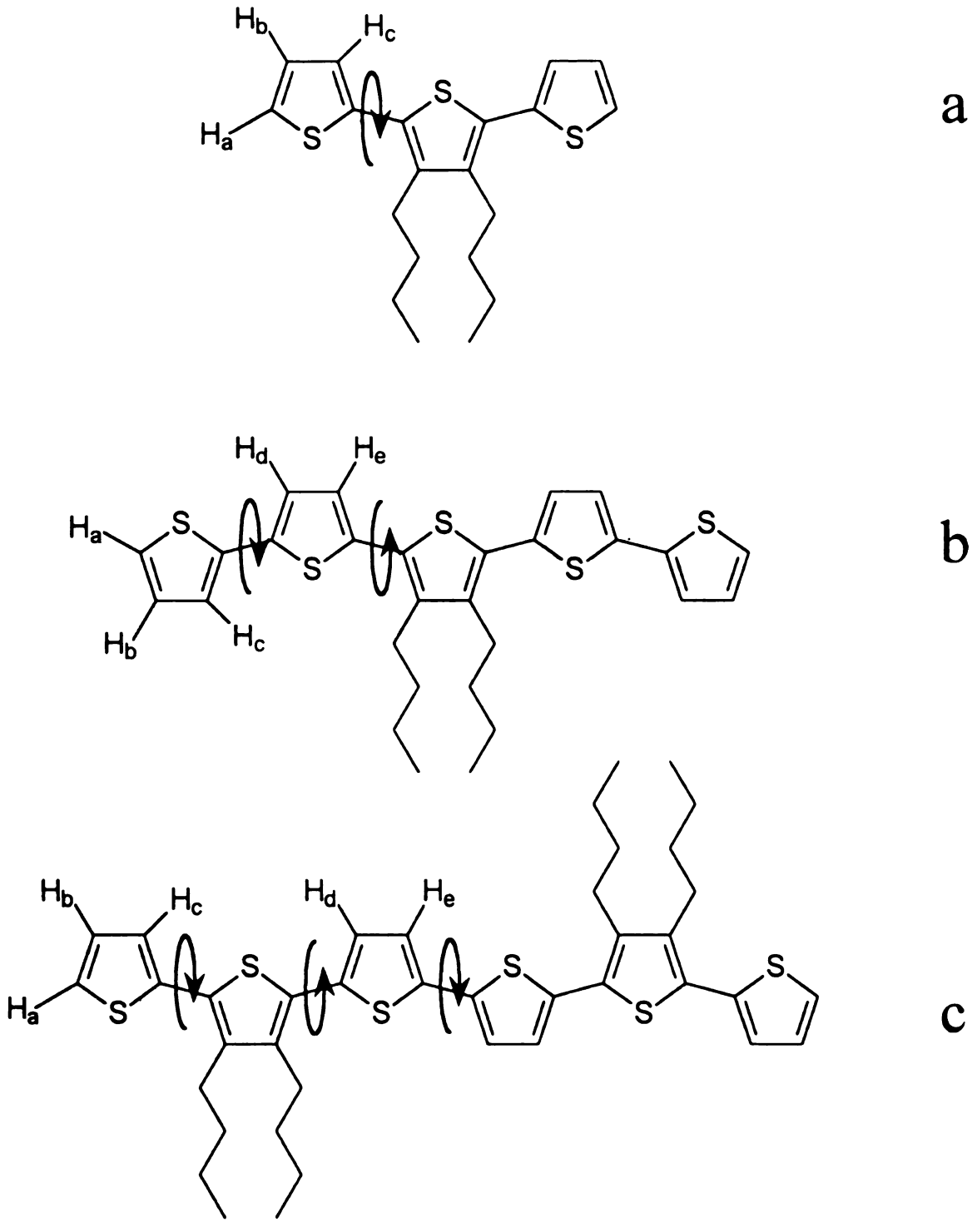

Figure 3.3 Structures and inter-ring rotations for the three thiophene oligomers. (a). 3',4'-dibutyl-2,2':5',2"-terthiophene (DBTT), (b) 3",4"-dibutyl-2,2':5',2":5",2"':5"', 2""-pentathiophene (DBPtT) and (c) 3',4',3"",4""-tetrabutyl-2,2':5',2":5",2"':5"',2"":5"",2""-sexithiophene (TBSxT).

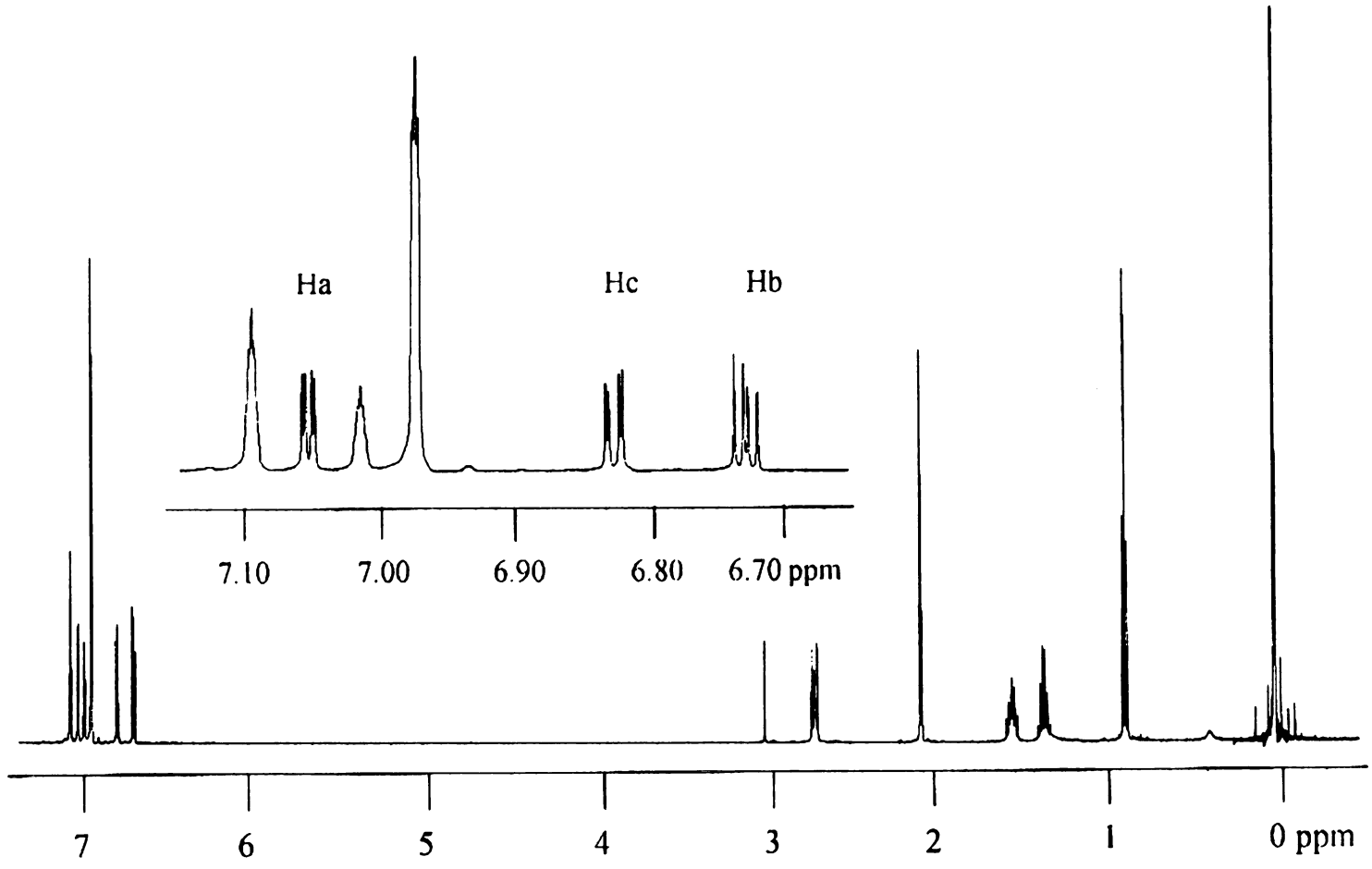

Figure 3.4 ^{1}H NMR spectrum of DBTT taken at -20°C. Inset: Expanded aromatic proton region with proton assignments for the aromatic protons. The designations of the protons are indicated in Figure 3.3.

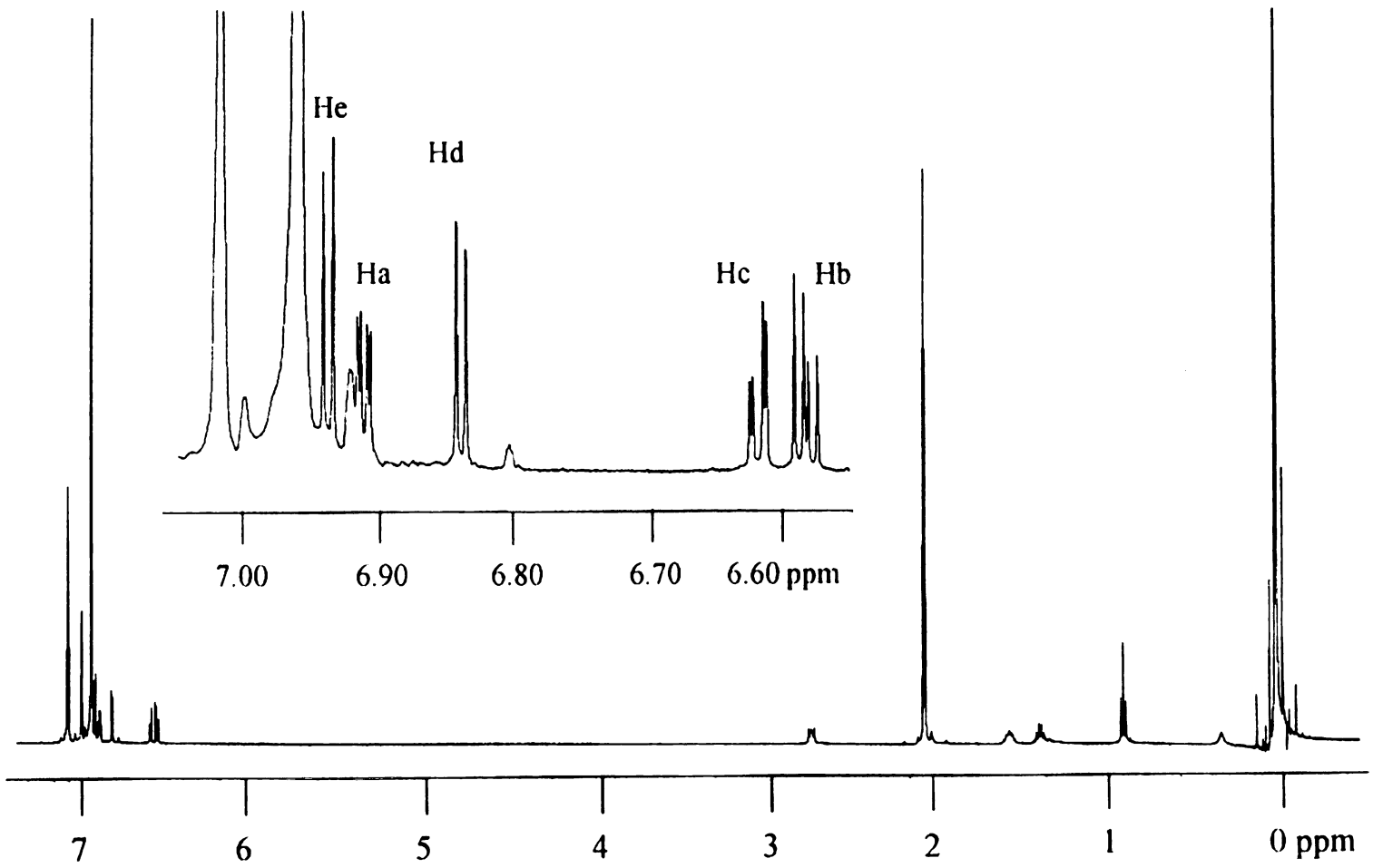

Figure 3.5 ^{1}H NMR spectrum of DBPtT taken at -20°C. Inset: Expanded aromatic proton region with proton assignments for the aromatic protons. The designations of the protons are indicated in Figure 3.3.

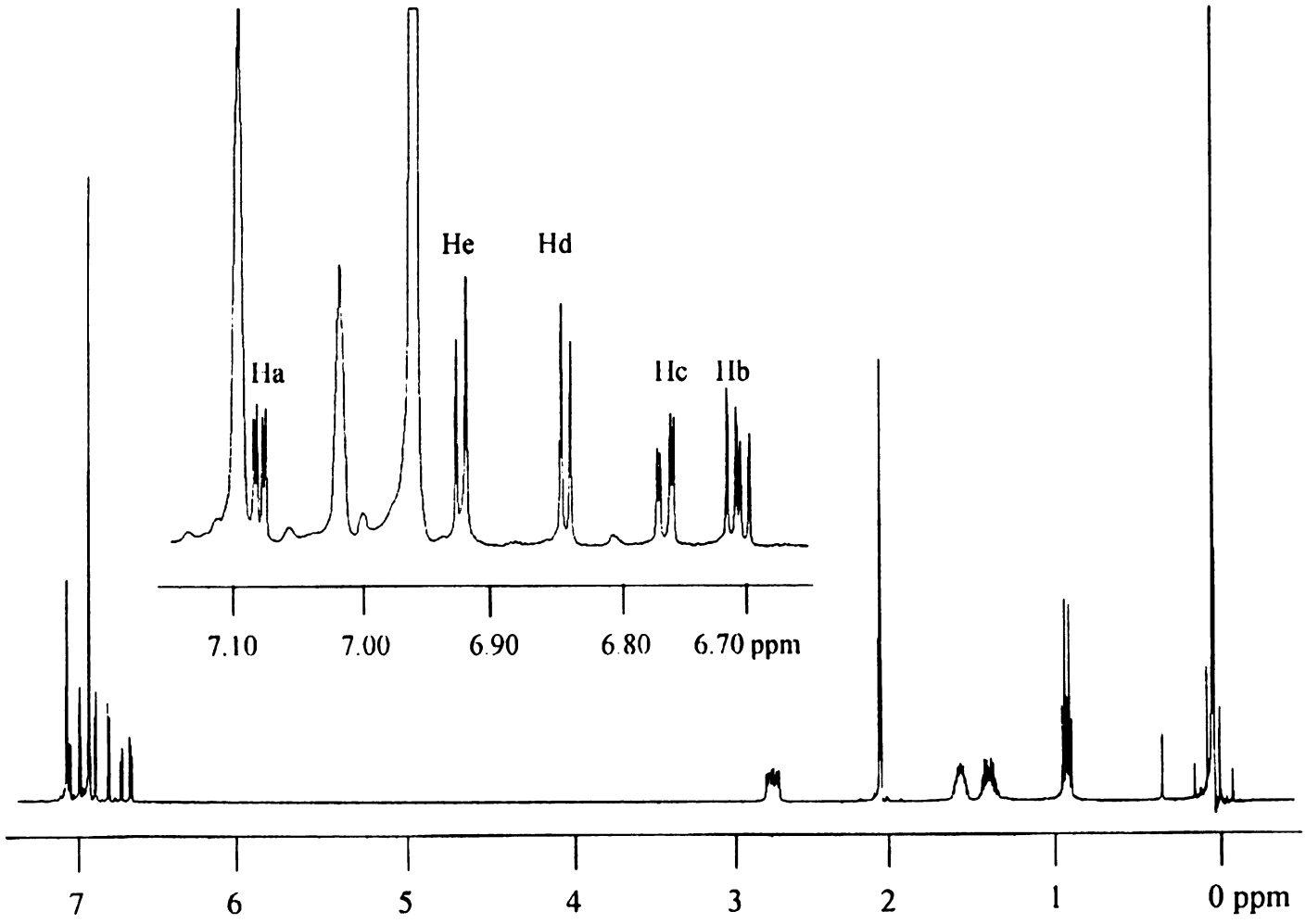

Figure 3.6 ^{1}H NMR spectrum of TBSxT taken at -20°C. Inset: Expanded aromatic proton region with proton assignments for the aromatic protons. The designations of the protons are indicated in Figure 3.3.

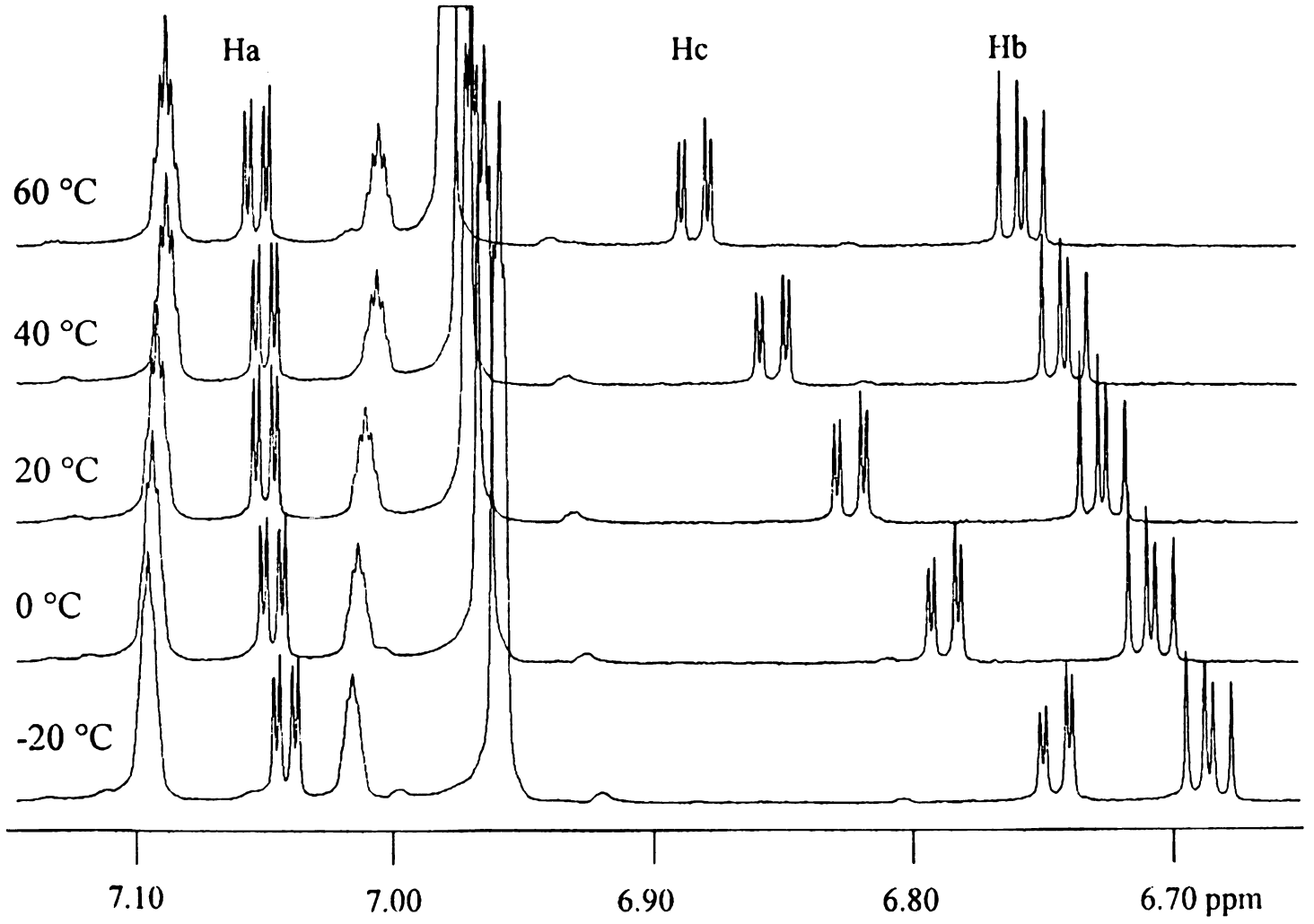

Figure 3.7 Temperature dependence of the aromatic proton resonances of DBTT, shown at five representative temperatures, as indicated in Figure 3.3.

NMR spectrometer, that the several doublet resonances split by ~1.5 Hz appeared to coalesce and, based on this information, an isomerization barrier of ~20 kcal/mol was reported for ground state DBTT.[4] Our subsequent measurements using a higher field spectrometer have shown that the apparent coalescence we reported earlier is actually only a loss of resolution. The split resonances for a given individual proton do not coalesce, because the splittings arise from *J*-coupling between non-adjacent protons. Based on the higher resolution data we report here for DBTT, DBPtT and TBSxT, we conclude that ring rotation is much faster than the time scale of the NMR experiment. That is, coalescence occurs at a temperature much lower than -40°C for these oligomers. The rotational isomerization barriers for these oligomers are, in fact, significantly smaller than 20 kcal/mol. Despite the absence of a coalescence in these data, the temperature-dependence of the proton chemical shifts for these oligomers can be used to infer the approximate energy of the isomerization barrier. We understand the temperature dependence of the individual proton resonances in these oligomers based on the temperature-dependent conformational distribution of the rotamers.

It is well established that the chemical shift of a proton bound to an aromatic system is related to the effective charge on the carbon atom to which the proton is bound.[32-34]

$$\Delta\delta_H = a\Delta q_C \qquad [3.1]$$

The effective charge (q_C) on the carbon of interest is determined by its electron density, and the ^{1}H NMR resonance energies (chemical shifts, δ) are also affected by secondary, inductive effects such as "ring current".[34-36] We expect the effective charge on the proton to play a central role in determining the chemical shift, although we are not aware of any

explicit treatments of the relationship between proton charge and chemical shift. We find, in fact, that the proton charges play a critical role in determining the proton NMR resonance frequency, and the carbon π electron density is important as well (*vide infra*). The proportionality constant a can be determined for a given system,[32,37] but is not expected to be constant for all molecules because of secondary, structure-dependent shielding effects. We understand and model the temperature-dependent proton resonance energies for the thiophene oligomers as follows. The charge of each proton is influenced by the inter-ring dihedral angle between individual thiophene rings. Because there is a finite energy barrier to inter-ring rotation, (Figures 3.8a, 3.9a, 3.10a) the extent to which each rotamer will contribute depends on the temperature of the system. We have calculated the conformation dependence of the proton and adjacent carbon charge, (Figures 3.8b,c; 3.9b,c; 3.10b,c) as well as the isomerization barrier for inter-ring rotation (Figures 3.8a, 3.9a, 3.10a) for each oligomer using semiempirical molecular orbital calculations with the PM3 parameterization. We calculated the charge for each aromatic proton and carbon at 5 degree increments between 0 and 180 degrees. We assume in our treatment that the there are no anomalies on this energy surface that would give rise to discontinuities (*e.g.* sudden polarization phenomena[38-41]). The *average* charge of a given proton or a given carbon for an oligomer isomerizing in solution, then, depends on the amount of time that the oligomer exists in each rotational conformation. This treatment presumes that ring rotation is fast compared to the time scale of the NMR measurement and that we sample a thermally-weighted portion of the isomerization surface. Changes in temperature thus alter the contribution of high energy portions of the isomerization surface to the average charges sampled in the NMR measurements. To determine the

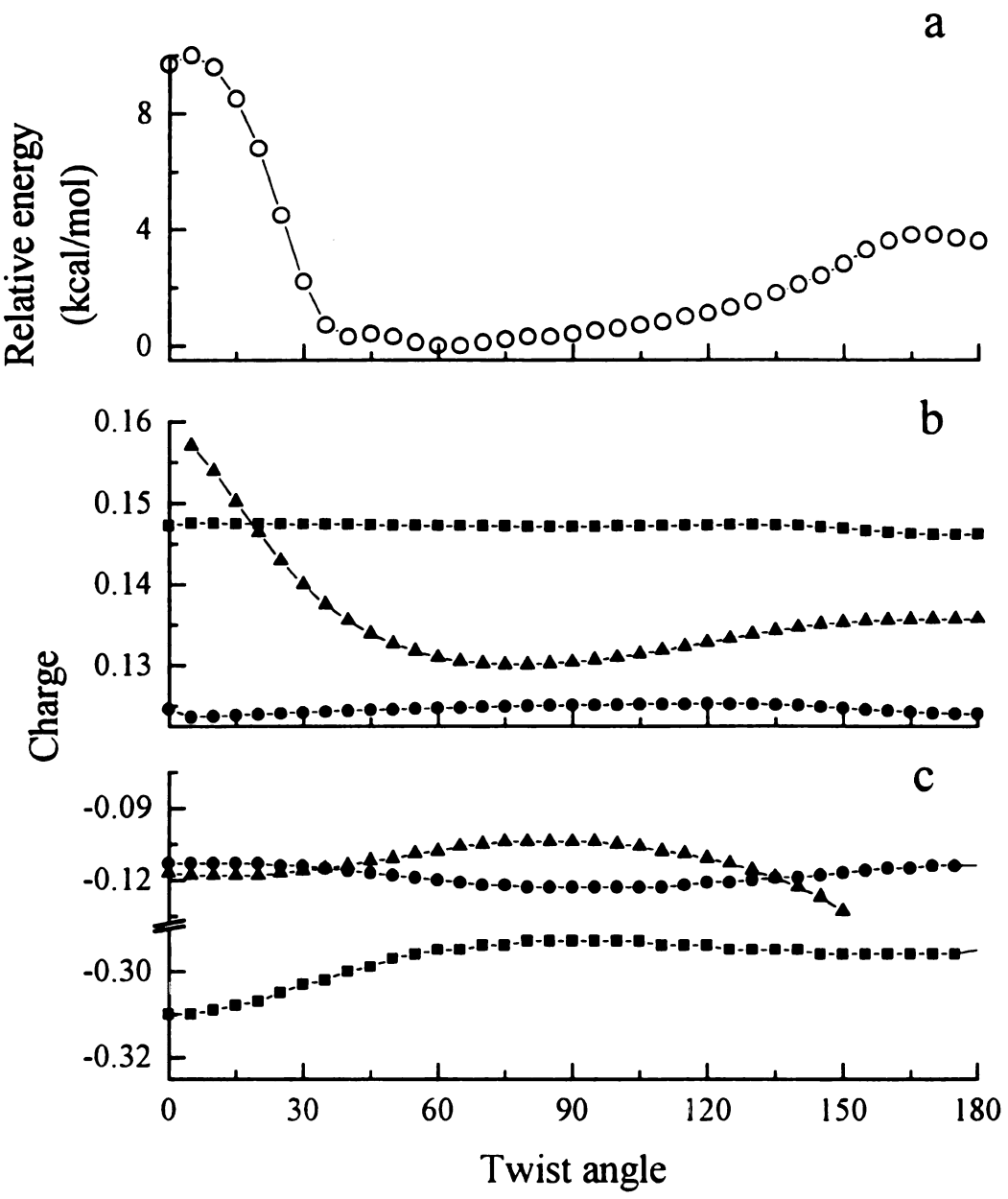

Figure 3.8 (a) Calculated isomerization barrier for DBTT, where the isomerization coordinate is taken as the inter-ring dihedral angle. (b) Dependence of the proton charges on inter-ring rotation angle; (●) = H_a, (■) = H_b, (▲) = H_c. (c) Dependence of the aromatic carbon charges on inter-ring rotation angle; (●) = C_a, (■) = C_b, (▲) = C_c.

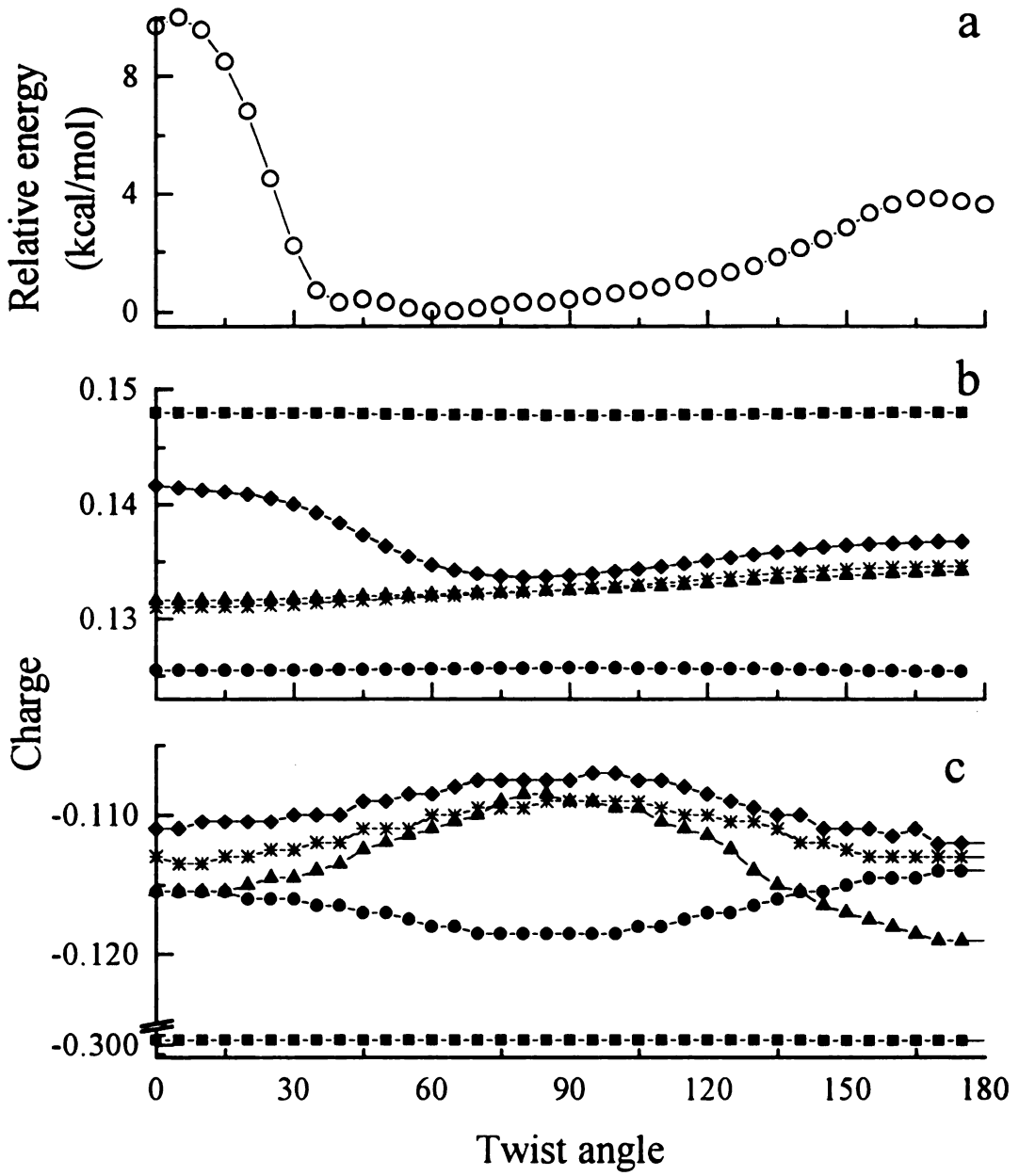

Figure 3.9 (a) Calculated isomerization barrier for DBPtT, where the isomerization coordinate is taken as the inter-ring dihedral angle. (b) Dependence of the proton charges on inter-ring rotation angle; (●) = H_a, (■) = H_b, (▲) = H_c, (+) = H_d, (◆) = H_e. (c) Dependence of the aromatic carbon charges on inter-ring rotation angle; (●) = C_a, (■) = C_b, (▲) = C_c, (✳) = C_d, (◆) = C_e.

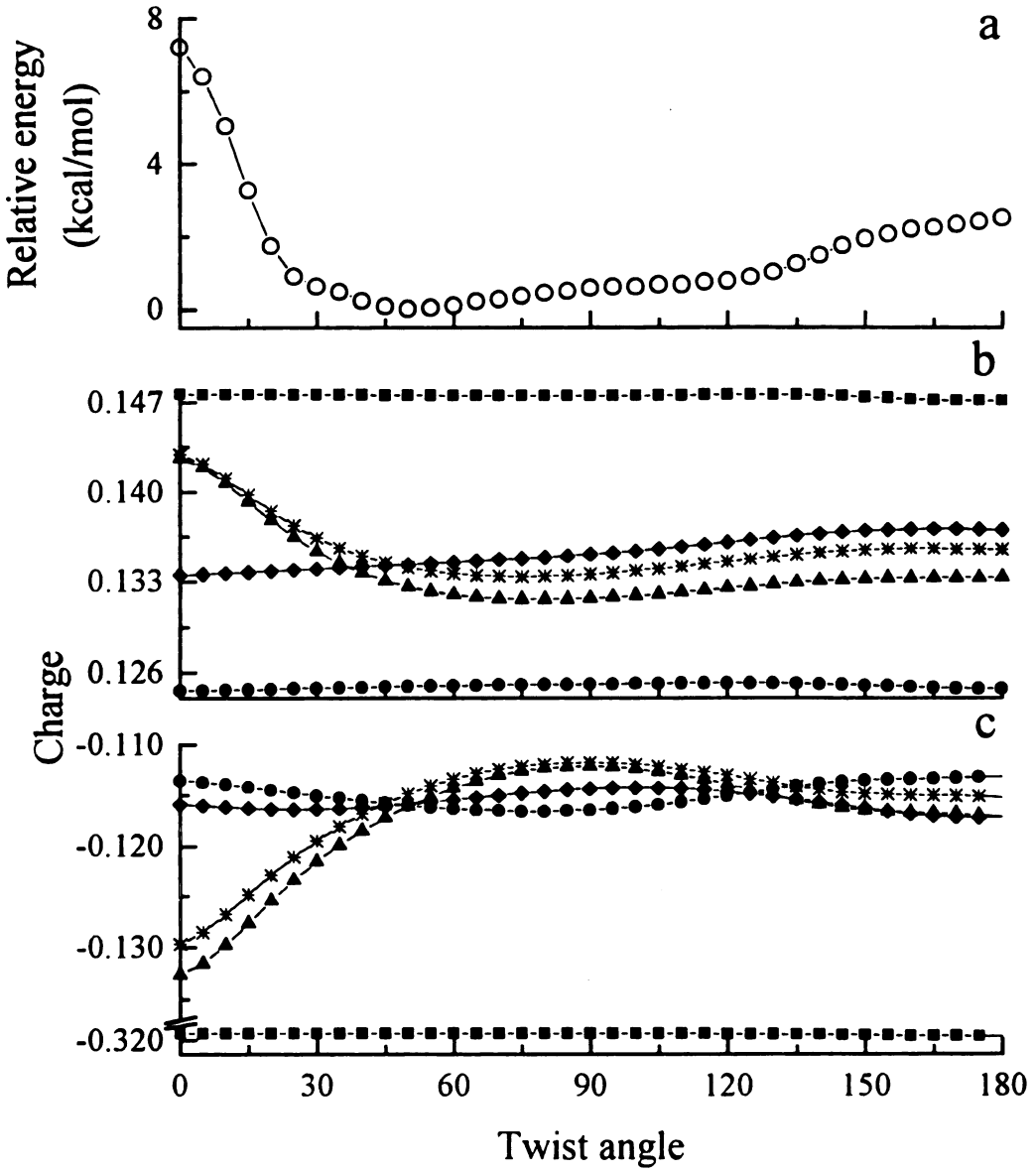

Figure 3.10 (a) Calculated isomerization barrier for TBSxT, where the isomerization coordinate is taken as the inter-ring dihedral angle. (b) Dependence of the proton charges on inter-ring rotation angle; (●) = H_a, (■) = H_b, (▲) = H_c, (+) = H_d, (◆) = H_e. (c) Dependence of the aromatic carbon charges on inter-ring rotation angle; (●) = C_a, (■) = C_b, (▲) = C_c, (✳) = C_d, (◆) = C_e.

fractional contribution of a given conformer to the average charge of a given proton or carbon, the energy of the oligomer was calculated as a function of inter-ring dihedral angle. For DBTT, there is one unique isomerization to consider. For DBPtT there are two distinct dihedral angles relevant to the isomerization surface and for TBSxT there are three relevant dihedral angles, as shown in Figure 3.3. In this treatment of DBPtT and TBSxT we assume that the individual isomerization coordinates are nominally uncoupled (this is a valid assumption because the barriers are small), and thus the average of the two isomerization barriers provides a useful one-dimensional potential well representation for these molecular motions on the time scale of the NMR measurement. This assumption allows us to calculate ring rotation-dependent atomic charges without accounting for inductive, multiple-ring effects. From these energy surfaces, reduced to one-dimensional representations of the overall molecular motion, we can determine the contribution (fractional population) of a given rotamer based on the Boltzmann distribution because the isomerization is driven thermally.

$$\frac{N_\theta}{N_0} = \exp\left(-\left(E_\theta - E_0\right)/k_B T\right) \qquad [3.2]$$

Where N_θ is the population of the rotamer with dihedral angle θ, N_0 is the population of the lowest energy conformation, and the energies E_θ and E_0 are the relative energies of the two conformers. We assume that the degeneracy of each conformer is the same, and include no degeneracy weighting factors in Equation 3.2. For each atom of interest, the average charge density at a given temperature T, $\bar{q}_T$, weighted for the appropriate rotamer distribution, can be calculated from

$$\bar{q}_T = \left(\frac{\sum_\theta N_\theta q_\theta}{\sum_\theta N_\theta} \right)_T \qquad [3.3]$$

The temperature dependence of $\bar{q}_T$ results from the Boltzmann terms. We obtain $\bar{q}_T$ for each relevant proton and carbon in these oligomers accordingly. A plot of the experimental temperature dependencies of the aromatic proton resonances for DBTT is shown in Figure 3.11a and a corresponding plot of $\bar{q}_T$ vs. T for these same protons is shown in Figure 3.11b. We present the same comparison for DBPtT and TBSxT in Figures 3.12 and 3.13, respectively. The temperature-dependence of the average charge on a given proton correlates well with the experimental chemical shift temperature-dependence. We note that the poorest agreement between experiment and calculation is for DBPtT, where the approximation of an average isomerization coordinate is expected to be most limiting. We recognize that the magnitude of the chemical shift(s) in Hz are not calibrated, necessarily, with the temperature-dependent charge variation on each proton, due in part to the inherently qualitative nature of the molecular orbital calculations we used to estimate the charges. Registration of these two scales (charge and chemical shift) would be empirical even with the appropriate standards.[32,37] Thus our qualitative agreement between experiment and model is encouraging in and of itself. Previous models, relating electronic charge to ^{1}H NMR chemical shift have focused on the carbon atom to which the proton is bound. We observe that the charge on the proton is a dominant factor in determining the deshielding and thus the NMR chemical shift. The relationship between the charges on each proton and carbon and the proton chemical shift will be determined by proportionality constants that are different for each species. Thus

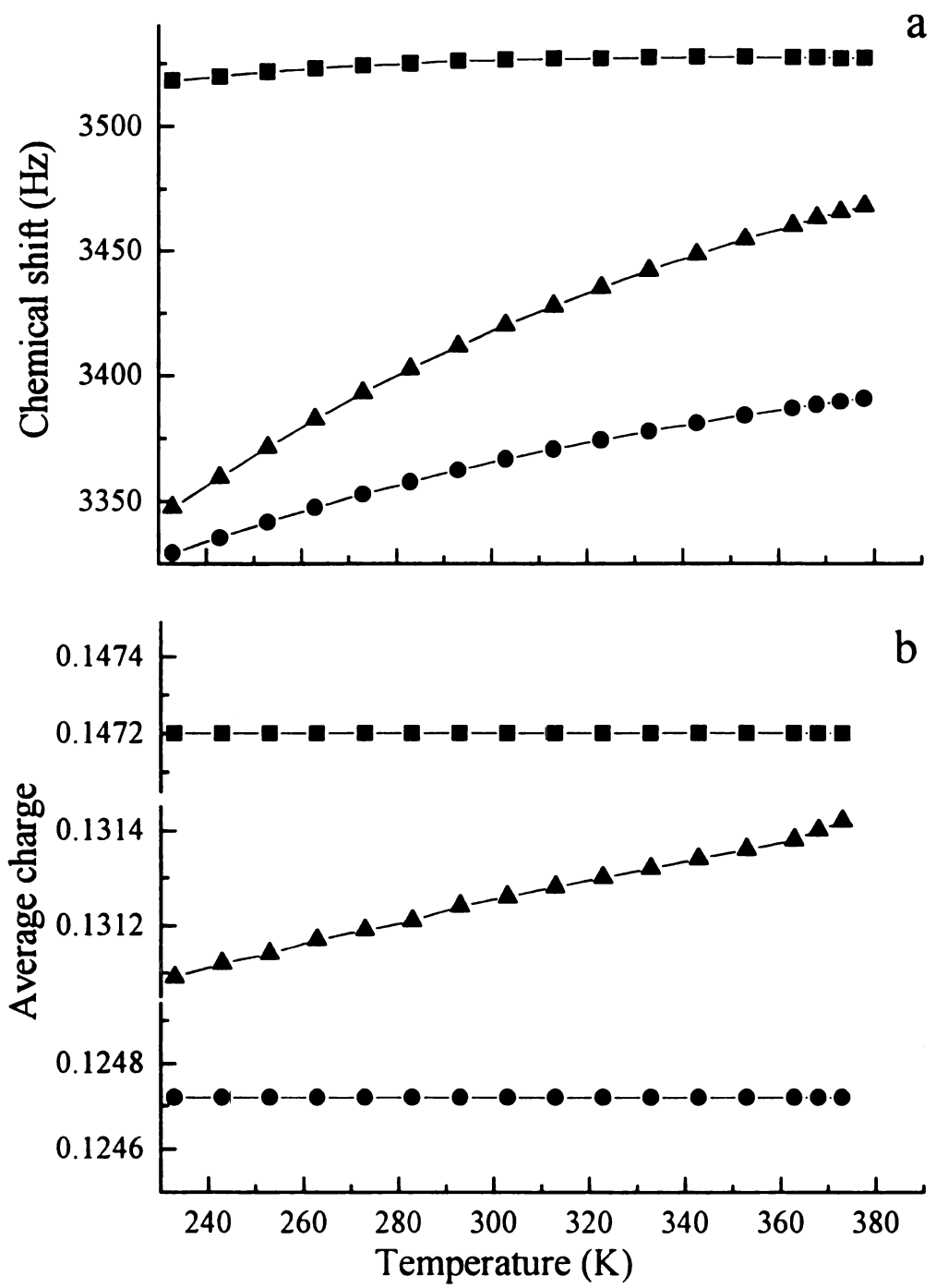

Figure 3.11 (a) Experimental temperature-dependence of ^{1}H NMR resonances for DBTT. (b) Temperature-dependence of aromatic proton charges, calculated as described in the text. For both (a) and (b), (●) = H_a, (■) = H_b, (▲) = H_c.

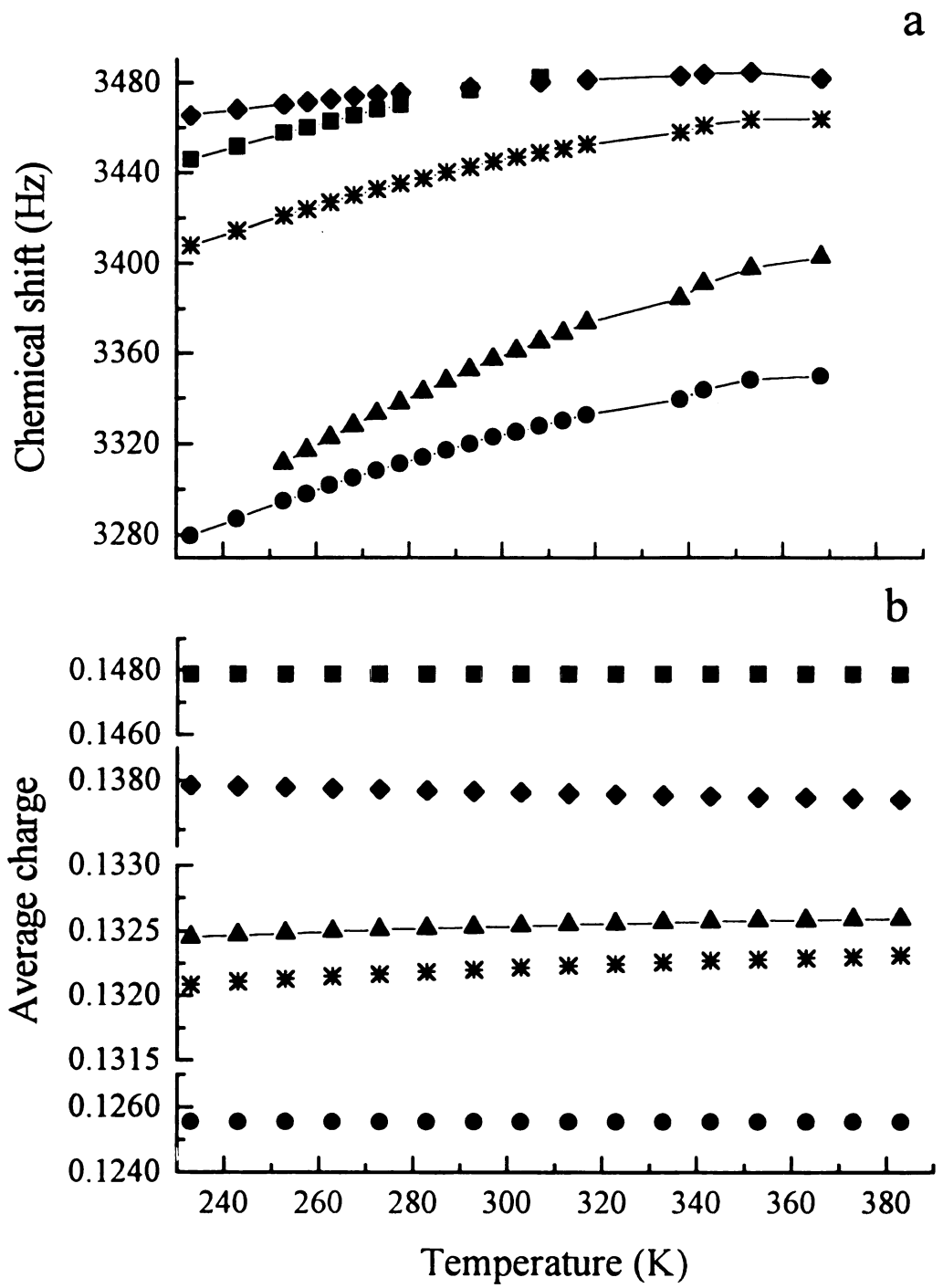

Figure 3.12 (a) Experimental temperature-dependence of ^{1}H NMR resonances for DBPtT. (b) Temperature-dependence of aromatic proton charges, calculated as described in the text. For both (a) and (b), (●) = H_a, (■) = H_b, (▲) = H_c, (+) = H_d, (◆) = H_e.

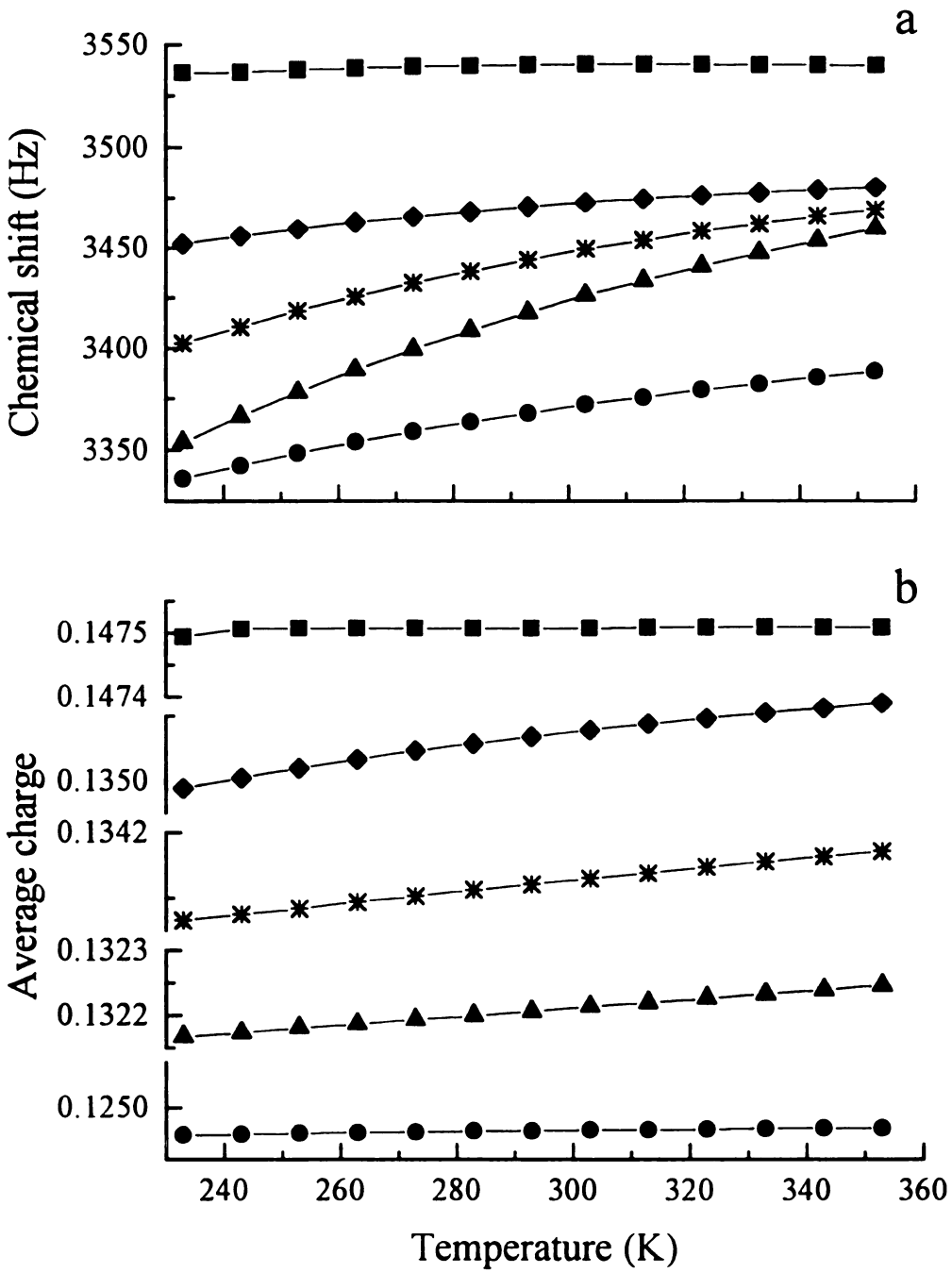

Figure 3.13 (a) Experimental temperature-dependence of ^{1}H NMR resonances for TBSxT. (b) Temperature-dependence of aromatic proton charges, calculated as described in the text. For both (a) and (b), (●) = H_a, (■) = H_b, (▲) = H_c, (✳) = H_d, (◆) = H_e.

Equation 3.1 can be modified to include these dependencies explicitly,

$$\Delta\delta_H = a_H \Delta q_H + a_C \Delta q_C \qquad [3.4]$$

where a_H and a_C are different. Consideration of either of these charges individually does not provide the optimum agreement, although it is clear from the experimental data that the dominant contribution to $\Delta\delta_H$ comes from $a_H \Delta q_H$. Consideration of $a_C \Delta q_C$ would lead to an improved correlation between experiment and model, as suggested by Figure 3.14. While we can calculate the terms q_C and q_H, the determination of each coefficient a is problematic because of the limited experimental information available. That is, we do not have sufficient experimental information to determine either a_C or a_H separately. Despite this limitation, we recognize that the trends presented in the experimental data are consistent with contributions from the electron densities of both the proton and carbon. Proton *a* of DBTT will exhibit relatively little temperature-dependence because the charge density on the carbon to which it is attached is comparatively rotation-independent. The temperature-dependence of the proton *b* NMR resonance will increase in slope due to the inductive effect of the adjacent carbon, and proton *c* will exhibit a slight decrease in its temperature-dependence. The comparisons between experimental NMR data and our calculated charge temperature dependencies are in excellent predictive agreement with the relationship between electronic charges and chemical shift indicated in Equation 3.4. The agreement between the experimental data and our model also provides justification for our estimation of an isomerization barrier on the order of 8 kcal/mol for ground state thiophene oligomers, as calculated. A few words are in order at this point on the meaning(s) of the isomerization barriers we report in Figures 3.8 – 3.10. For DBTT, there is only one unique dihedral angle, and the barrier height of ~10 kcal/mol calculated for this

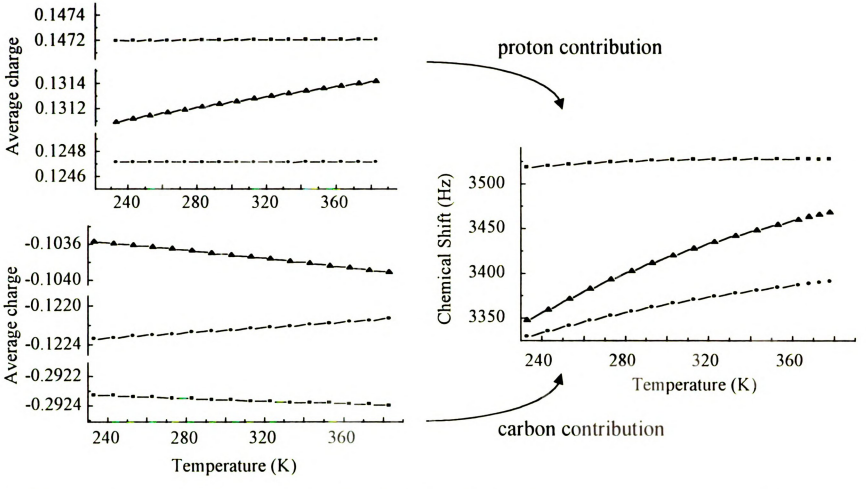

Figure 3.14 Calculated temperature dependent proton charges (top, left) and aromatic carbon charges (bottom, left) for DBTT, compared to experimental ^{1}H NMR chemical shift temperature-dependent data. The comparison is necessarily qualitative. See text for a discussion of this point. Symbol assignments are the same as in Figure 3.8.

isomerization is determined almost exclusively by steric constraints imposed by the *n*-butyl moieties at the 3' and 4' positions of the molecule. Our calculation did not take into account the ability of these aliphatic groups to move in such a way as to minimize steric hindrance to the ring rotation, and we thus believe that the calculated barrier is a slight overestimate of the actual experimental barrier. For the larger oligomers, DBPtT and TBSxT, the barriers we report in Figures 3.9 and 3.10 are averages of the isomerization barriers for the 2 (DBPtT) or 3 (TBSxT) dihedral angles involved. We recognize that the ~8 kcal/mol barrier is an over-estimate for the DBPtT terminal ring because steric hindrance by the *n*-butyl groups will not play a role. For rotation of only the DBPtT terminal ring, we calculate an isomerization barrier of ~1 kcal/mol. The relatively poorer agreement between experiment and calculation for this oligomer (Figure 3.12) is therefore an expected result. For TBSxT, the rotation of each thiophene ring will be hindered to some extent by the presence of the *n*-butyl groups on an adjacent ring, and thus the average of the barriers will provide a reasonably accurate one-dimensional representation of the isomerization surface of this molecule. Because of the qualitative nature of the calculations, and the limitations intrinsic to our reduction of these complex, large amplitude molecular motions to a one-dimensional coordinate, we do not imply that 8 kcal/mol is an explicit upper or lower bound on the isomerization barrier energy for these molecules. We assert, however, that the experimental barriers must be close to those we calculate. If the barriers to ring rotation were much higher than 8 kcal/mol, the temperature-dependence of the NMR resonances would be much weaker because the oligomers would remain in energetically favored conformations even at elevated temperatures, *i.e.* a small portion of the multidimensional isomerization surface would be

sampled. Conversely, if the isomerization barrier were negligible compared to k_BT, then the isomerization surface would be sampled uniformly for all temperatures and we would observe a temperature-independent ^{1}H NMR response. The correlation between the semiempirical calculations and the experimental NMR data also indicates that the electron density on the protons is at least as important as the charge on the carbons in determining the proton chemical shift for aromatic systems.

Excited State Isomerization. Dilute (~10^{-4} M) solutions of DBPtT and TBSxT in methanol, *n*-butanol, *n*-heptanol, and *n*-decanol were excited at 390 and 406 nm, respectively, and fluorescence was collected at the wavelengths indicated in Table 3.1. The lifetimes were observed by collecting fluorescence polarized at 54.7° with respect to the exciting electric field to eliminate any rotational diffusion contributions to the data. In a previous report, the lifetime of DBTT showed a linear dependence on viscosity, which can be understood in the context of the existence of an excited state rotamer that is coupled efficiently to the ground state surface. For this model, there is essentially ~90° of uncertainty in the inter-ring dihedral angle at which efficient relaxation occurs. Many organic molecules exhibit a minimum energy in their S_1 isomerization surfaces at an inter-ring dihedral angle of 90°, because of the decoupling of the π system (break in conjugation) at this dihedral angle.[42,43] Relaxation from this conformation is thought to be rapid, and the limiting rate in the relaxation of the excited electronic state in this model is therefore mediated by the time required to execute an activated isomerization along the S_1 surface. The other possibility is that there is no 90° conformer that relaxes efficiently, but rather, one conformer is significantly shorter lived than the other conformer. These two conformers are expected to differ by an inter-ring dihedral angle of ~180°. In other

words, the *~syn* conformer excited state lifetime is expected to be significantly different than that of the *~anti* conformer. The obvious difference between these conformers is the extent to which S atoms on adjacent rings can interact. We speculate that such an interaction, enhanced in the *~syn* conformer, would serve to decrease the excited state lifetime, although there is no direct data to support this speculation. Semiempirical calculations of the S_1 thiophene oligomers (not shown) predict isomerization surfaces that do not exhibit energetic minima at 90° dihedral angles, but rather indicate the presence of energetic maxima at 90°. Regardless of the model used, the time required for an excited thiophene oligomer to relax is mediated by two barriers to the ring rotation; one intrinsic to the molecule and one imposed by the surrounding solvent medium. The extrinsic portion of the isomerization barrier, contributed by frictional interactions between the oligomer and the surrounding solvent, can be controlled by changing the solvent viscosity. In this model, a high viscosity solvent will impede the intramolecular ring rotation significantly, producing a comparatively long excited state lifetime. For a low viscosity solvent, where intramolecular motion is comparatively unhindered, the lifetime is expected to be shorter due to the greater rotational mobility of the rings. In order to estimate the intrinsic barrier to ring rotation for the thiophene oligomers, the viscosity dependence of the S_1 lifetime was extrapolated to zero viscosity. The experimental data for DBTT were regressed to a 123 ps zero-viscosity fluorescence lifetime. This lifetime can be interpreted in the context of an activated process,

$$k_{isom} = A \cdot \exp\left(-\left(E_{isom} + E_{vis}\right)/k_B T\right) \qquad [3.5]$$

using a preexponential factor of 10^{13}, which is appropriate for the *n*-alcohols. From this

time constant, E_{isom} was determined to be 4.2 ± 0.4 kcal/mol, with the uncertainty in this value being determined by uncertainty in the value of A. For the longer thiophene oligomers DBPtT and TBSxT, we find that there is no discernible viscosity dependence, as shown in Figure 3.15. Despite the outward difference in the appearance of the DBPtT and TBSxT data compared to the data for DBTT, we believe that the same model applies because of the structural similarity of these molecules. We are confident in this assertion based on the similarity of the ground state barriers for all of these oligomers, as well as the qualitative similarities in their linear optical responses. If the intrinsic barrier to rotation is greater than the extrinsic isomerization barrier, due to solvent frictional forces, then little or no viscosity dependence will be observed. The lifetimes for DBPtT and TBSxT are 676 ± 4 ps and 779 ± 8 ps, from which rotational barriers of 5.1 ± 0.4 and 5.2 ± 0.4 kcal/mol were calculated. These barriers are approximately 1 kcal/mol higher than that of DBTT,[4] and we can rationalize this behavior in the context of a more delocalized π system for the longer oligomers. We expect that the excited state of polythiophenes should be qualitatively similar to that of other conjugated polymers, such as polyaniline or poly(phenylenevinylene). For such polymers, the excited electronic state is expected to increase the bond order of the inter-ring bond(s). The longer the oligomer, the more capable it will be of supporting a "quinoid-like" resonance structure,[9] and the larger will be the expected isomerization barrier. The experimental data and intuitive reasoning we describe above are consistent with semiempirical calculations of the excited thiophene oligomers, which indicate an S_1 barrier height of ~5 kcal/mol for both DBPtT and TBSxT.

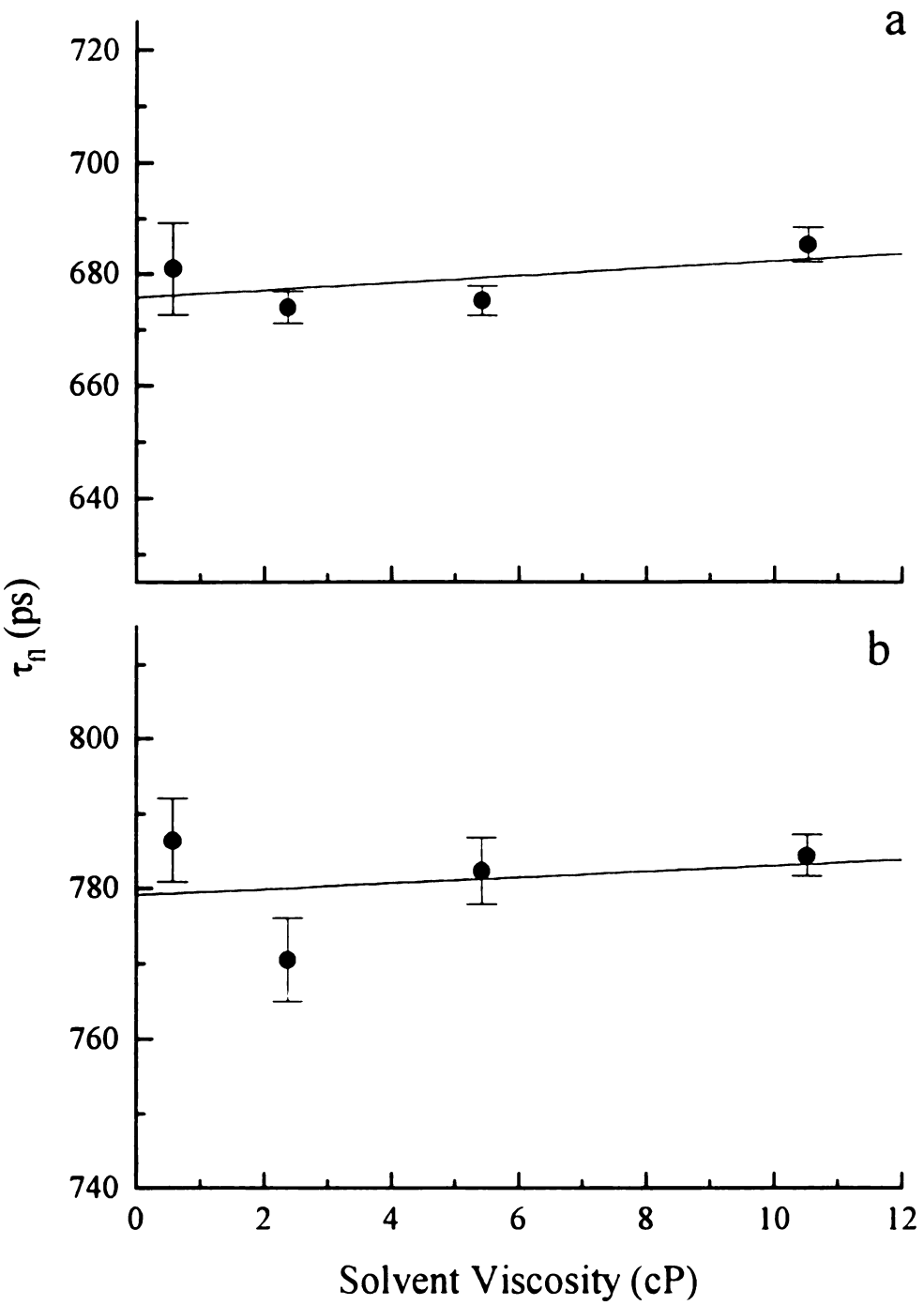

Figure 3.15 (a) Viscosity dependence of fluorescence lifetimes for DBPtT. (b) Viscosity dependence of fluorescence lifetimes for TBSxT.

3.4 Conclusions

We have investigated the isomerization characteristics of several thiophene oligomers in order to understand the dependence of oligomer length on the intrinsic disorder in resulting polythiophenes. We find that the inter-ring isomerization barrier is ~8 kcal/mol for rotation in the S_0 state of all oligomers we have examined. This estimation is based on the temperature-dependence of the ^1H NMR resonances for the aromatic protons, and is not derived from a coalescence measurement. For the S_1 DBPtT and TBSxT oligomers, we have determined isomerization barriers of 5.1 ± 0.4 and 5.2 ± 0.4 kcal/mol respectively. These barrier heights are ~1 kcal/mol larger than that found for DBTT, and we rationalize this difference in the context of the longer oligomers being able to support a more quinoid-like excited electronic state. Our findings imply that the small barrier height values we have determined preclude the existence of corresponding long-term order in the polymers synthesized from these materials. The similarities of the isomerization barriers in these two states indicates that there is no significant basis for favoring a photopolymerization scheme over an electrochemical route. We speculate, based on these data that the ground state inter-ring isomerization barrier for poly(thiophene)s are on the order of ~8 kcal/mol plus any additional frictional contribution associated with the motion of associated aliphatic moieties. Thus rotational defects in poly(thiophene)s do not likely contribute significantly to the material properties because any mesoscopic or macroscopic material response is averaged over a large number of rotations of each thiophene ring. If the ground state ring rotations in the polymer can be treated as an activated process, then the time constant for a ring rotation should be on the order of 60 ns. In this limit, extrinsic frictional effects in the solid state polymer will likely

dominate the speed of ring rotation in these materials, but in any event such rotation will be relatively fast.

3.5 Literature Cited

1. Hambir, S. A.; Blanchard, G. J.; Baker, G. L. *J. Chem. Phys.* **1995**, *102*, 2295.

2. Hambir, S. A.; Wolfe, D.; Blanchard, G. J.; Baker, G. L. *J. Am. Chem. Soc.* **1997**, *119*, 7367.

3. Wang, C; Benz, M. E.; LeGoff, E.; Schindler, J. L.; Allbritton-Thomas, J.; Kannewurf, C. R.; Kanatzidis, M. G. *Chem. Mater.* **1994**, *6*, 401.

4. DeWitt, L., Blanchard, G. J.; LeGoff, E.; Benz, M. E.; Liao, J.-H.; Kanatzidis, M. G. *J. Am. Chem. Soc.* **1993**, *115*, 12158.

5. Wang, C.; Benz, M. E.; LeGoff, E.; Schindler, J. L.; Kannewurf, C. R.; Kanatzidis, M. G. *Polym. Preprints* **1993**, *34*, 422.

6. McCullough, R. D.; Lowe, R. D. *J. Chem. Soc., Chem. Commun.* **1992**, 70.

7. Guay, J.; Kasai, P.; Diaz, A.; Wu, R.; Tour, J. M.; Dao, L. H. *Chem. Mater.* **1992**, *4*, 1097.

8. Roncali, J. *Chem. Rev.* **1992**, *92*, 711.

9. Nunzi, J.-M.; Pfeffer, N.; Charra, F. *Chem. Phys. Lett.* **1993**, *215*, 114.

10. Robitaille, L.; Leclerc, M.; Callender, C. L. *Chem. Mater.* **1993**, *5*, 1755.

11. Beljonne, D.; Shuai, Z.; Bredas, J. L. *J. Chem. Phys.* **1993**, *98*, 8819.

12. Thienpont, H.; Rikken, G. L. J. A.; Meijer, E. W.; ten Hoeve, W.; Wynberg, H. *Phys. Rev. Lett.* **1990**, *65*, 2141.

13. Zhao, M.-T.; Singh, B. P.; Prasad, P. N. *J. Chem. Phys.* **1988**, *89*, 5535.

14. Gamaggi, G. M.; Deluca, G.; Tundo, A. *J. Chem. Soc. Perkin II* **1972**, 1594.

15. Jen, K. Y.; Miller, G. G.; Elsenbaumer, R. L. *J. Chem. Soc., Chem. Commun.* **1986**, 1346.

16. Sato, M.; Tanaka, S.; Kaeriyama, K. *J. Chem. Soc., Chem. Commun.* **1986**, 873.

17. Hotta, S.; Rughooputh, S. D. D. V.; Heeger, A. J.; Wudl, F. *Macromolecules* **1987**, *20*, 212.

18. Nowak, M.; Rughooputh, S. D. D. V.; Hotta, S.; Heeger, A. J. *Macromolecules* **1987**, *20*, 965.

19. Rughooputh, S. D. D. V.; Nowak, M.; Hotta, S.; Heeger, A. J.; Wudl, F. *Synth. Met.* **1987**, *21*, 41.

20. Rugooputh, S. D. D. V.; Hotta, S.; Heeger, A. J.; Wudl, F. *J. Polym. Sci. Polym. Phys.* **1987**, *25*, 1071.

21. McCullough, R. D.; Tristam-Nagle, S.; Williams, S. P.; Lowe, R. D.; Jayaraman, M. *J. Am. Chem. Soc.* **1993**, *115*, 4910.

22. Tour, J. M.; Wu, R. *Macromolecules* **1992**, *25*, 1901.

23. Benz, M. E.; Ph.D. Thesis, Michigan State University, East Lansing, MI 1992.

24. Dewar, M. J. S.; Zoebisch, E. G.; Healy, E. F.; Stewart, J. J. P. *J. Am. Chem. Soc.* **1985**, *107*, 3902.

25. Dewar, M. J. S.; Dieter, K. M. *J. Am. Chem. Soc.* **1986**, *108*, 8075.

26. Stewart, J. J. P. *Comput.-Aided Mol. Des.* **1990**, *4*, 1.

27. Dewar, M. J. S.; Thiel, W. *J. Am. Chem. Soc.* **1977**, *99*, 4899.

28. Dewar, M. J. S.; Thiel, W. *J. Am. Chem. Soc.* **1977**, *99*, 4907.

29. Liao, J.-H.; Benz, M. E.; LeGoff, E.; Kanatzidis, M. G. *Adv. Mater.* **1994**, *6*, 135.

30. Snyder, S.; Demas, J. N.; Private Communication.

31. Allinger, N. L. *J. Am. Chem. Soc.* **1977**, *99*, 8127.

32. Fraenkel, G.; Carter, R. E.; McLachlan, A.; Richards, J. H. *J. Am. Chem. Soc.* **1960**, *82*, 5846.

33. Cobb, T. B.; Memory, J. D. *J. Chem. Phys.* **1969**, *50*, 4262.

34. Memory, J. D.; Wilson, N. K. *NMR of Aromatic Compounds*, John Wiley and Sons, New York, 1982.

35. Pauling, L. *J. Chem. Phys.* **1936**, *4*, 673.

36. Bernstein, H. J.; Schneider, W. G.; Pople, J. A. *Proc. Royal. Soc.* **1956**, *A236*, 515.

37. Musher, J. I. *J. Chem. Phys.* **1962**, *37*, 34.

38. Bonacic-Koutecky, V. *J. Am. Chem. Soc.* **1978**, *100*, 396.

39. Salem, L. *Acc. Chem. Res.* **1979**, *12*, 87.

40. Malrieu, J. P. *Theo. Chim. Acta* **1981**, *59*, 251.

41. Lam, B.; Johnson, R. P. *J. Am. Chem. Soc.* **1983**, *105*, 7479.

42. Rulliere, C. *Chem. Phys. Lett.* **1976**, *43*, 303.

43. Awad, M. M.; McCarthy, P. K.; Blanchard, G. J. *J. Phys. Chem.* **1994**, *98*, 1454.

Chapter 4

Dynamics Within a Single Molecular Layer. Aggregation, Relaxation and the Absence of Motion

Summary

We report on the transient and steady state optical responses of the chromophore 2,2'-bithiophene-5,5'-diylbis(phosphonic acid) (BDP) incorporated within a single zirconium phosphonate layer as a function of chromophore density. While the dilute solution optical response of BDP reveals no anomalous behavior, its characteristics are substantially different when confined within a monolayer. We vary the concentrations of layer constituents to determine the extent of interaction between BDP moieties within a single monolayer. We observe limited initial aggregation of BDP, the extent of which is determined largely by the conditions under which the monolayer is formed. Over time, the fractional contribution of BDP aggregates to the total optical response decreases to a limiting value, implicating surface adsorption site density as the dominant factor in determining the morphology of the organobisphosphonate layer. Motional relaxation measurements of BDP within the layer show that the chromophores are immobile on the hundreds-of-picoseconds time scale of our experiments.

4.1 Introduction

In this chapter, we consider intra-layer relaxation processes of MP monolayers from a fundamental perspective using 2,2'-bithiophene-5,5'-diylbis(phosphonic acid) (BDP, Figure 4.1) as the chromophore. To gain the information of interest here, we vary the concentration of the chromophore within a Zr-phosphonate (ZP) monolayer. An optically inactive component can be used either for spacing between chromophore layers or for dilution of the chromophore within layers. In these experiments, we dilute the chromophore within a single layer using 1,6-hexane diylbis(phosphonic acid). (HBPA) This spacer molecule, in its all-*trans* form, is approximately the same length as the chromophore, so that the thickness of the monolayer is uniform. (Figure 4.1). We discuss below the extent of synthetic control we have over the composition of an individual layer, the steady-state optical response of BDP, and how it is related to the measured dynamical relaxation processes operating within the layer. Our data indicate that both aggregated and non-aggregated forms of the chromophore exist within a monolayer, and that the relative amount of each is determined primarily by the silanized site density of the surface and not simply by the chromophore density.

4.2 Experimental

Synthesis of Bisphosphonates. 2,2'-Bithiophene-5,5'-diylbis(phosphonic acid) (BDP) was synthesized by modification of a published procedure on a longer (α,ω)-bisphosphonated thiophene oligomer, as reported in Chapter 2. Briefly, bithiophene was phosphorylated at both termini by lithium coupling to a phosphochloridate, followed by acid hydrolysis. The synthesis of 1,6-hexanediylbis(phosphonic acid) (HBPA) is also

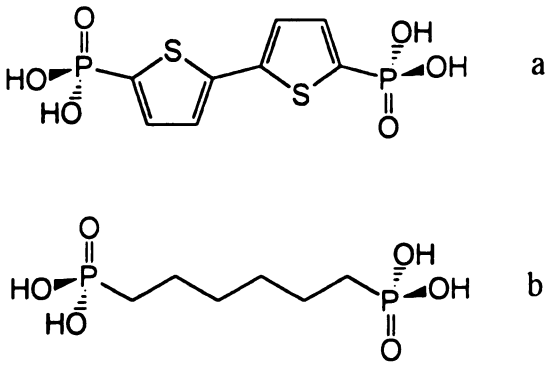

Figure 4.1 Structures of bisphosphonates used in this work. (a) 2,2'-Bithiophene-5,5'-diylbis(phosphonic acid) (BDP) and (b) 1,6-hexane diylbis(phosphonic acid) (HBPA).

reported in Chapter 2. HBPA was synthesized from 1,6-dibromohexane by the Michaelis-Arbuzov reaction, followed by acid hydrolysis.

Metal-Phosphonate Multilayer Synthesis. Silica substrates, cut from quartz slides, were cleaned by immersion in piranha solution (1 H_2O_2:3 H_2SO_4) for 15 minutes, rinsed with distilled water, and dried under a N_2 stream. The substrate surface was silanized by refluxing in 1% v/v (3-aminopropyl) triethoxysilane in anhydrous octane under Ar atmosphere for 10 minutes, followed by thorough rinsing with reagent grade *n*-hexane. This amine primer layer was derivatized to the phosphonate by reaction with 100 mM $POCl_3$ and 100 mM collidine in anhydrous acetonitrile under Ar for 1 hour and rinsed with solvent grade acetonitrile. The phosphonic acid surface was zirconated overnight with a 5 mM solution of $ZrOCl_2$ in 60% EtOH/H_2O. Subsequent layers were added by sequential reaction with bisphosphonate (1.25 mM in 95% EtOH, three hours at 55 °C) and zirconium (5 mM in 60% EtOH, 30 minutes) solutions, with extensive rinsing (H_2O) between each step. The pH of the solutions was maintained between 2 and 4.

Steady-State Optical Spectroscopy. The absorption spectra of BDP monolayers were measured using a Hitachi U-4001 UV-visible spectrophotometer. The samples were held vertically in place at 45° with respect to the incident beam and were collected with 5 nm spectral resolution. The emission spectra of the monolayers and solutions were collected using a Hitachi F-4500 fluorescence spectrophotometer. Monolayer samples were excited at 320 nm through a 10 nm slit. The emission bandpass was adjusted according to spectral intensity. The samples were held vertically, at 45° with respect to the excitation beam propagation in such a way as to minimize reflection of excitation radiation into the emission collection optics.

Time Correlated Single Photon Counting Spectroscopy. The spectrometer we used for the fluorescence dynamics measurements of BDP solutions and monolayers is described in detail in Chapter 3, and we present here only a brief overview of the system. The light pulses used to excite the sample are generated with a cavity-dumped, synchronously pumped dye laser (Coherent 702-2) excited by the second harmonic of the output of a mode-locked CW Nd:YAG laser (Quantronix 416). All samples were excited at 320 nm (Kiton Red, Exciton; $LiIO_3$ Type I SHG). Monolayer samples were held approximately horizontally, with 5° tilts away from horizontal in two directions: toward the excitation beam and toward the detector. Fluorescence from the sample was imaged through a reflecting microscope objective. Lifetimes were collected across the emission bands at 54.7° with respect to the excitation polarization for solutions, and without polarization bias for monolayers. Fluorescence was collected at 390 nm (5 nm FWHM bandwidth for solution, 20 nm for monolayers) with polarizations of 0° and 90° for rotational diffusion dynamics measurements on all samples.

Data Analysis. The lifetimes we report here were fit to sums of exponentials using Microcal Origin v. 4.1 software , and are reported as the values and uncertainties of the fit to individual decays. Rotational diffusion information for solution measurements is reported as the average of six data sets with their associated 95% confidence limit uncertainty. For monolayers, eight pairs of alternating parallel and perpendicular scans were used to produce an average anisotropy function. R(0) was determined to ± 0.01 by regression of data at times after the instrument response, and several data sets were averaged for each sample.

Calculations. Semiempirical calculations[1-5] were performed using Hyperchem Release 4.0 (Hypercube, Inc.) on an IBM compatible PC (Gateway 2000 P5-120). The PM3 parametrization, used for these calculations, is a modification of the AM1 parametrization that treats molecules containing heteroatoms, such as sulfur, more accurately than previous parametrizations. An initial optimization of the structure was performed using a molecular mechanics routine (MM+)[6] followed by geometry optimization at the semiempirical level using an SCF algorithm. The torsion of the 2,5' BDP σ bond was set at 10° increments, and semiempirical optimization was performed until the lowest energy conformation for the fixed inter-ring bond torsion was attained. The heat of formation and $S_0 \leftrightarrow S_1$ transition energy were calculated for each geometrically optimized conformation.

4.3 Results and Discussion

We are concerned with understanding the optical response of (α,ω)-bisphosphonated chromophores, specifically oligomeric thiophene derivatives, as constituents of metal-phosphonate multilayer structures. As discussed above, the structural regularity attainable in these systems allows for the selective examination of intermolecular interactions between layers and within layers. Our initial work in this area focuses on the simplest case, that of a single layer containing a variable chromophore density. We want to discern, ultimately, how intermolecular interactions and photophysical processes within one layer will affect the optical response of, and relaxation dynamics within, more complex layered structures.

There are several factors that can, in principle, contribute to the optical response of this system. One factor is the stoichiometry of the monolayer deposition, which we can determine using UV-visible absorption spectrometry. The spontaneous emission response of the monolayer is also a rich source of information on how the components of the monolayer are assembled and how they interact. Fluorescence lifetime and reorientation dynamics data obtained using transient emission spectroscopy provide insight into the local environment(s) of the chromophores within a monolayer. Semiempirical calculations performed on the chromophore aid in our interpretation of the experimental data and thus our understanding of monolayer properties. We consider in the following sections each of these aspects in the characterization of mixed ZP monolayers.

Stoichiometry of Monolayer Formation. Little is known about the competition between different bisphosphonates for active metal ion sites. There is some evidence that the formation of different mixed monolayers does not follow the stoichiometry of the solution from which they are formed precisely,[7] and thus we need to determine whether or not such is the case for the BDP/HBPA system. In addition to complications arising from competition for binding sites, the stoichiometry of a multi-component deposition solution may not be reflective of the resulting monolayer concentration if solution phase aggregation of one or more of the constituents is occurring. For these reasons, it is important to establish a direct means of calibration for this particular system. To study the deposition stoichiometry of mixed monolayers relative to the solution from which they are formed, we varied the proportions of the chromophore (BDP) and the optically inactive component (HBPA) in ethanol solution and compared these data to absorbance measurements of the resulting monolayers. The total concentration of bisphosphonates

(BDP + HBPA) in the deposition solutions was 1.25 mM, with the concentration of BDP fixed in increments from 1.25 mM (100%) to 0.0125 mM (1%). The absorption spectra of the resulting monolayers are shown in Figure 4.2. These data are background subtracted using a separate primed and zirconated substrate as the background (Figure 4.2 inset). This background spectrum is identical to that of a pure HPBA monolayer. The raw spectra exhibit a slight sample-to-sample variation in absorbance baseline, which can be attributed to slight absorptive differences between individual quartz substrates and positioning of the sample in the instrument. To correct for this baseline variation, the absorbances reported in Figure 4.3 are the differences between the absorbance at λ_{max} and the interpolated baseline. A linear regression fits the data well, indicating that there is a direct relationship between the deposition stoichiometry and the fractional concentrations of the components present in the deposition solution. These data reveal that the correspondence between solution composition and monolayer composition is not one-to-one. Beer's law requires there to be no residual sample absorption at [BDP] = 0, and the experimental background corrected data produce a linear regression to a measurable absorbance. Clearly for [BDP] = 0, A_{BDP} = 0, and the regression to a nonzero intercept implies that monolayer composition is offset from solution composition. In other words, for low fractional BDP concentrations (<1%), the relationship between solution and monolayer composition is curvilinear. From these data we can establishing a working relationship between solution and layer composition that is straightforward. For monolayer formation where BDP is the only phosphonate containing constituent in the deposition solution, we assert that a limiting layer of the chromophore is present, and we know experimentally that a pure HBPA monolayer represents a zero-absorbance

condition. We further assert that Beer's Law holds for this system so that the absorbance of monolayers formed from mixed solutions is indicative of the chromophore concentration. For high fractional chromophore coverage, a direct correspondence between solution and monolayer composition is recovered, but for lower fractional coverage, we find significant preference for adsorption of BDP compared to HBPA (Table 4.1).

Table 4.1 Comparison of fractional BDP concentrations in deposition solution and in the resulting monolayer, determined according to absorbance.

% BDP in deposition solution	% BDP in monolayer
100	100
50	58
10	34
5	29
1	26

This is not an unexpected result. For many ionic association processes, the formation constant of the complex depends sensitively on the identity of the species involved, and there is no reason to expect that not to be the case here. This result is observed, at least in part, because there is a ~25 fold stoichiometric excess of BDP relative to the number of substrate active sites (~1.5×10^{15}) for the 1% BDP deposition solution. This ratio correlates remarkably well with the observed monolayer concentration for this solvent system. We expect that it would be possible to achieve lower fractional coverages of the SiO_x surface by using smaller absolute amounts of BDP in the deposition solution, and we recognize that the relative efficiency of adsorption of both species will be determined by

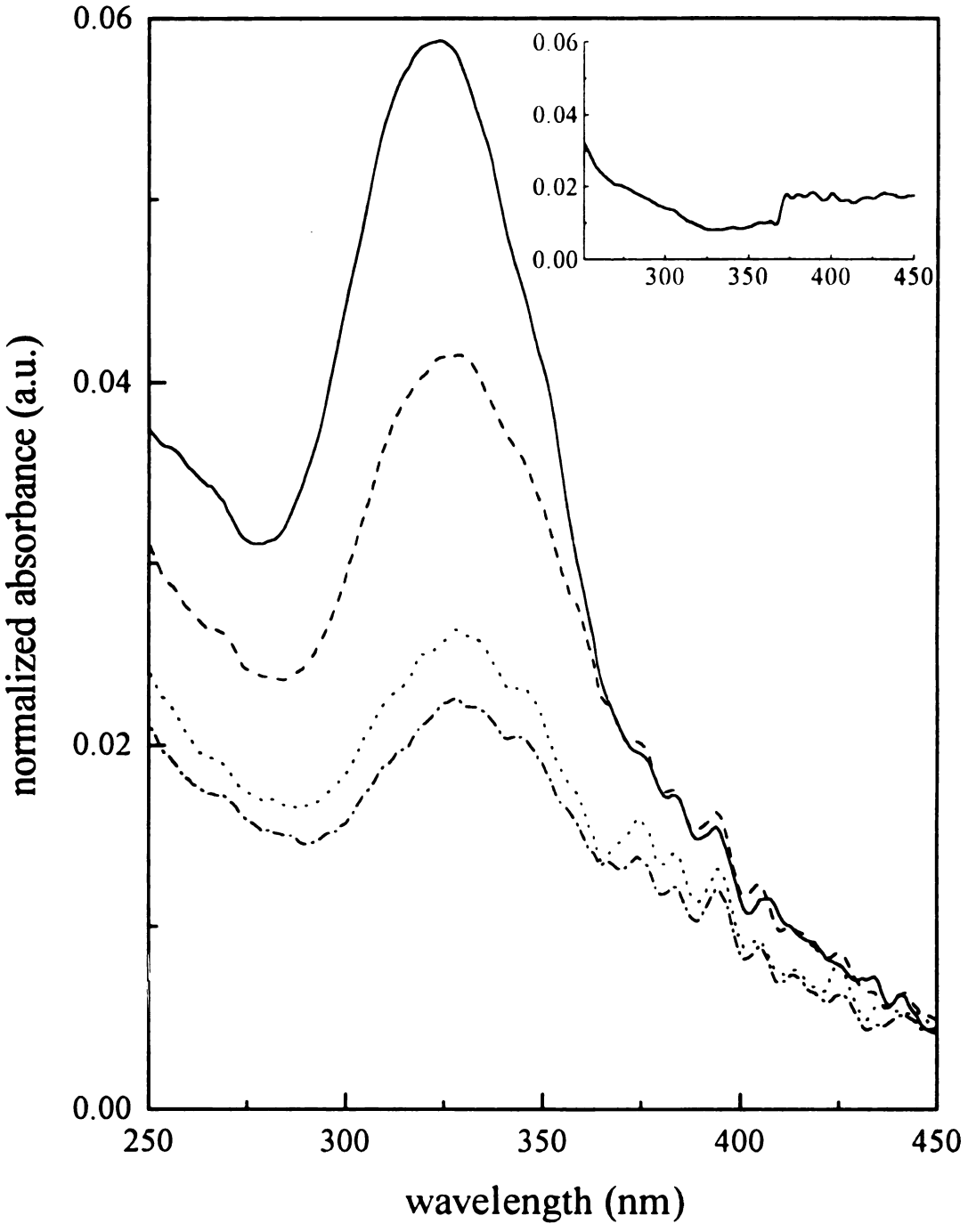

Figure 4.2 Background corrected absorbance spectra of BDP monolayers: (——) 100%; (- - - -) 58%; (· · · ·) 34%; (· - · - ·)26%. Inset: Background spectrum.

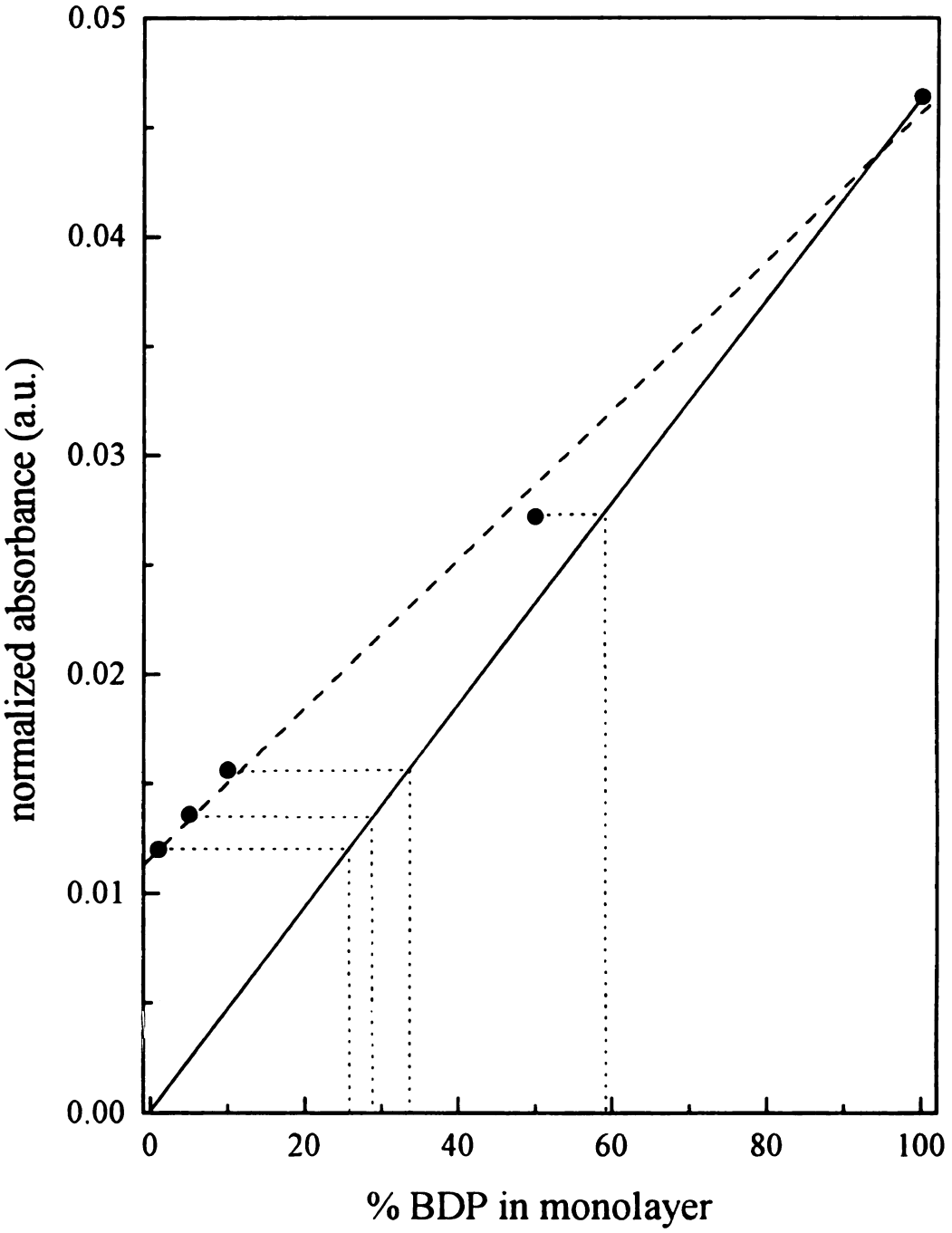

Figure 4.3 Dependence of monolayer absorbance on concentration of BDP in deposition solution. Solid line: Beer's Law predicted dependence, dashed line: Regression of experimental data.

the solvent system.

The monolayer emission intensities varied with each sample, but did not follow any trend, suggesting that the quantum efficiency of the monolayer samples is related to some factor(s) in addition to the amount of chromophore present. Part of the variation, again, may be due to inconsistency in the positioning of the sample. The relatively complicated behavior of the emission response for this system is also not a surprising result, and the details of this complexity contain useful chemical information as we will discuss below.

Monolayer Composition. The dilute solution behavior of BDP is typical of a simple chromophore. Its absorption and emission spectra have well-defined bands, and it exhibits a single exponential fluorescence intensity decay in time. With monolayer samples, a double exponential decay is observed, with a fast component that is the same as the solution lifetime, ~200 ps, and a slow component, ~1 ns, as shown in Figure 4.4. This decay functionality is observed for all monolayer samples, and the time constants recovered for each component are the same over the entire concentration range studied, as shown in Figures 4.5a and b. We observe that, as we collect lifetime data at several wavelengths within the BDP emission band, the form of the decay changes, as indicated Figure 4.6. Fitting these data recovers the same two time constants, but the fractional contribution of each decay component varies as a function of the wavelength at which the data are collected. Specifically, the relative contribution of the longer lifetime increases on the red side of the emission band for all samples. (See Figures 4.7a and b).

Such behavior has been observed previously for different chromophores imbedded in ZP layers, although its origin was not determined.[8] One explanation for the existence of two lifetime components in these monolayers is the interaction of the chromophore with

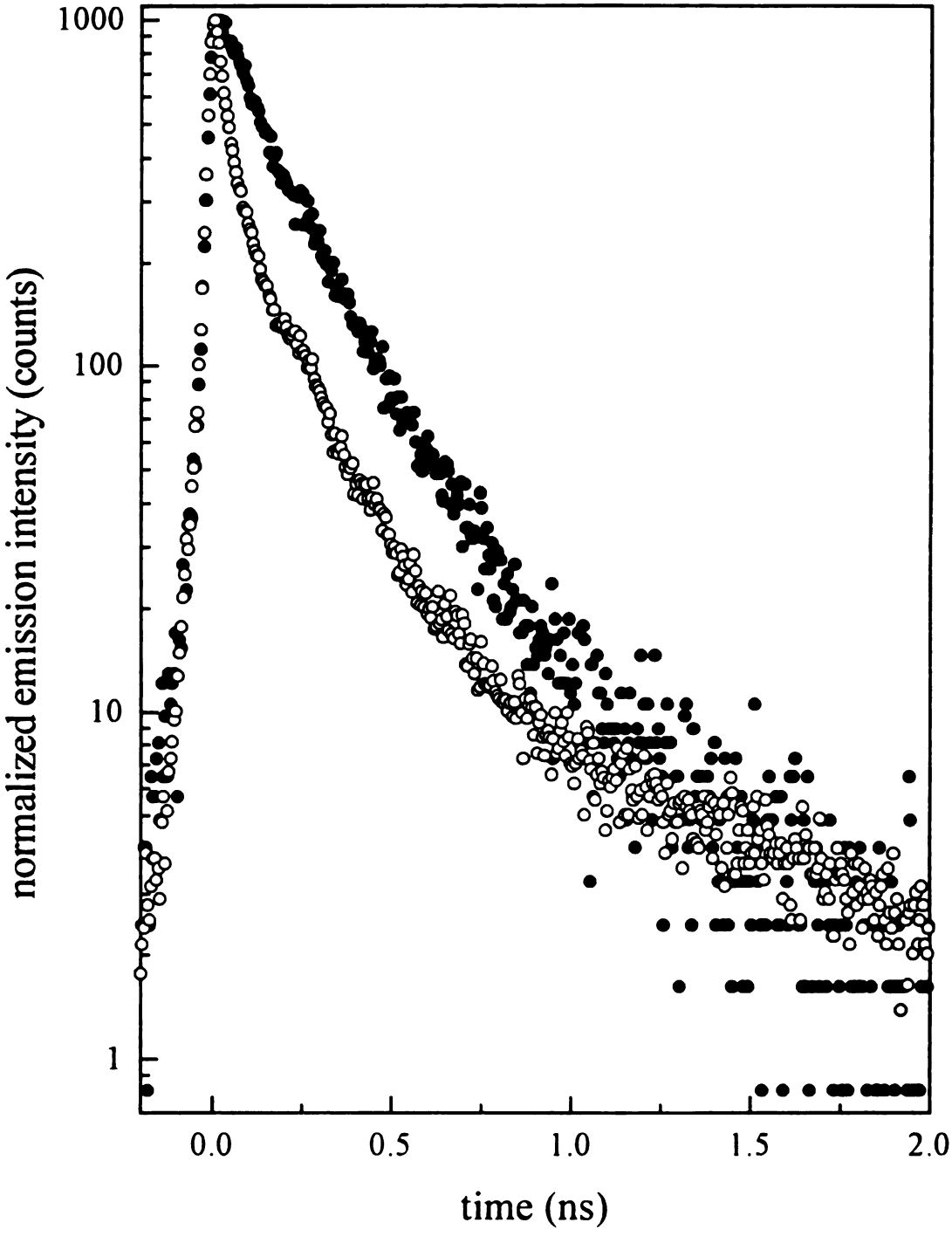

Figure 4.4 Representative fluorescence lifetimes of (●) 10^{-6} M BDP solution and (○) 26 % BDP/HBPA monolayer collected at 390 nm.

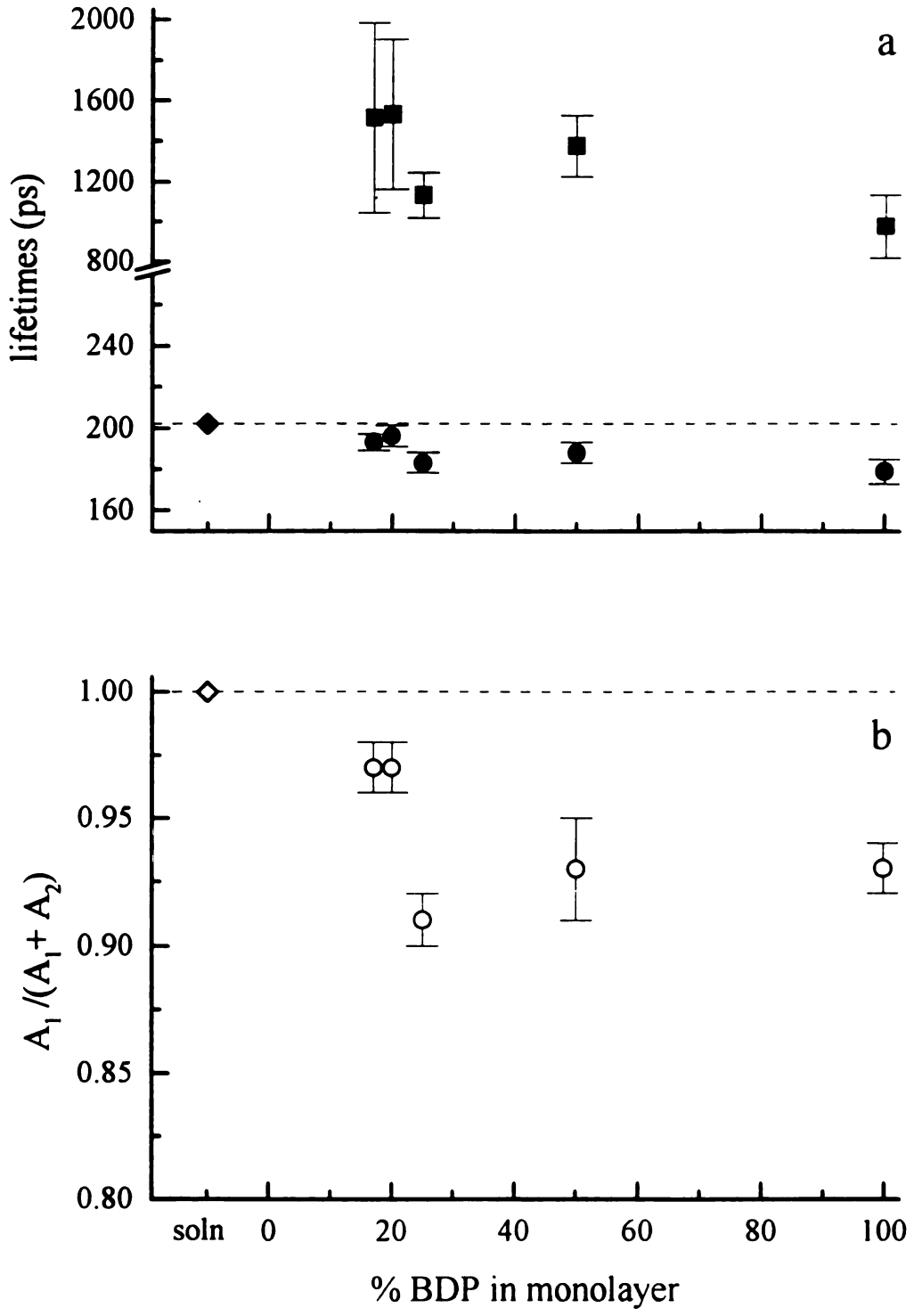

Figure 4.5 (a) Fluorescence lifetimes of BDP monolayers and solution at 400 nm. The data were fit to the function $f(t) = A_1\exp(-t/\tau_1) + A_2\exp(-t/\tau_2)$. (b) Normalized prefactors of fast exponential decay component for data taken at 400 nm.

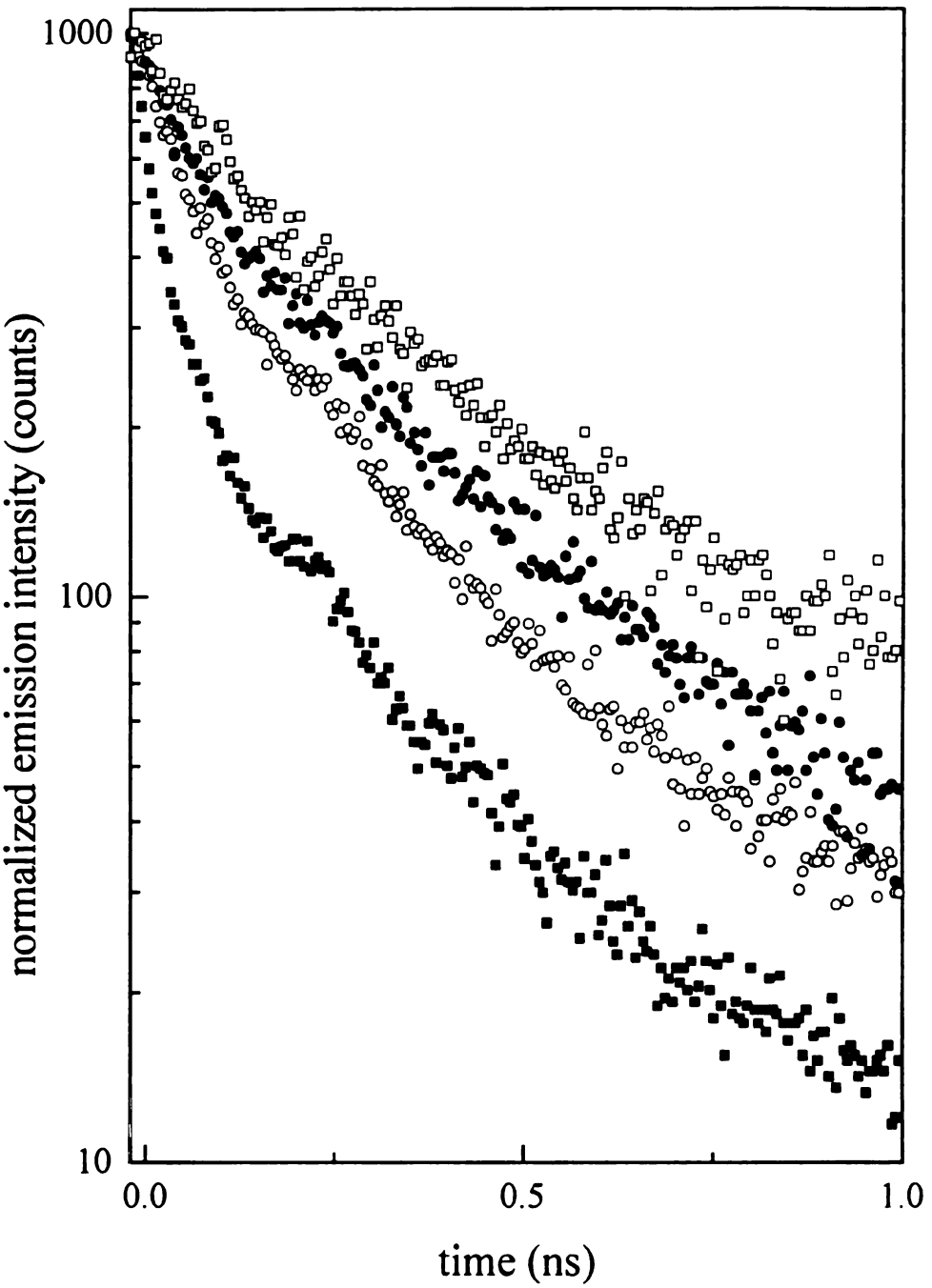

Figure 4.6 Fluorescence lifetime decays of BDP monolayers at (■) 390 nm, (○) 475 nm, (●) 525 nm, and (□) 575 nm.

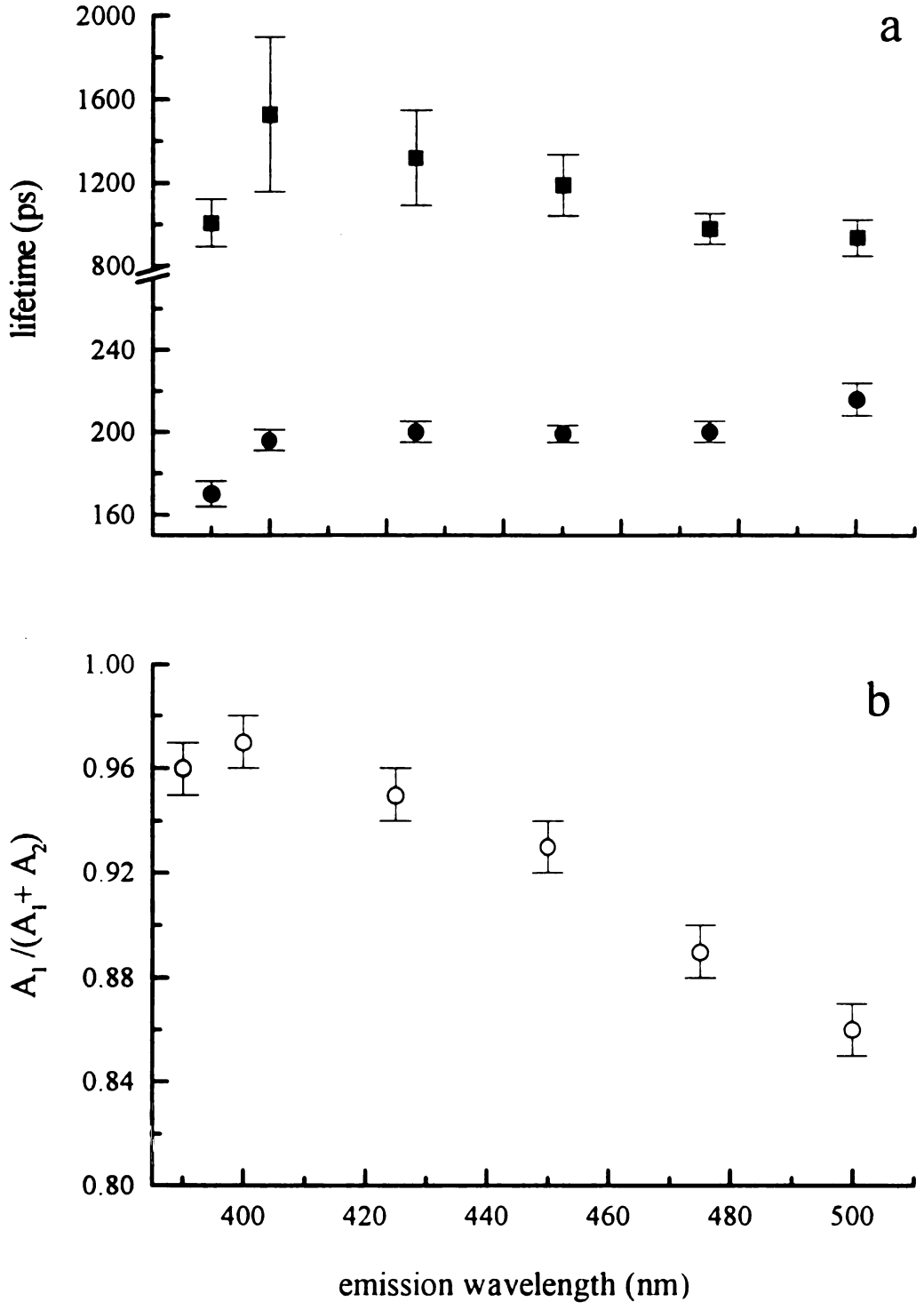

Figure 4.7 Emission wavelength dependence of (a) lifetimes and (b) Normalized fast exponential prefactors for 29% BDP monolayer.

active hydroxyl sites on the silica surface. Wang and Harris found similar lifetime behavior for pyrene on silica, and determined that it was due to the existence of two distinguishable active silanol sites on the surface.[9] To explore the possible role of chromophore-substrate interactions, we synthesized a multilayer structure with a ~26% BDP layer spaced away from the SiO_x surface by three HBPA layers. This structural motif prevents the chromophore from interacting with the surface. The same lifetime measurements were made, and the results were identical to those of the monolayers that were not isolated from the substrate, indicating that the presence of the second lifetime component is not the result of a single chromophore interacting with different silica sites on the same surface.

We consider next the possibility that we are observing emission from an aggregate or excimer moiety that forms at short intermolecular spacings, such as are found in a monolayer. Aggregation has been observed for several molecules, such as pyrene, which is known to form excimers in concentrated solutions and at solid interfaces.[10] The steady state emission spectra of the monolayer samples are consonant with this explanation, as we find two distinct classes of spectra; one which has been observed at all chromophore concentrations and is similar to the dilute solution spectrum, and one seen for chromophore monolayer concentrations above 34%. (See Figures 4.8a and b). This latter feature, which we designate as the aggregate spectrum, is broader and red shifted by about 50 nm from the dilute solution, or monomer, spectrum. The intensity of the monomer emission spectrum is several times that of the aggregate spectrum, although quantitative intensity comparisons are difficult. We observe both monomer and aggregate peaks in the 100% BDP (1.25 mM) deposition solution, implying that the resulting monolayer will be comprised of both monomer and aggregate, with the ratio of the two forms being

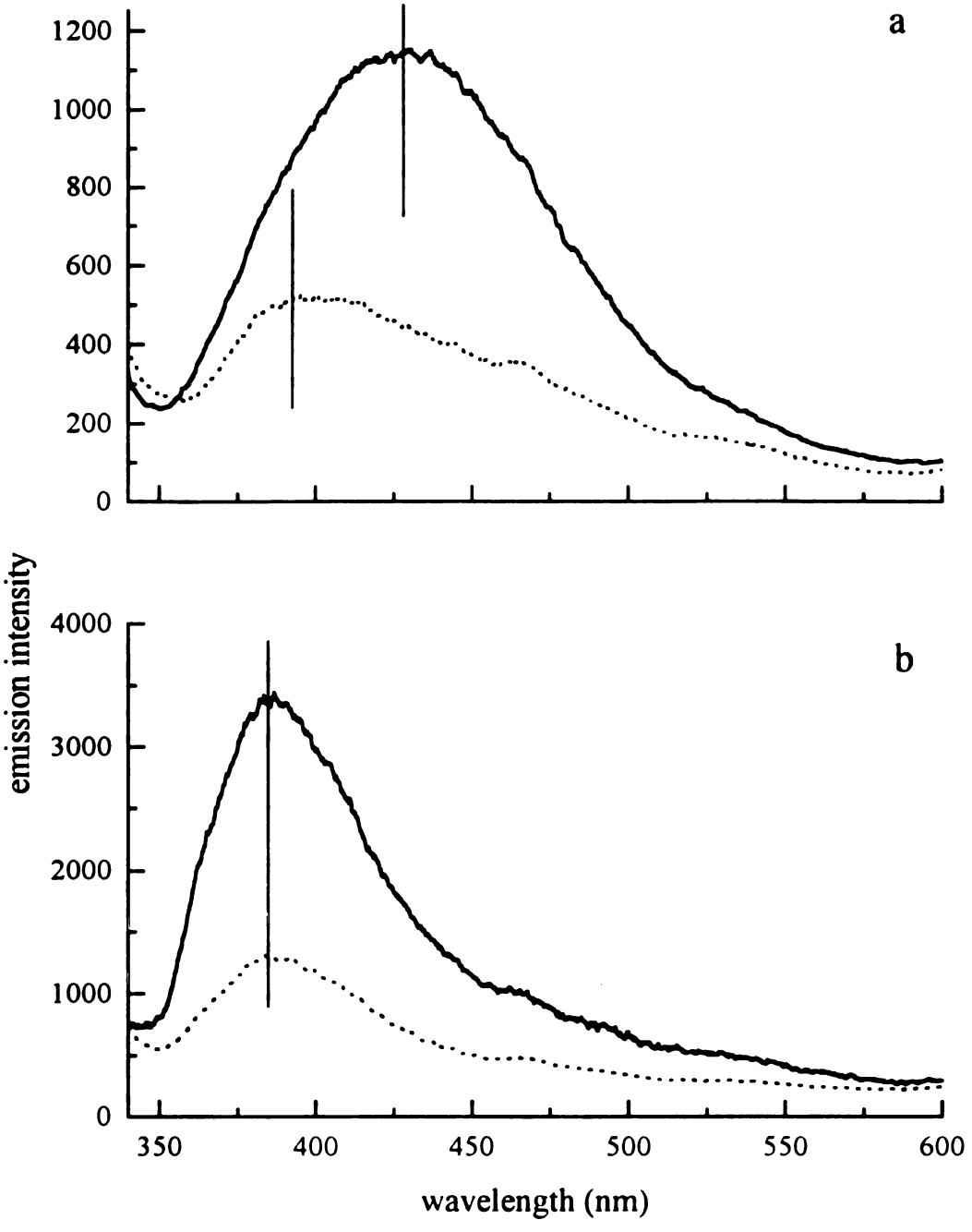

Figure 4.8 Emission spectra of fresh samples (solid lines) and aged (two-months) samples (dashed lines) for (a) aggregate-like and (b) monomer-like samples. The vertical lines are guides for the eye to the band maxima.

determined, at least initially, by their deposition kinetics. We note that, occasionally, a monolayer synthesized from concentrated BDP solution yields a monomer-like spectrum, which we believe is due to incomplete monolayer formation.

The monolayer aggregate spectra anneal over time to more monomer-like spectra, but samples that were characterized initially by a monomer-like emission response stayed the same except for diminution of intensity, as seen in Figure 4.8. There is evidence in the literature that the packing density of the organic portions of the ZP structures is mediated by the lateral spacing of the inorganic inter-layer linking functionalities.[11-13] The ZP lattice has been shown to cause disorder in layers because the spacing it enforces is larger than the molecular area of most organic moieties.[14,15] This means that the spacing between individual chromophores may be larger than the intermolecular distance that is optimum for aggregate formation, so that, even if the chromophores are deposited onto the surface as pairs, they are likely to separate over time, giving rise to the spectral "annealing" we observe. This finding is fully consistent with our FTIR data on HBPA monolayers on SiO_x (see Chapter 2) indicating some structural heterogeneity within the layer. Also, we detect an apparent photodegradation of the chromophores within the layer (Figure 4.8a) which may indicate that the aggregates, as well as the monomer, are being destroyed, resulting in a sample with a higher proportion of monomer and a spectrum reflecting that change.

We expect that, based on the ionic nature of the metal-phosphonate bond(s), surface dissociation and diffusion will play a role in achieving the annealed condition for these layers. Our linear response data, however, do not provide significant insight into the role of diffusion for this system. If bound BDP aggregation was mediated by surface

diffusion, we would observe aggregate-like absorption spectra in proportion to the surface concentration of the BDP for the annealed layers. Instead, we observe that the stable long-term condition for these films is in the form of monomeric chromophores, regardless of the initial BDP concentration. While the implications of these data remain to be explored more completely, it is clear that, for this system, surface diffusion is not the only process at work in determining the absorption properties of these films.

The existence of two measurably different spectra based on two chromophore species can be understood from a structural perspective with the aid of semiempirical calculations. We calculated the inter-ring rotational energy barriers for both the ground state and the first singlet excited state of BDP, as shown in Figure 4.9. The S_0 potential energy surface is essentially independent of thiophene inter-ring torsion angle, with rotational barriers of less than 1 kcal/mol. However, the S_1 surface has 12 kcal/mol barriers at 90° and 270° (rings perpendicular). The energetic minima occur at 0°, the *anti* conformer, and 180°, the *syn* conformer, where the molecule can adopt a quinoid-like S_1 resonance structure. In a system where there is freedom of motion, such as in solution, the conformational distribution of the chromophore is unbiased with respect to inter-ring rotation prior to excitation. Upon excitation, the conformational distribution of BDP is biased toward the S_1 minima, where the molecules take on the planar, quinoidal structure. Planar BDP chromophore pairs are more likely to aggregate than non-planar species if they are in close proximity, by a dipole coupling mechanism. In a monolayer, we expect different behavior, because the chromophores are not able to rotate freely (*vide infra*). In the monomer limit within a monolayer, chromophores are spaced such that the probability of intermolecular interactions between chromophores is low, so the chromophores are

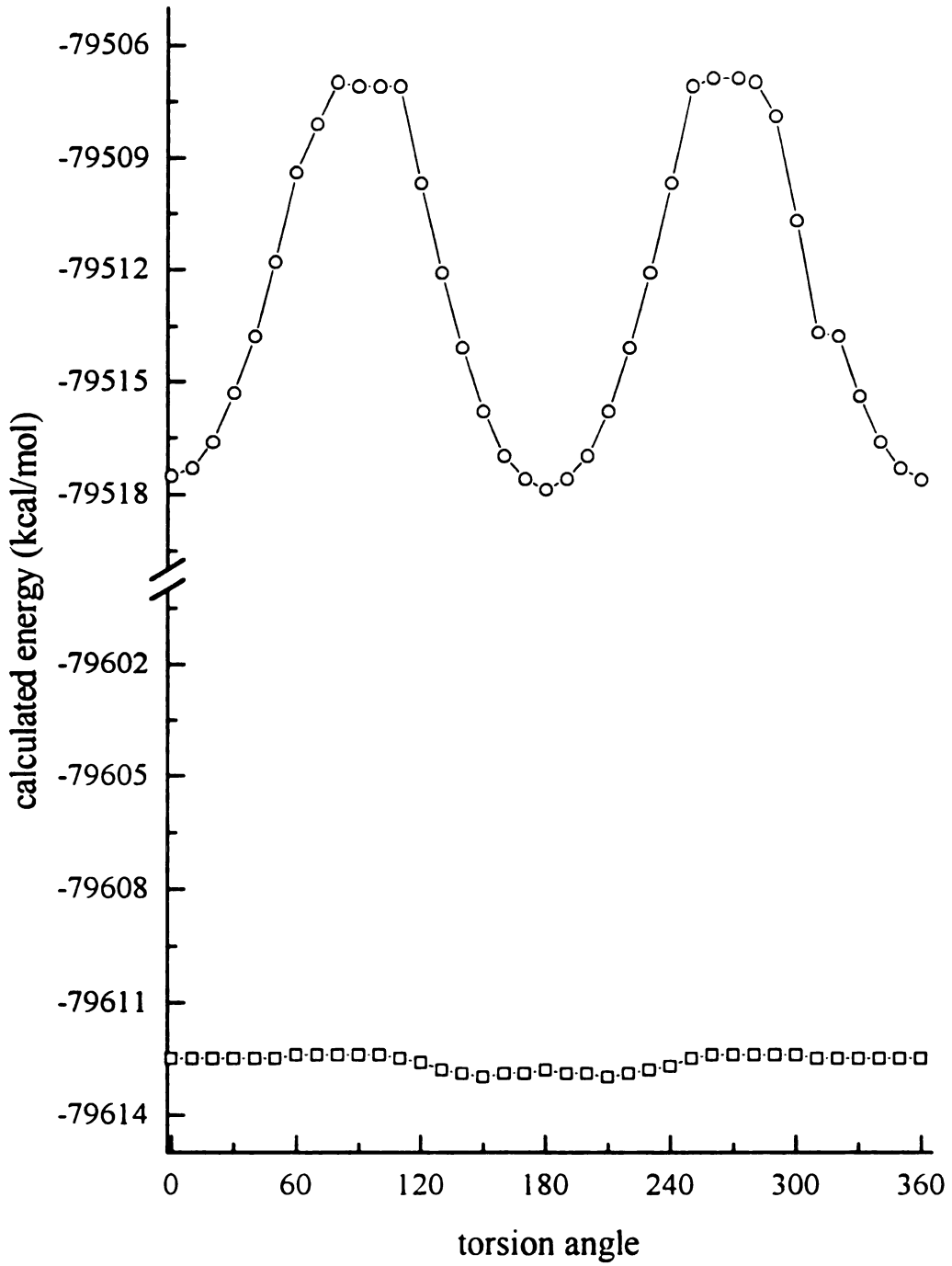

Figure 4.9 Calculated rotational energy barriers for BDP: (□) S_0 and (○) S_1.

excited from an average of all conformations, resulting in an emission spectrum with a distribution of energies skewed to high energies by S_1 emission contributions from twisted conformers. In more concentrated monolayers, chromophores are likely to be close enough to allow interaction which would serve to fix the molecules in more planar conformations, and resulting in the lower energy spectrum. In addition, aggregation is expected to yield a spectral red shift, as is seen for the pyrene excimer.[10]

Rotational Dynamics. The rotational dynamics of the chromophores within a monolayer are an information-rich component of the optical response. Molecular reorientation measurements are well established as sensitive indicators of intermolecular interactions.[16-21] Most rotational diffusion measurements are performed on probe molecules in solution, where the orientational distribution of the chromophore can be completely random while for a (partial or complete) monolayer of the same molecule, we expect its motional freedom to be constrained both by surface attachment and by interactions with neighboring molecules. For such a system, the hindered rotor model is appropriate for interpreting anisotropy data.[22,23] In this model, the surface-bound probe molecule is confined to a cone of rotation, where the base of the cone is defined by the attachment point of the probe to the surface and the cone semiangle is designated as θ_0. The optical and geometric properties of the tethered probe molecule also affect the form of the experimental signal. We select a non-random orientational distribution of chromophores within the monolayer with a laser pulse and monitor the change in emission intensity as a function of time following excitation. This measurement is made for emission signals polarized parallel and perpendicular to the excitation polarization and

these data are combined to produce the induced orientational anisotropy function, R(t), (Figure 4.10)

$$R(t) = \frac{I_{\parallel}(t) - I_{\perp}(t)}{I_{\parallel}(t) + 2I_{\perp}(t)} \qquad [4.1]$$

The function R(t) is related to the properties of the probe molecule through[23]

$$R(t) = \tfrac{2}{5} P_2(\cos\delta)\left\langle P_2\left[\mu(0)\cdot\mu^*(t)\right]\right\rangle \qquad [4.2]$$

where δ is the angle between μ and μ^*, the excited and emitting transition moments and P_2 is the second order Legendre polynomial. For the hindered rotor model, it is important to consider two limiting cases, t = 0 and t = ∞. At t = 0, where the second term in Equation 4.2 is unity, the information available from the measurement is determined by the optical properties of the probe molecule and thus we can determine δ directly. For BDP in solution we measure R(0) = 0.24, yielding $\delta = 31° \pm 2°$. At t = ∞, any re-randomization of the chromophores will be complete and the information available from the measurement is related only to the average tilt angle of the chromophore ensemble within the layer according to the hindered rotor model.[23]

$$R(\infty) = \tfrac{2}{5} P_2(\cos\theta_{ex}) P_2(\cos\theta_{em}) \left\langle P_2(\cos\theta)\right\rangle^2 \qquad [4.3]$$

In Equation 4.3, θ_{ex} is the angle of the excited transition moment with respect to the cone center axis, θ_{em} is the emitting transition moment angle with respect to this same axis and θ is the average tilt angle of the chromophore within the cone. The terms for θ_{ex} and θ_{em} are, together, representative of the angle δ, and for simplicity, we take $\theta_{ex} = 0$ and $\theta_{em} = \delta$. From these quantities we can extract the average tilt angle, θ, from the experimental data.

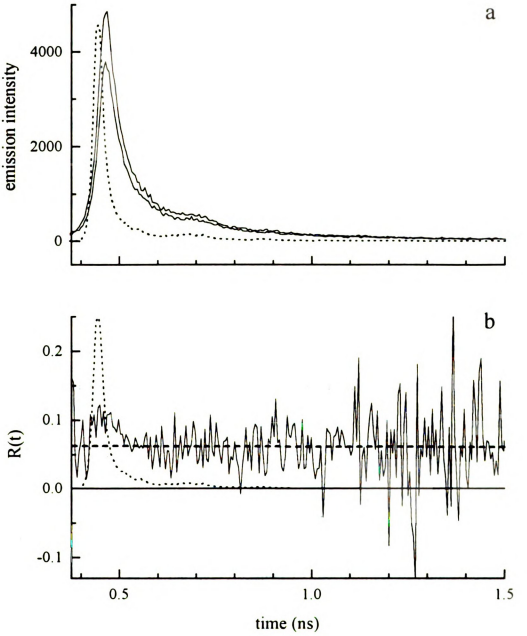

Figure 4.10 Reorientation data for a 26% BDP monolayer. (a) Raw transient signal intensities for emission polarized parallel (upper) and perpendicular (lower) to excitation pulse polarization. Included is the instrumental response function. (b) Induced orientational anisotropy function derived from the data presented in panel (a) and regressed fit.

In the hindered rotor model, there can also be a measurable relaxation associated with the randomization of chromophore orientations within the confining cone, with the time constant of this relaxation being related to the motion of the chromophore about its tether and the semi-angle of the cone. It is evident from the experimental data presented in Figure 4.10 that we do not detect a transient relaxation of the chromophore within the monolayer, once contributions from the instrumental response function are accounted for. This finding is important in and of itself because it implies the rigidity of these systems on a ~nanosecond timescale, and from the infinite time response, we can derive useful information on the average tilt of the chromophore in the cone.

It is fair to question whether the absence of a decay in R(t) is reflective of the absence of dynamics or the presence of unresolved, fast motion. We expect that the motion of BDP in a low viscosity solvent will place a qualitative lower bound on the time constant for any such motion in the monolayer. For BDP in 95% ethanol, the reorientation time we measure, $\tau_{OR} = 299 \pm 41$ ps, is on the same order of magnitude as the monomer lifetime. This reorientation time is significantly slower than would be predicted by the Debye-Stokes-Einstein model[24] in the stick limit[25] (60 ps) and we attribute this difference to partial deprotonation of the terminal phosphonate moieties. Ionic charge will give rise to strong association with the solvent, slowing rotation of the chromophore. In a monolayer, the dynamics are expected to be mediated by attachment of the chromophore to the substrate as well as by dipole-dipole interactions between molecules and by the proximity of its neighbors. We expect that, if the chromophore were to exhibit a dynamical response within the monolayer, it would occur on a timescale at least similar to that seen for BDP in ethanol, if not longer. We believe that the absence of

a measurable decay in R(t) is indicative of a highly rigid environment. We recover the same value for the steady-state anisotropy for all monolayer concentrations studied, as shown in Table 4.2, another indication that the chromophores are unable to randomize on the timescale of the BDP excited state lifetime.

Table 4.2 Dependence of infinite time anisotropy on fractional composition of monolayer.

% BDP	R(∞)
100	0.06 ± 0.01
58	0.05 ± 0.01
34	0.07 ± 0.01
26	0.05 ± 0.01

From the monolayer data, R(∞) = 0.06 ± 0.01, yielding θ = 35° ± 2°. This value for the tilt angle is similar to that recovered for alkane bisphosphonates[126] but, for the BDP chromophores, indicates that organization within the layer is not determined fully by the structure of the (presumably all-*anti*) chromophore, which would suggest a tilt angle of ~17°. It appears that there is either a contribution to the measured tilt angle of BDP from the metal-phosphonate coordination or from intermolecular interactions between the organic functionalities of the bisphosphonate species. Unfortunately, we do not have sufficient knowledge of the surface roughness or active site spacing to resolve this question, especially in light of the several possible coordination numbers of Zr^{4+}.[27]

We can use the rotational dynamics results to clarify some ambiguity about the origin of the aggregates. One explanation for the presence of aggregate is that all of the

chromophore within the layer is initially monomer. Upon excitation, BDP relaxes to its S_1 conformational minima, where it is planar, and if other planar chromophores are in close proximity, they will aggregate. The second possibility is that the chromophore is pre-aligned as aggregates in solution, and is deposited onto the surface as such. We found no evidence of motion in the dynamical data, likely ruling out the possibility that aggregate formation in BDP monolayers is driven by optical excitation. We note also that, if aggregation were mediated by excitation of BDP, then the measured population relaxation dynamics would be more complex than the double exponential decay functionality we recover, and we would expect a chromophore concentration dependence, which we fail to observe. We believe that the deposition of pre-formed aggregates is more likely, based on both the dynamics data and the observation of monomer and aggregate bands in concentrated BDP deposition solution spectra.

4.4 Conclusions

Our initial investigation of the optical response of a chromophore-containing ZP monolayer indicates that these assemblies are ideal for the selective examination of inter-layer and intra-layer energy relaxation phenomena. We have demonstrated control over the concentration of chromophore in the layer, which is limited by the higher affinity of BDP for the metal binding sites. Some degree of aggregation occurs in the BDP monolayers, as verified by the presence of the two species detected with both the steady-state and fluorescence lifetime spectroscopies. The presence of aggregated chromophore does affect the population relaxation dynamics within the monolayer, but in a way that can be monitored. The time constants for the fluorescence decays remain concentration

independent, ~200 ps for the monomer and ~1 ns for the aggregate, although the contribution of each species' lifetime varies across the emission band. The rotational motion data are constant within the chromophore concentration range of 26% to 100% BDP. We find a steady-state anisotropy of ~0.06, consistent with the restrictions of monolayer attachments and interactions, from which we determine an average tilt angle of 35°. The absence of rotational motion demonstrates that the chromophores are in a highly rigid environment on the hundreds of picoseconds timescale of our experiments. This finding will simplify the interpretation of results on interlayer transport within multilayer structures, because the chromophores should be even more restricted in an environment with attachments at both phosphonate functionalities.

4.5 Literature Cited

1. Dewar, M. J. S.; Zoebisch, E. G.; Healy, E. F.; Stewart, J. J. P. *J. Am. Chem. Soc.* **1985**, *107*, 3902.

2. Dewar, M. J. S.; Dieter, K. M. *J. Am. Chem. Soc.* **1986**, *108*, 8075.

3. Stewart, J. J. P. *Comput.-Aided Mol. Des.* **1990**, *4*, 1.

4. Dewar, M. J. S.; Thiel, W. *J. Am. Chem. Soc.* **1977**, *99*, 4899.

5. Dewar, M. J. S.; Thiel, W. *J. Am. Chem. Soc.* **1977**, *99*, 4907.

6. Allinger, N. L. *J. Am. Chem. Soc.* **1977**, *99*, 8127.

7. Rabolt, J. F.; private communication.

8. Katz, H. E.; Bent, S. F.; Wilson, W. L.; Schilling, M. L.; Ungashe, S. *J. Am. Chem. Soc.* **1994**, *116*, 6631.

9. Wang, H.; Harris, J. M. *J. Phys. Chem.* **1995**, *99*, 16999.

10. Berlman, I. B. *Handbook of Fluorescence Spectra of Aromatic Molecules;* Academic Press: New York, 1971.

11. Frey, B. L.; Hanken, D. G.; Corn, R. M. *Langmuir* **1993**, *9*, 1815.

12. Schilling, M. L.; Katz, H. E.; Stein, S. M.; Shane, S. F.; Wilson, W. L.; Buratto, S.; Ungashe, S. B.; Taylor, G. N.; Putvinski, T. M.; Chidsey, C. E. D. *Langmuir* **1993**, *9*, 2156.

13. Cao, G.; Hong, H.-G.; Mallouk, T. E. *Acc. Chem. Res.* **1992**, *25*, 420.

14. Thompson, M. E. *Chem. Mater.* **1994**, *6*, 1168.

15. Bent, S. F.; Schilling, M. L.; Wilson, W. L.; Katz, H. E.; Harris, A. L. *Chem. Mater.* **1994**, *6*, 122.

16. Jiang, Y.; Blanchard, G. J. *J. Phys. Chem.* **1994**, *98*, 6436.

17. Blanchard, G. J. *J. Phys. Chem.* **1991**, *95*, 5293.

18. Blanchard, G. J. *J. Phys. Chem.* **1989**, *93*, 4315.

19. Blanchard, G. J. *Anal. Chem.* **1989**, *61*, 2394.

20. Blanchard, G. J. *J. Phys. Chem.* **1988**, *92*, 6303.

21. Blanchard, G. J.; Cihal, C. A. *J. Phys. Chem.* **1988**, *92*, 5950.

22. Szabo, A. *J. Chem. Phys.* **1984**, *81*, 150.

23. Lipari, G.; Szabo, A. *Biophys. J.* **1980**, *30*, 489.

24. Debye, P. *Polar Molecules;* Chemical Catalog Co.: New York, 1929.

25. Hu, C. M.; Zwanzig, R. *J. Chem. Phys.* **1974**, *60*, 4354.

26. Yang, H. C.; Aoki, A.; Hong, H.-G.; Sacket,, D. G.; Arendt, M. F.; Yau, S.-L.;Bell, C. M.; Mallouk, T. E. *J. Am. Chem. Soc.* **1993**, *115*, 11855.

27. Fay, R. C.; Pinnavaia, T. J. *Inorg. Chem.* **1968**, *7*, 508.

Chapter 5

The Role of Substrate Identity in Determining Monolayer Motional Relaxation Dynamics

Summary

We report on the lifetime and motional dynamics of zirconium phosphonate (ZP) monolayers containing oligothiophene chromophores in a range of concentrations. Monolayers were formed on fused silica substrates and on a 15 Å oxide layer formed on crystalline Si(100) substrates. For both interfaces, the fluorescence lifetime behavior of the chromophores is identical and does not depend on chromophore concentration within the monolayer. Transient anisotropy measurements reveal that, for both substrates, the chromophores are oriented at ~35° with respect to the surface normal. For monolayers formed on silica, there is no evidence for chromophore motion, while motion is seen for monolayers formed on silicon. Despite the substantial similarity between the two families of monolayers, the surface roughness of the primed silicon substrate allows for greater motional freedom of the chromophores in the monolayers. We discuss these findings in the context of the differences in substrate surface roughness and domain sizes as measured by atomic force microscopy (AFM).

5.1 Introduction

Our focus in this Chapter is to understand the energy migration and motional dynamics that occur within an optically active layer. By using simple chromophores, we can observe the presence or absence of excitation transport and motional dynamics without complications associated with large scale chromophore isomerization. We use 2,2'-bithiophene-5,5'-diylbis(phosphonic acid) (BDP) and 2,2':5',2":5",2"'-quaterthiophene-5,5"'-diylbis(phosphonic acid) (QDP) (Figure 5.1) because the BDP emission band overlaps the QDP absorption band, as shown in Figure 1.1. The spectral overlap of the two chromophores is useful for excitation transport studies. These chromophores can photoisomerize via ring rotation and this property is of value in understanding their dynamical response in layered assemblies (*vide infra*).

In these initial studies, we concentrate on the intralayer motional relaxation properties of each chromophore by varying the chromophore concentration in a series of BDP and QDP monolayers. The chromophore concentration is controlled by incorporating optically inactive, alkanebisphosphonate diluents into the monolayer. We chose 1,6-hexanediylbis(phosphonic acid) and 1,12-dodecanediylbis(phosphonic acid) as diluents because, in their all-*trans* conformations, they are approximately the same lengths as BDP and QDP, respectively, enabling us to make the monolayer thickness as uniform as possible, at least on molecular length scales.

We have characterized the chromophore dynamics of a single layer of BDP on fused silica substrates in Chapter 4. In this work, we compare the behavior of QDP to BDP on fused silica and oxidized Si(100) substrates. For BDP on silica, we do not detect

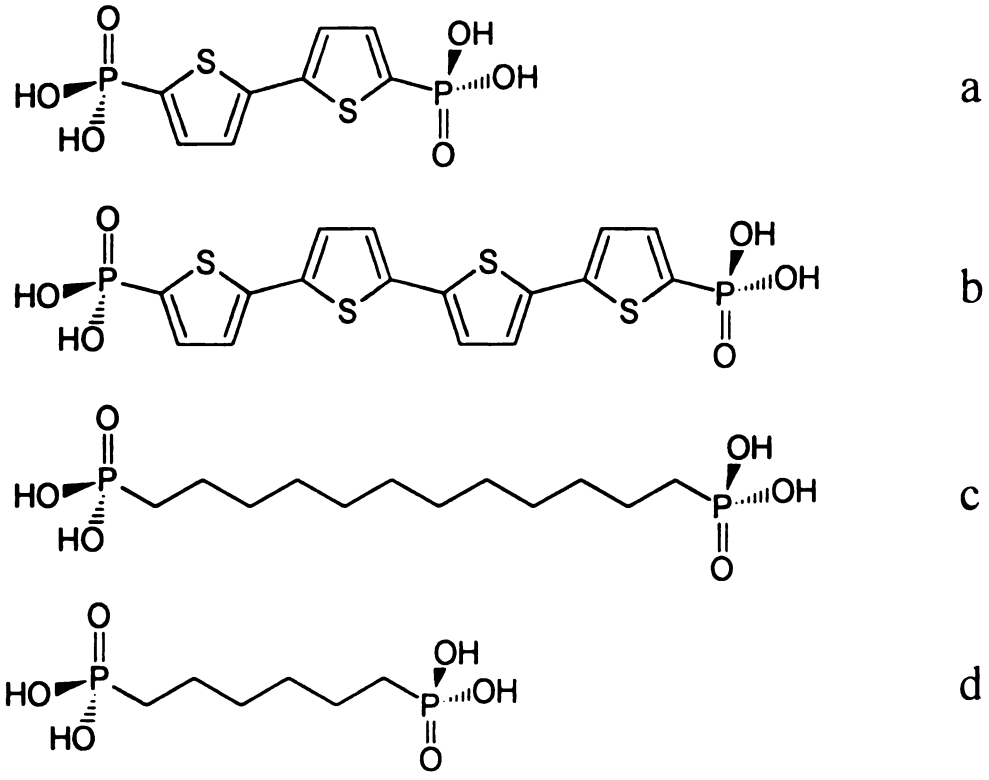

Figure 5.1 Structures of oligobisphosphonates used in this work. (a) 2,2'-bithiophene-5,5'-diylbis(phosphonic acid) (BDP); (b) 2,2':5',2":5",2"'-quaterthiophene-5,5"'-diylbis(phosphonic acid) (QDP); (c) 1,12-dodecanediylbis(phosphonic acid) (DDBPA); (d) 1,6-hexanediylbis(phosphonic acid) (HBPA).

any chromophore rotational motion. The fluorescence dynamics of QDP on silica are essentially the same, as we describe below in more detail.

The identity of the substrate affects the dynamical behavior of the chromophores. The 15 Å oxide layer on Si(100) possesses the same active sites (-OH) as silica, but there are fundamental differences in site density and surface roughness on oxidized silicon that affect the primer density and organization and thus influence the adlayers. The steady-state optical response and the fluorescence lifetime behavior were identical on both substrates, for a given chromophore. We detect chromophore motion on silicon, and this finding suggests substantially different organization and structural freedom in the two systems. The active sites on silica appear to allow a higher chromophore density on the initial phosphonate primer layer than is seen for silicon, giving rise to an improvement in the ordering of the first layers. We present AFM images of the SiO_x substrates that complement the dynamic spectroscopic measurements and demonstrate the differences in surface roughness of the substrates.

5.2 Experimental

Synthesis of 2,2':5',2'':5'',2'''-Quaterthiophene-5,5'''-diylbis(phosphonic acid) (QDP); 2,2'-bithiophene-5,5'diylbis(phosphonic acid) (BDP); 1,12-dodecanediylbis (phosphonic acid) (DDBPA) and 1,6-hexanediylbis(phosphonic acid) (HBPA). The syntheses of these compounds were described in more detail in Chapter 2. Briefly, bithiophene and quaterthiophene were derivatized to the phosphonic acid by lithium coupling to a phosphochloridate, followed by acid hydrolysis. DDBPA and HBPA were

synthesized by the Michaelis-Arbuzov reaction[1] of the corresponding dibromoalkane with triethylphosphite, followed by acid hydrolysis.

Metal-phosphonate multilayer synthesis. Fused silica and polished Si(100) (MultiScanning Plus) substrates were cleaned by piranha solution for 10 minutes and rinsed with flowing distilled water. Samples were dried with a N_2 stream and used shortly after for deposition. The substrates were primed by reflux in a 1% v/v solution of 3-(aminopropyl) triethoxysilane in anhydrous octane for 10 minutes, followed by rinses with hexane and water. After drying with N_2, the amine surface was derivatized to the phosphonate in a solution of 0.1M $POCl_3$ and 0.1M collidine in anhydrous CH_3CN for one hour, followed by rinses with CH_3CN and water. The resulting surface was functionalized with Zr^{4+} by immersion in a 5 mM solution of $ZrOCl_2$ in 60% aqueous ethanol solution for 10 minutes. Monolayers were deposited from bisphosphonate solutions with a total 1 mM concentration ([chromophore] + [alkane] = 1 mM). Alkanebisphosphonate, BDP, and mixed alkanebisphosphonate/BDP solutions were made in 90% EtOH (*aq*); QDP and mixed alkanebisphosphonate/QDP were made in 80% DMSO, 20% (90% EtOH (*aq*)). The substrates were immersed in the appropriate bisphosphonate solution for 4 hours at 55°C.

Steady-state optical spectroscopy. The absorbance spectra of oligothiophene chromophores in solution and on surfaces were measured using a Hitachi U-4001 UV-visible spectrophotometer. Monolayer samples were held vertically in place at a 45° angle with respect to the incident beam. Spectra were collected with 5 nm resolution. Fluorescence spectra of solutions were measured on a Hitachi F-4500 fluorescence spectrophotometer. Excitation and emission slits were adjusted according to spectral

intensity. Monolayer emission spectra were collected on a SPEX Fluorolog 2 spectrophotometer. Samples were mounted vertically and at a 45° angle with respect to excitation, to minimize reflection of excitation light into the emission collection optics. Slits were adjusted according to spectral intensity.

Time correlated single photon counting spectroscopy (TCSPC). TCSPC was used to measure excited state fluorescence lifetimes and rotational dynamics of the chromophores. This system has been described in detail previously in Chapter 3, and we review it briefly here. The light pulses used to excite the sample are generated with a cavity dumped, synchronously pumped dye laser (Coherent 702-2) pumped by the second harmonic output of a mode-locked CW Nd:YAG laser (Quantronix 416). The excitation beam was frequency doubled ($LiIO_3$ Type I SHG) to excite BDP samples at 320 nm (640 nm fundamental, Kiton Red, Exciton) and QDP samples at 390 nm (780 nm fundamental, LDS 821, Exciton). Monolayer samples were held approximately horizontally, with 5° tilts away from the horizontal in two directions: toward the excitation beam and toward the detector. Fluorescence from the sample was imaged through a reflecting microscope objective. Lifetimes were collected across the emission bands at 54.7° with respect to the excitation polarization for solutions and without polarization bias for monolayers. While such collection can, in principle, lead to small contributions to the measured relaxation from motional dynamics, for our experimental conditions this is not a problem.[2,3] Fluorescence was collected at 390 nm and 465 nm (5 nm FWHM bandwidth for solution, 30 nm for monolayers) for BDP and QDP, respectively, with polarizations of 0° and 90° for orientational anisotropy measurements on all samples. A representative lifetime decay and instrument response function (~ 35 ps FWHM) are shown in Figure 5.2.

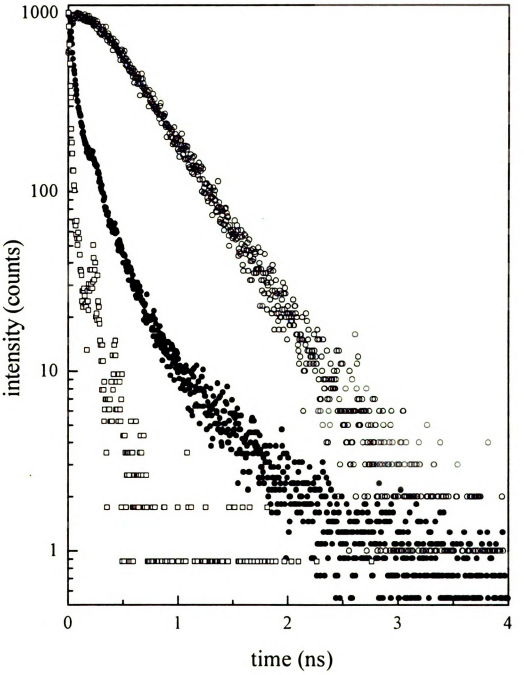

Figure 5.2 Representative instrument response function (□), excited state population decay for QDP in DMSO (10^{-5} M) (○) and excited state population decay for QDP in a monolayer (1%) (●).

Data analysis. The lifetimes we report here were fit to sums of exponentials using commercial software (Microcal Origin v. 4.1) and are reported as the averages and standard deviations of 4-6 individual decays. Rotational dynamics parameters were determined in two ways. For monolayers on silica, eight pairs of alternating parallel and perpendicular scans were used to produce an average anisotropy function. Each scan pair was recorded for a different physical location on the substrate. R(0) was determined to ± 0.01 by regression of data at times after the instrumental response, and several data sets were averaged for each sample. For monolayers on oxidized Si(100), the rotational diffusion information is reported as the averages and standard deviations of data from several decays. Four pairs of alternating parallel and perpendicular scans were used to produce an average anisotropy function, which was fit with Origin to determine the parameters R(0), τ_{MR}, and R(∞).

Calculations. Semiempirical calculations were performed using Hyperchem Release 4.0 (Hypercube, Inc.). The PM3 parameterization used for these calculations is a modification of the AM1 parameterization that treats molecules containing heteroatoms, such as sulfur, more accurately than previous parameterizations. An initial optimization of the structure was performed using a molecular mechanics routine (MM+) followed by geometry optimization at the semiempirical level using an SCF algorithm. The torsions of the QDP 2-2' and 5'-5" σ bonds were set at 10° increments, and semiempirical optimization was performed until the lowest energy conformation for the fixed interring bond torsions was reached. The heat of formation and $S_0 \leftrightarrow S_1$ transition energy were calculated for each geometrically optimized conformation.

5.3 Results and Discussion

In this section we compare the steady-state and transient optical responses of four optically active chemical systems using two chromophores and two substrates. A basic understanding of the optical response and the intralayer relaxation effects of each chromophore is necessary for future investigation of interlayer energy transport between the two chromophores in complex multilayer structures. In addition to the determination of the optical properties of these layers, the effect of substrate must also be considered. Several measurements contribute to our understanding of the optical response, including UV-visible absorption, fluorescence emission, excited state population decays, and induced orientational anisotropy. The results from the anisotropy measurements are critical for comparing the systems. We detail the subtle differences between the systems below.

Monolayers on fused silica

Steady state spectroscopy. BDP monolayers on silica were characterized in Chapter 4. For BDP and HBPA mixed monolayers, we found a linear relationship between the proportion of chromophore in the deposition solution and the proportion of chromophore in the resulting monolayer. The calibration did not regress through the origin, however. This is a simple partitioning effect and can be understood in terms of preferential solvation of HBPA over BDP in ethanol. For QDP and DDBPA mixed monolayers, we also observe a calibration that is linear in QDP concentration, shown in Figure 5.3. In this case, the solvent system used for the monolayer deposition solution gives rise to a calibration curve that passes through the origin. The implication of these

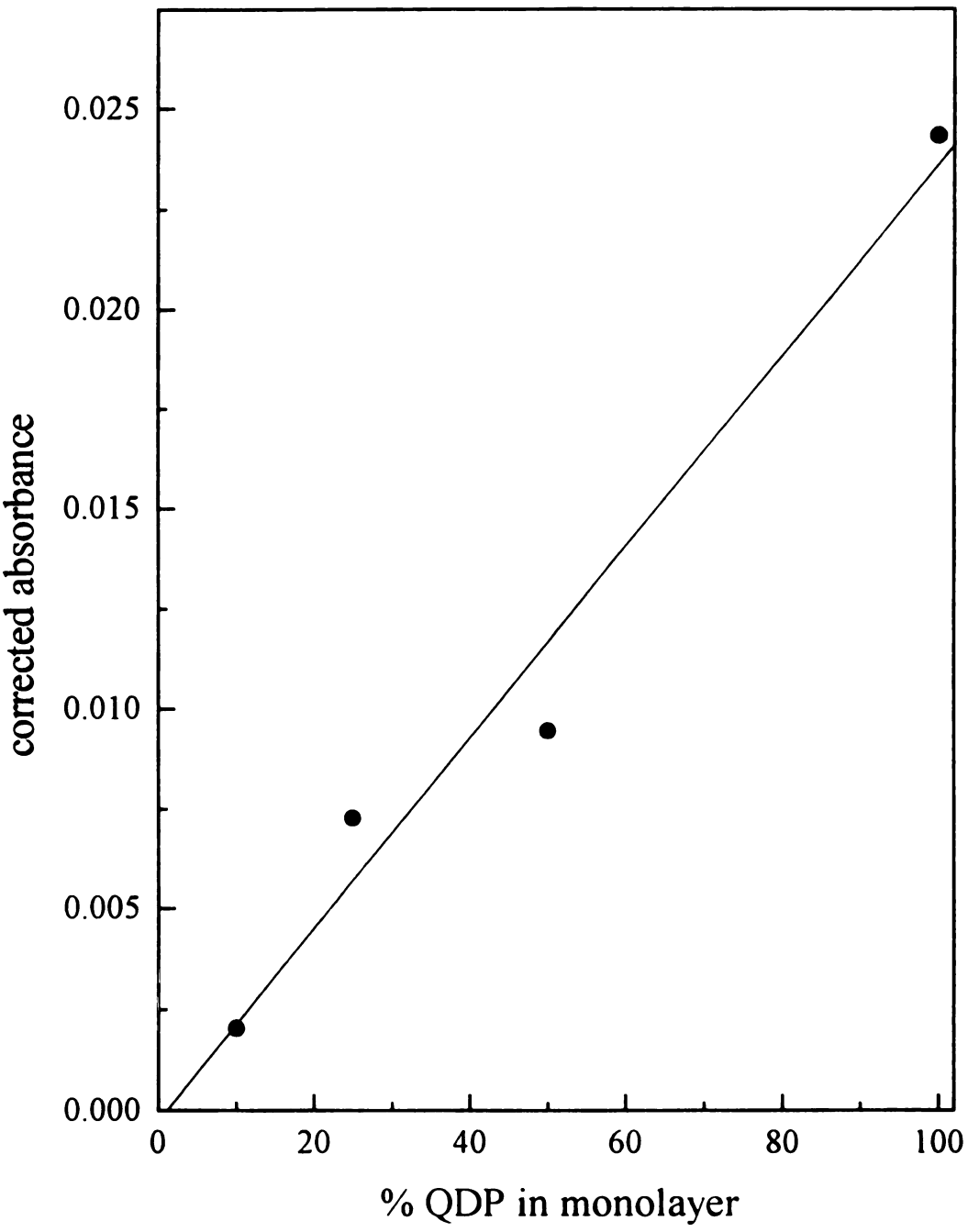

Figure 5.3 Dependence of monolayer absorbance on concentration of QDP in deposition solution and regression of experimental data.

data is that solution concentration ratios will result in a monolayer with the same constituent ratio, if the solvent system is chosen correctly. The proportions of constituents that are incorporated into a mixed monolayer depend mostly on their solubilities in the solvent used.

The steady-state emission spectra for both BDP and QDP are similar in the sense that they reveal more than one form of the chromophore in the monolayer. The BDP spectrum has two features, a narrow peak at 390 nm that we see for dilute (< 35% BDP) monolayers and a broader, less intense peak at 425 nm that we observe for concentrated monolayers. These bands correspond to the two peaks present in concentrated solution spectra. QDP exhibits four unresolved bands in solution and typically three are present in monolayer spectra (see Figure 5.4). For the monolayers, the 445 nm band is not observed. The QDP spectra also depend on concentration in the monolayer. Blue-shifted peaks are prominent in the dilute monolayer spectra, and red-shifted features dominate the concentrated monolayer spectra. Over time, the BDP spectra anneal to spectrum dominated by the blue band, (Figure 4.8) but it is not clear from our data that QDP monolayers exhibit this same evolution. The complexity of these monolayer spectra is also manifested in the temporal evolution of emission intensity. We will discuss this behavior in more detail in Chapter 6.

Transient spectroscopies. The dilute solution behavior of both BDP and QDP is that of a simple chromophore. The absorption and emission bands of the steady-state spectra are well-defined, and dilute solution lifetimes are fit to a single exponential decay for both chromophores. The lifetime for dilute solutions is approximately 200 ps for BDP and 450 ps for QDP. The population decays of monolayers approximate a double

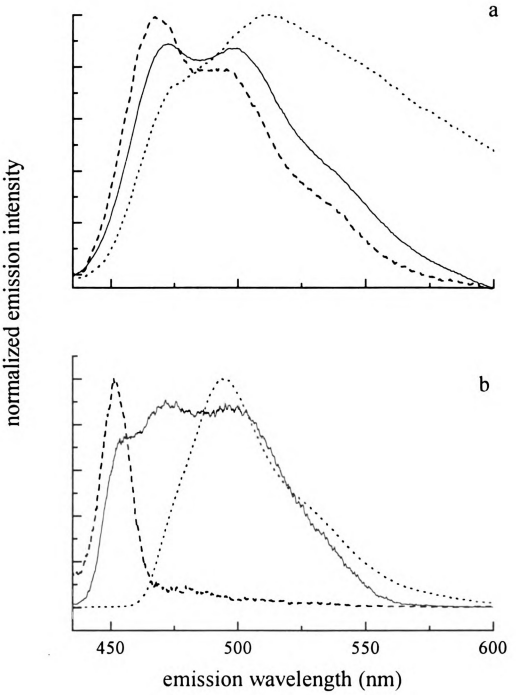

Figure 5.4 Emission spectra of (a) QDP monolayers (- - -) 1%; (——) 5%; (· · · ·) 100%; and (b) QDP solution in DMSO (- - -) 10^{-7} M; (——)10^{-6} M; (· · · ·) 10^{-3} M. Spectra were normalized for presentation and no information about fluorescence quantum yield should be inferred from these plots.

exponential, as shown in Figure 5.2. The fast component of the monolayer lifetimes is ~ 200 ps for both chromophores and the longer lifetime is ~ 1.2 ns, as shown in Table 5.1.

Table 5.1 Excited state lifetimes of monolayers. The time constants refer to fits of the experimental data to the function $f(t) = A_1\exp(-t/\tau_1) + A_2\exp(-t/\tau_2)$.

	τ_1 (ps)	τ_2 (ps)
BDP on silica	187 ± 11	1140 ± 337
QDP on silica	232 ± 16	1265 ± 138
BDP on silicon	213 ± 12	1277 ± 96
QDP on silicon	243 ± 23	1115 ± 156

We interpret the fast monolayer lifetime as that due primarily to an isolated chromophore species in an alkane-like environment, owing to its similarity to the solution phase value, and the long lifetime primarily to a chromophore within an aggregated island. These assignments are, of course, only approximations and the actual contributions to the measured decay are not as clear-cut. This relaxation behavior is well understood and we will present a detailed treatment in Chapter 6. The lifetimes do not vary with respect to either chromophore density in the monolayer or emission wavelength collected for either chromophore. For this reason, the lifetimes reported in Table 5.1 are averages over all concentrations and emission wavelengths used for chromophore monolayers. However, the fractional contribution of each lifetime component varies with chromophore concentration and emission wavelength. For BDP, as the chromophore concentration is increased or as emission is collected on the red edge of the emission band, the relative

contribution of the long lifetime increases. This trend is not observed with QDP, as the contributions of the different species to the total signal varied with no simple pattern. This effect may be due to the greater complexity of the QDP emission spectrum compared to BDP.

Rotational motion measurements are not complicated by population decay functionality effects and can provide insight into how the chromophores move within their environment, offering an indication of how ordered the layers are. Rotational diffusion measurements are most typically made on probe molecules in solution, where the chromophores can relax into all possible orientations. We have measured the dynamics of BDP and QDP in monolayers. Because one end of each chromophore is attached to a substrate, the motion of the chromophore is confined to a conic volume. The cone dimensions are described by Lipari and Szabo's hindered rotor model,[14] where the base of the cone is the point of attachment of the chromophore to the substrate, and the semiangle of the cone is designated θ_0. A nonrandom orientational distribution of the chromophore ensemble in the monolayer is selected with a polarized excitation pulse, and components of the emission that are polarized parallel and perpendicular to the excitation polarization are collected. These data (Figure 5.5a, for example) are combined to construct the induced orientational anisotropy function, R(t):

$$R(t) = \frac{I_{\parallel}(t) - I_{\perp}(t)}{I_{\parallel}(t) + 2I_{\perp}(t)} \qquad [5.1]$$

The decay of R(t) (see Figure 5.5b) is fit to:

$$R(t) = R(\infty) + [R(0) - R(\infty)]\exp\left(-t/\tau_{MR}\right) \qquad [5.2]$$

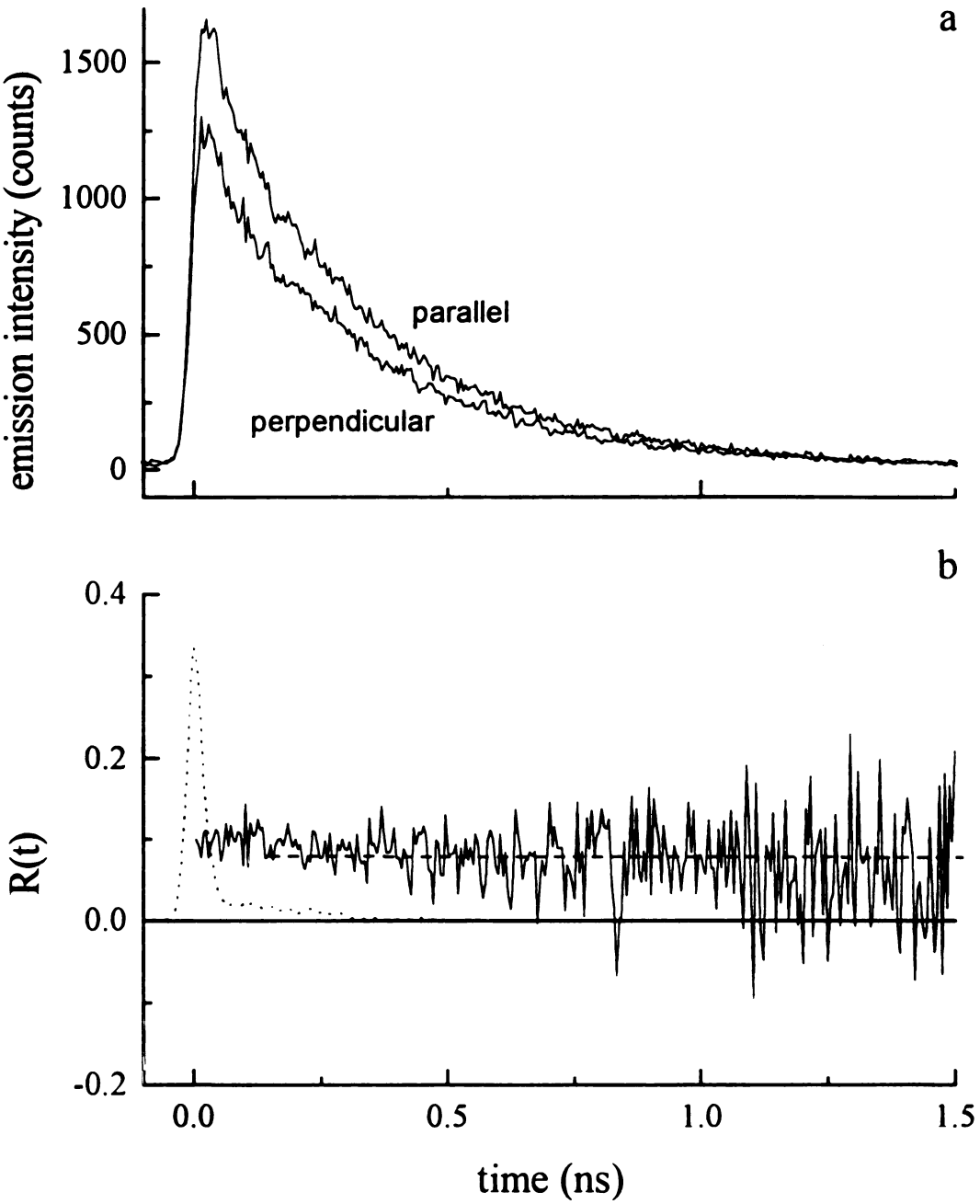

Figure 5.5 Reorientation data for a 50% QDP monolayer on silica. (a) Emission intensity data for parallel and perpendicular polarizations. (b) Induced orientational anisotropy function of above data with fit (- - -).

τ_{MR} is the motional relaxation time constant and the quantity R(0) is related to the angle between the chromophore absorbing and emitting transition moments, δ,

$$R(0) = \frac{2}{5} P_2(\cos\delta) \qquad [5.3]$$

where P_2 is the second order Legendre polynomial. For BDP in solution, R(0) = 0.24, which corresponds to an angle of δ = 31°. For QDP in solution, R(0) = 0.40, indicating parallel transition moments. We consider that the QDP transition moments lie along the long molecular axis. We use these values for δ in the treatment of monolayer data because this quantity is intrinsic to the chromophore and, for the solution data, represents an average over all conformers. We note that R(0) does depend to a certain extent on environment because the intramolecular rotational freedom available to the chromophore depends on the limitations imposed by its surroundings (*vide infra*). Specifically, *syn* and *anti* conformers are likely to exhibit different values of δ.

For chromophores in solution, R(∞) = 0 because they can completely re-randomize at infinite time. For chromophores in monolayers, |R(∞)| > 0 because of the geometric restriction on their motional freedom. R(∞), the steady-state anisotropy, is related to θ, the average tilt angle of the chromophore within the cone by[14]

$$R(\infty) = \frac{2}{5} P_2(\cos\theta_{ex}) P_2(\cos\theta_{em}) \langle P_2(\cos\theta) \rangle^2 \qquad [5.4]$$

The angles θ_{ex} and θ_{em} are the transition moment angles with respect to the cone center axis. The calculation of θ is simplified by setting θ_{ex} = 0° and θ_{em} = δ. In our previous work we reported that BDP on SiO_x exhibited a concentration-independent steady-state anisotropy of 0.06 ± 0.01, which yields an average tilt angle of 35° ± 2°. We report here

that QDP on silica has a similar, concentration-independent steady-state anisotropy of 0.07 ± 0.05, and an average tilt angle of 39° ± 7° (Table 5.2).

Table 5.2 Induced orientational anisotropy data for monolayers. For BDP, the angle between the transition moments is δ = 31° and for QDP, δ = 0°. Angles θ were determined from δ and R(∞) data using Equation 5.4.

	R(0)	τ_{MR} (ps)	R(∞)	θ (degrees)
BDP on silica	-	-	0.06 ± 0.01	35 ± 2
QDP on silica	-	-	0.07 ± 0.05	39 ± 7
BDP on silicon	0.40 ± 0.15	393 ± 119	0.18 ± 0.08	19 ± 11
QDP on silicon	0.32 ± 0.06	479 ± 153	0.13 ± 0.06	32 ± 7

Our measurement of the same tilt angles for both chromophores implies that the oligothiophene/alkane environment is not affected by the lengths of the constituent molecules. We note that the angles we report here for layer tilt are quite similar to the tilt angle of ~30° seen for alkanethiol monolayers on gold.[5,6] In the case of alkanethiol/gold SAMs, the tilt angle is determined by aliphatic inter-chain interactions and the registry of the thiol head groups on the crystalline gold substrate surface. For ZP layers, it is not as obvious that intermolecular interactions dominate the tilt angle because, for the substrates we use, the spacing between primed sites is significantly less well determined than for a crystalline metal surface. In the case of ZP layers, it may be the bonding geometry of the metal-phosphonate connecting layers that determines the range of structural properties available to the system.

We do not detect any chromophore motion in either BDP or QDP monolayers on silica, as indicated by the absence of a decay in R(t). At times after the instrument response function, regression of R(t) yields a line of zero slope. We can evaluate the possibility that the chromophores are reorienting significantly faster than our detection system time resolution (~ 35 ps). The time constants of reorientation in solution are 299 ± 15 ps for BDP in ethanol and 1.2 ± 0.2 ns for QDP in DMSO. Based on viscosity considerations, we believe that the chromophore imbedded in the monolayer will not reorient more rapidly than in low viscosity solvents such as ethanol or DMSO. If there was any motion of the chromophore in the monolayer, it would occur on a time scale we can determine because of the proximity of neighboring molecules and dipolar and van der Waals interactions between them.

Monolayers on silicon

The substrate on which self-assembling structures are synthesized affects the ordering of the adlayers.[5-11] This effect is seen for alkanethiol layers on various metal surfaces, because the infrared-active symmetric and asymmetric CH_2 stretching modes are sensitive indicators of aliphatic chain ordering. We compare the optical response of the chromophore monolayers on silica to that on oxidized Si(100) substrates to evaluate the role of substrate-induced chromophore ordering in determining the dynamical response of the system. Frey and coworkers have shown effects of the substrate on the order of ZP layers,[12] but this effect is seen in the inorganic portion of the IR spectrum (ν_a (PO_3^{2-})) rather than in the aliphatic CH_2 stretching region. We chose silicon substrates for the comparison because the surface priming chemistry is identical to that of

silica, due to the 15 Å thick layer of native oxide that is present on silicon under our experimental conditions.

It is fair to consider that vibrational spectroscopy could address the question of monolayer order for ZP layers on these two substrates.[12] Aside from the different dielectric responses of the two substrates, especially in the IR spectral region, vibrational spectroscopy will not be as sensitive to order for our samples as they are for pure alkanebisphosphonate layers. Contributions from the thiophene rings combined with the structural perturbations they may induce in adjacent aliphatic domains will serve to obscure structural information for our samples. The strong absorbance of SiO_x at low energies obscures information about the inorganic portion of the structures. We therefore rely on lifetime and anisotropy measurements that are sensitive to the local environment of the oligothiophene chromophores.

The concentration dependence of the lifetime data is important in understanding excitation transport in these monolayers. If excitation transport does play a significant role in the transient response of these systems, then we would expect a highly concentration-dependent population decay.[13] The fact that we observe concentration independent lifetime behavior indicates that either excitation transport in this system does not play an important role in determining the observed motional dynamics, excitation transport dynamics are faster than can be resolved for all of the systems we examined, or the double exponential decay is itself characteristic of the excitation transport dynamics. We consider this issue in detail in Chapter 6. The chromophores we have chosen possess moderately high fluorescence quantum yields and large absorption cross sections (ε_{max} = 27,200 $\underline{M}^{-1}cm^{-1}$ for BDP and 27,300 $\underline{M}^{-1}cm^{-1}$ for QDP). Because the oligothiophene

chromophores relax primarily by radiative decay and they possess a large Stokes shift (Figure 1.1), the oligothiophene chromophores are ideal candidates for energy transport studies. We are presently characterizing intralayer excitation transport in mixed monolayers of BDP and QDP. Multilayer assemblies of these chromophores will be useful in investigating interlayer excitation transport phenomena.

While the lifetime data for the chromophores reveal no discernible dependence on the identity of the substrate, the rotational dynamics of BDP and QDP on silicon are fundamentally different than those on silica. As we show in Figures 5.6 and 5.7, a measurable decay of the anisotropy is present for BDP and QDP, with an average reorientation time of ~ 435 ps for both, that was not seen for these chromophores bound to silica. These data were taken over a broad spectral range, with emission collected at 465 nm ± 15 nm, and the values reported in Table 5.2 are averaged over all concentrations because there was no statistically meaningful concentration dependence. The average tilt angles, θ, calculated from $R(\infty)$ using Equation 5.4, are approximately the same for both QDP and BDP monolayers, ~ 35°, (Table 5.2) which correlates well with tilt angles determined for other MP monolayers.[12,14] We note that the average tilt angles of the chromophores on silica are similar, so measurement of θ cannot explain the existence of motion on the oxidized silicon substrate and not silica.

Origins of Chromophore Motion. A necessary first step is to determine the nature of the molecular motion we sense in a single layer. In particular, we need to distinguish between inter-ring isomerization and large amplitude precessional motion. The hindered rotor model describes the physics of a chromophore imbedded in a monolayer. It is typically assumed that a decay in R(t) is related to large amplitude motion of a

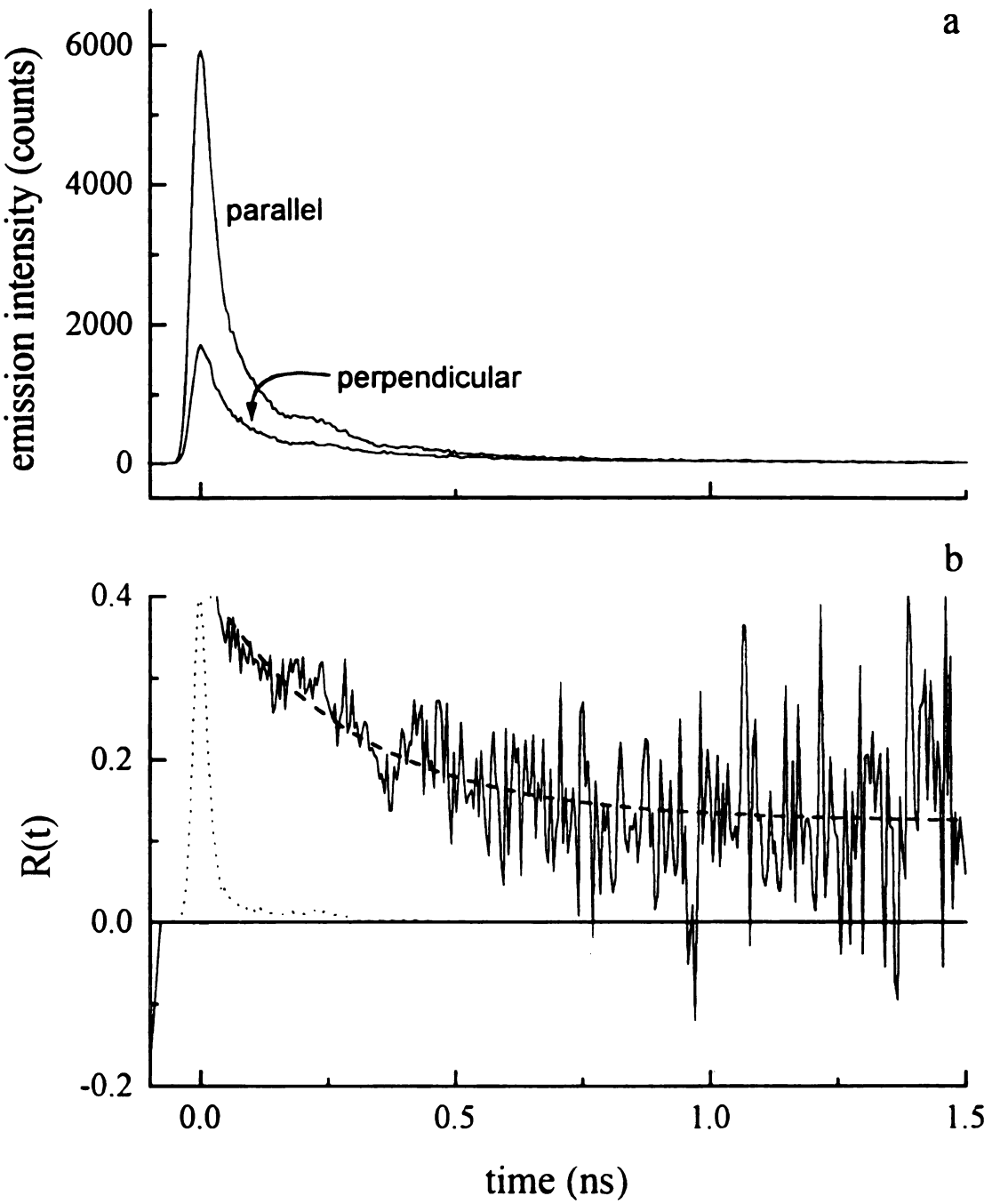

Figure 5.6 Emission intensities (a) and induced orientational anisotropy function (b) for a 26% BDP monolayer on silicon.

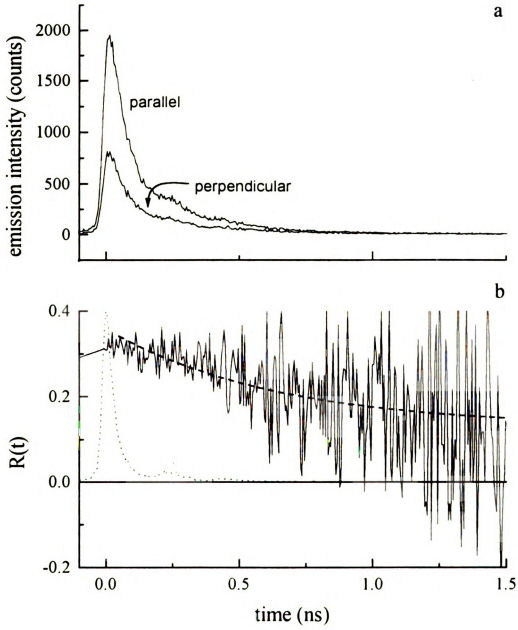

Figure 5.7 Emission intensities (a) and induced orientational anisotropy function (b) for a 1% QDP monolayer on silicon.

chromophore in its environment about its tether to the surface, which is one possible explanation for the dynamics we detect. If this is the dominant motion in our systems, a larger or longer chromophore would experience more hindered movement, and would exhibit a correspondingly longer relaxation time. This is essentially a viscous drag argument, borrowing from the underlying principles of the Debye-Stokes-Einstein model for rotational diffusion in liquids.[15,16]

If large amplitude motion dominates our experimental data then we would also expect to see a concentration dependence, since the thiophene chromophores occupy a larger "footprint" in the lattice sites than alkanes do. A chromophore with chromophore neighbors will move more slowly in its environment than if it were surrounded by aliphatic constituents because of geometric constraints and dipolar coupling. The average motional relaxation time, τ_{MR}, (Table 5.2) for BDP and QDP on silicon are the same to within the experimental uncertainty, arguing that the relaxation we measure is *not* large amplitude precessional motion within a conic volume.

Another type of motion that is important in these chromophores is intramolecular relaxation, specifically the rotation of the thiophene rings about their connecting bonds. This motion is intrinsic to the molecule, and is not limited to a hindered environment. As seen in Figure 5.8, a transition from an all-*anti* to an all-*syn* conformation of QDP represents a substantial change in the orientation of the transition moments relative to the substrate. We believe that rotation of the ring(s) is more reasonable and it can account for our data (*vide infra*). The optical anisotropy decay is a correlation function for the transition moment relaxation, so the dynamics we observe can be accounted for by inter-ring conformational changes in QDP and large amplitude motion does not need to be

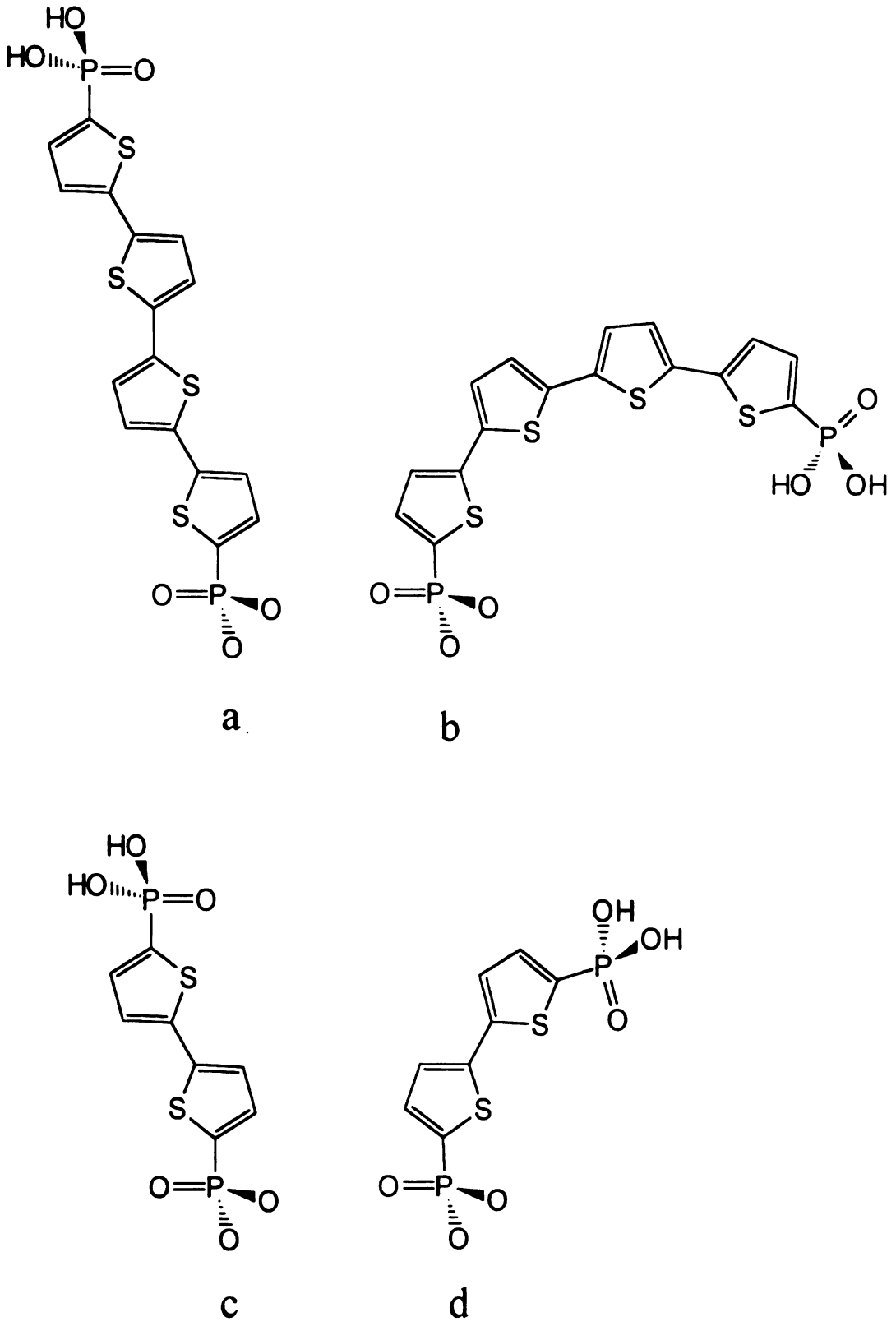

Figure 5.8 Conformations of QDP with thiophene rings (a) all *anti* and (b) all *syn*. Conformations of BDP with thiophene rings (c) *anti* and (d) *syn*.

invoked. The anisotropy decay due to isomerization is not as pronounced for BDP as it is for QDP because BDP possesses fewer conformational degrees of freedom, but there is still a discernable change in the transition moment angle with respect to the substrate normal (Figure 5.8). The BDP and QDP measured parameters of R(0), τ_{MR}, and R(∞) are likely similar because they are constrained to the same molecular area, as dictated by the substrate, primer, and metal phosphonate lattice structure. Within the constraints of a well-packed, uniform monolayer, BDP and QDP may actually have the same net change in transition moment direction, because QDP will not be able to access all of the degrees of conformational freedom available to an isolated molecule (Figure 5.8).

Based on semiempirical calculations,[17-21] rotation of the thiophene rings of an isolated ground state chromophore is a low energy activated process, and certainly occurs at room temperature. We reported in Chapter 4 that the BDP chromophore possesses low barriers to rotation between conformations in the ground state (< 1 kcal/mol). This finding implies that there will be a statistical distribution of conformers that are excited, with any bias in their conformational distribution being induced by environmental, not structural constraints. In Figure 5.9, we show results from semiempirical calculations on QDP for twists between two end rings and between the two center rings. These plots are representative of most energetically favorable conformations, with the exclusion of contributions from the twist between the other two end rings, which were held at 0° in the *anti* conformation. In the first excited singlet state, energetic minima are present at approximately 0° and 180° ring torsion (*anti* and *syn*), while a maximum of ~ 10 kcal/mol is calculated for an inter-ring angle of 90°. This maximum is the result of the tendency of thiophenes to form a planar quinoid structure in the excited state. The *syn* and *anti*

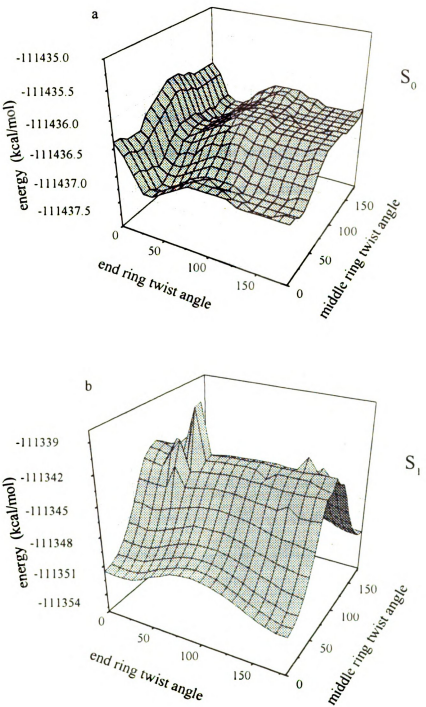

Figure 5.9 Calculated energy barriers for QDP inter-ring rotation for the first two inter-ring bonds: (a) S_0 and (b) S_1. Twist angles indicated are for angles with respect to their adjacent ring.

conformations correspond to the lowest energy difference between S_0 and S_1, so transitions associated with these conformations are expected to produce the red shifted features we see. From these calculations we can see that QDP exhibits facile interconversion between all conformations in the ground state and the excited state possesses definite minima. These calculations are, of course, qualitative and are limited by the utility of the PM3 parameterization in the calculation of S_1 surfaces. Despite these limitations, they do demonstrate the likelihood for the chromophores to exhibit ring rotation in the S_1, consistent with intramolecular relaxation being the dominant phenomenon we detect in the dynamical measurements.

The semiempirical calculations serve to limit the possible explanations for why we observe motional relaxation for monolayers on oxidized Si(100) and not on fused silica. The observation of motion on the silicon substrate could be taken to imply that we are observing motion in this system because the rotation of the chromophore rings is not hindered. It is clear based on the data for the Si(100) substrate and comparison to bulk liquid data that motion of the thiophene rings on silica would occur within a time window accessible to our measurements. We believe that thiophene ring rotation on the silica substrate must be hindered in some way. A simple difference in the dielectric responses of the two substrates cannot account for the differences in motional behavior, because the population dynamics, which depend sensitively on the dielectric response of the substrate, do not vary.

The surface morphology of the substrates is more likely to provide an explanation for our observations. As shown in atomic force microscopy (AFM) images[122] (Figure 5.10), the two substrates are characterized by very different surface features. The silica

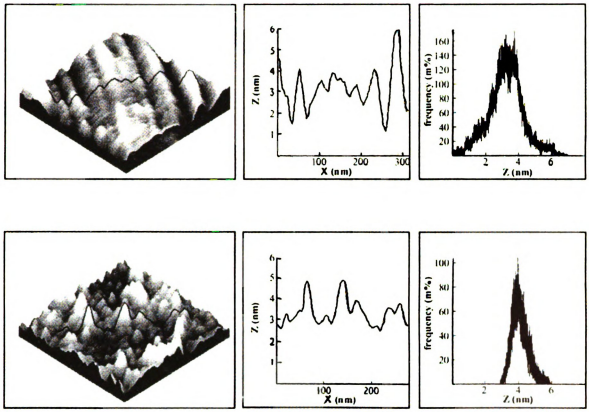

Figure 5.10 Atomic force microscopy images for 300 nm x 300 nm areas of oxidized silicon (top) and fused silica (bottom) substrates. Cursor plots show height profiles along the line indicated in the 3-D images. Image histograms indicate surface relief (Δz) distribution of area imaged.

has a granular, irregular surface, and the oxidized silicon exhibits striations, probably a result of polishing. The grooves in the oxidized Si surface are 200 – 500 Å apart, and 10 – 30 Å deep. The roughness of the two surfaces was determined from the FWHM of a histogram of the imaged area, which is slightly narrower for the silica substrate. On a length scale more relevant to our spectroscopic measurements (50 Å),[23] the variations in height across the surfaces reveal much flatter domains on silica (± 2 Å) than on silicon (± 10 Å). Because of the greater variation in surface relief, chromophores on silicon should have more motional freedom than on a corresponding monolayer formed on silica. An additional piece of information that corroborates this explanation is that for SiO_x, $x_{silicon} < x_{silica}$, which could result in a less dense layer on silicon. Haller has shown that, for this priming chemistry on silicon, under all except the most stringent conditions, the triethoxysilane primer polymerizes easily, resulting in large islands on the surface instead of a single layer.[24] It is possible that the higher density of hydroxyl active sites on the silica surface precludes much of the polymerization because the tighter packing does not allow as much multilayer buildup. For silicon, with fewer active sites on which to grow the bisphosphonate monolayer, the chromophores will be spaced further apart and therefore ring rotation is less hindered. The relative active site density for the two substrates does not explain, however, why we observe a larger fluorescence signal from the monolayers on silicon than on silica. One factor is that the polished silicon substrate is more reflective, so that a larger fraction of emitted light is collected. A more important factor is that, in the more dense monolayers on silica, aggregation of the chromophores is likely. Aggregates typically exhibit lower emission quantum yields than isolated chromophores,[25] and the less densely packed monolayers on silicon will, on average,

have more non-aggregated chromophores. Regardless of these qualitative observations relating to emission intensity, our motional relaxation data can be understood in the context of substrate roughness, as characterized by the AFM data.

5.4 Conclusions

The lifetime and motional dynamics of oligothiophene chromophores within ZP monolayers reveal a subtle difference in the monolayers formed on different substrates. For both silica and oxidized Si(100) substrates, the fluorescence lifetime behavior of each chromophore is identical and is concentration independent, pointing to the limited contribution of intralayer excitation transport in these systems. Transient anisotropy measurements reveal that, for both substrates, the chromophores are oriented at ~35° with respect to the surface normal. For monolayers formed on silica, there is no evidence for chromophore motion, while motion is seen for monolayers formed on the silicon substrate. Despite the substantial similarity between the two families of monolayers, the surface roughness of the polished silicon substrate allows for greater motional freedom of the chromophores in the monolayers. The comparatively lower site density for active hydroxyl groups on the oxidized Si(100) surface likely also plays a role in determining the observed dynamics. These data underscore the important role of substrate morphology in determining the properties of molecular interfaces and provide a foundation for the examination of inter-layer excitation transport studies.

5.5 Literature Cited

1. Bhattacharya, A. K.; Thyagarajan, G. *Chem. Rev.* **1981**, *81*, 415.

2. Flory, W. C.; Blanchard, G. J. *Appl. Spectrosc.* **1998**, *52*, 82.

3. Spencer, R. D.; Weber, G. *J. Chem. Phys.* **1970**, *52*, 1654.

4. Lipari, G.; Szabo, A. *Biophys. J.* **1980**, *30*, 489.

5 Ulman, A. *Chem. Rev.* **1996**, *96*, 1533

6 Dubois, L. H.; Nuzzo, R. G. *Annu. Phys. Chem.* **1992**, *43*, 437.

7. Smith, E. L.; Porter, M. D. *J. Phys. Chem.* **1993**, *97*, 8032.

8. Fenter, P.; Eisenberger, P.; Li, J.; Camillone, N. III; Bernasek, S.; Scoles, G.; Ramanarayanan, T. A.; Liang, K. S. *Langmuir* **1991**, *7*, 2013.

9. Chau, L.-K.; Porter, M. D. *Chem. Phys. Lett.* **1990**, *167*, 198.

10. Chen, S. H.; Frank, C. W. *Langmuir* **1989**, *5*, 978.

11. Sondag, A. H. M.; Raas, M. C. *J. Chem. Phys.* **1989**, *91*, 4926.

12. Frey, B. L.; Hanken, D. G.; Corn, R. M. *Langmuir* **1993**, *9*, 1815.

13. Gochanour, C. R.; Andersen, H. C.; Fayer, M. D. *J. Chem. Phys.* **1979**, *70*, 4254.

14. O'Brien, J. T.; Zeppenfeld, A. C.; Richmond, G. L.; Page, C. J. *Langmuir* **1994**, *10*, 4657.

15. Debye, P. *Polar Molecules* Chemical Catalog Co.: New York, 1929.

16. Fleming, G. R. *Chemical Applications of Ultrafast Spectroscopy* Academic Press: New York, 1986.

17. Dewar, M. J. S.; Zoebisch, E. G.; Healy, E. F.; Stewart, J. J. P. *J. Am. Chem. Soc.* **1985**, *107*, 3902.

18. Dewar, M. J. S.; Dieter, K. M. *J. Am. Chem. Soc.* **1986**, *108*, 8075.

19. Stewart, J. J. P. *Comput.-Aided Mol. Des.* **1990**, *4*, 1.

20. Dewar, M. J. S.; Thiel, W. *J. Am. Chem. Soc.* **1977**, *99*, 4899.

21. Dewar, M. J. S.; Thiel, W. *J. Am. Chem. Soc.* **1977**, *99*, 4907.

22. We are grateful to Prof. Gang-Yu Liu and Yan Huang (Wayne State University) for providing the AFM images shown in Figure 5.10.

23. We estimate the Förster critical transfer radius for these chromophores to be 25 Å. For rotational diffusion measurements, the relevant distance is probably shorter, on the order of the nearest neighbor spacing. Due to the amorphous nature of these surfaces, we can only estimate this distance to be ≤ 10 Å.

24. Haller, I. *J. Am. Chem. Soc.* **1978**, *100*, 8050.

25. Song, Q.; Bohn, P. W.; Blanchard, G. J. *J. Phys. Chem. B.* **1997**, *101*, 8865.

Chapter 6

The Effect of Layer Morphology on Population Dynamics and Intralayer Excitation Transport in Zirconium-Phosphonate Monolayers

Summary

We use fluorescence relaxation dynamics in conjunction with atomic force microscopy (AFM) to understand the morphology of zirconium-phosphonate monolayers containing oligothiophene chromophores. The population relaxation dynamics we measure are non-exponential, chromophore concentration-independent and identical for two different chromophores. We account for these data in the context of an excitation hopping model in a system where the surface is characterized by islands of aggregated chromophores as well as non-aggregated monomers. From the spectroscopic data we infer the sizes of the aggregated islands to be between ~50 Å and 100 Å in diameter, in excellent agreement with the size range of 40 Å to 100 Å measured directly using atomic force microscopy (AFM). The AFM images also reveal that the nearest neighbor spacing of the chromophore islands varies from 80 Å to 200 Å, a separation sufficient to preclude efficient inter-island excitation transport. The data, taken collectively, indicate that the silanol group distribution on the surface determines the heterogeneity of the initial primer layer, and chromophore aggregation plays an additional role in mediating the size of the aggregated islands.

6.1 Introduction

In this work, we are interested in elucidating the details of excitation transport within a given molecular layer. The bisphosphonated oligothiophene chromophores we use are not candidates for optical information storage applications but, because of their spectroscopic properties, they allow us to determine the worst-case effects of excitation transport in a molecular layer. Isomerization about the inter-ring bond in oligothiophenes is facile in both the S_0 and S_1 states, as determined in Chapter 3, and this process does not interfere with the measured population dynamics. We can thus study excitation transport in the absence of complications associated with large amplitude molecular motion. We use 2,2'-bithiophene-5,5'-diylbis(phosphonic acid) (BDP) as the donor chromophore and 2,2':5',2":5",2"'-quaterthiophene-5,5"'-diylbis(phosphonic acid) (QDP) for the acceptor chromophore. The structures of these molecules are shown in Figure 6.1.

We have characterized the optical response of each chromophore separately in monolayer environments as well as in mixed monolayer systems where both BDP and QDP are present in varying concentrations. These two chromophores represent a limiting case in the context of information storage applications because the BDP (donor) emission band overlaps the QDP (acceptor) absorption band, making radiative energy transfer favorable (Figure 1.1). For all of the monolayer assemblies, we recover the same non-exponential population decay, independent of chromophore concentration. These data are not consistent with Förster excitation transport in a homogeneous system. The fact that the population relaxation dynamics are the same for both molecules suggests that the optical response for these monolayers is mediated by structure on a length scale significantly greater than the individual molecules. The origin of the apparently anomalous

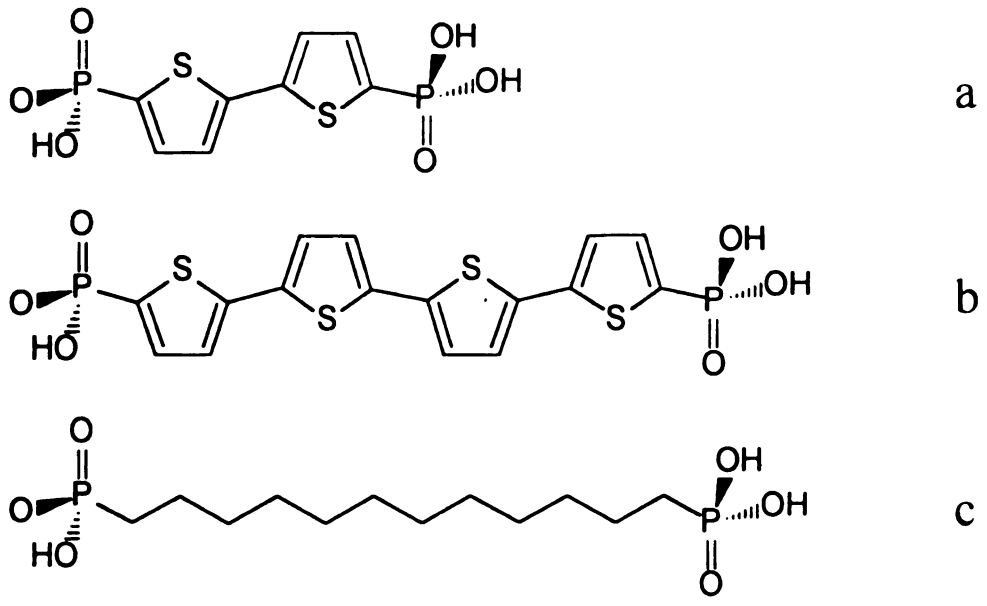

Figure 6.1 Structures of oligobisphosphonates used in this work. (a) The donor 2,2'-bithiophene-5,5'-diylbis(phosphonic acid) (BDP); (b) the acceptor 2,2':5',2":5",2"'-quaterthiophene-5,5"'-diylbis(phosphonic acid) (QDP); (c) the diluent 1,12-dodecanediylbis(phosphonic acid) (DDBPA).

relaxation behavior is the structural heterogeneity of the monolayer. Our lifetime data are consistent with the formation of aggregates. Based on an excitation transport model used previously for stilbazolium dyes in Langmuir-Blodgett films,[1] we predict aggregate domain sizes on the order of 50 Å to 100 Å. Atomic force microscopy (AFM) images reveal that the diameter of aggregates typically ranges from 40 Å to 100 Å. The nearest neighbor spacing of these islands varies from 80 Å to 200 Å, which is sufficient separation to preclude efficient inter-island excitation transport. The agreement between the spectroscopic and physical (AFM) measurements of the surface morphology shows that the domain size sensed by spectroscopic experiments is the same as that measured by AFM, implying a significant degree of intermolecular alignment within the individual aggregate domains. These findings indicate that the surface silanol group distribution determines the initial priming layer heterogeneity, and chromophore aggregation plays an additional, key role in the development of the observed layer morphology.

6.2 Experimental

Metal-phosphonate monolayer synthesis. Polished silicon (100) substrates (MultiCrystal Optics) were cleaned by piranha solution etch for 10 minutes and rinsed with flowing distilled water. Samples were dried with a N_2 stream and were primed immediately. The substrates were primed with 3-(aminopropyl) triethoxysilane (APTES) or 3-(aminopropyl) dimethylethoxysilane (APDMES). Substrates were refluxed in a 1% v/v solution of APTES in anhydrous octane for 10 minutes, followed by rinses in hexane and water. Alternatively, they were immersed in a 0.5% v/v solution of APDMES in anhydrous toluene overnight and rinsed with methanol and water. After drying with N_2,

the aminated surface was derivatized to the phosphonate using a solution of 0.2 M $POCl_3$ and 0.2 M collidine in anhydrous CH_3CN for 20 minutes, followed by rinses with CH_3CN and water. The resulting surface was exposed to Zr^{4+} by immersion in a 5 mM solution of $ZrOCl_2$ in 60% aqueous ethanol for 10 minutes. The syntheses of 2,2'-bithiophene-5,5'-diylbis(phosphonic acid) (BDP) and 2,2':5',2":5";2"'-quaterthiophene-5,5"'-diylbis(phosphonic acid) (QDP) and 1,12-dodecanebisphosphonic acid (DDBPA), were reported in Chapter 2, and we show their structures in Figure 6.1. Monolayers were deposited from solutions having a total 1 mM concentration of organobisphosphonate ([BDP] + [QDP] + [DDBPA] = 1 mM) in 80% DMSO, 20% (90% EtOH (*aq*)). The primed and zirconated substrates were immersed in the bisphosphonate solution overnight to allow formation of the layer of interest. The relative amount of each constituent in solution is related directly to the fraction of each in the formed monolayer for this solvent system.

Lifetime Measurements. Time correlated single photon counting spectroscopy (TCSPC) was used to measure the fluorescence lifetimes of the chromophores within the monolayers. This system has been described in Chapter 3, and we recap its salient features here. Short light pulses (~5 ps FWHM) are generated with a cavity-dumped, synchronously pumped dye laser (Coherent 702-2) pumped by the second harmonic of the output of a mode-locked CW Nd:YAG laser (Quantronix 416). The dye laser output is frequency doubled ($LiIO_3$, Type I SHG) to excite the samples at 315 nm (630 nm fundamental, Kiton Red, Exciton). Monolayer samples were held approximately horizontally, with 5° tilts away from the horizontal in two directions, toward the excitation beam and toward the detector. Fluorescence from the sample was imaged through a

reflecting microscope objective and collected across the emission bands of the chromophores with 30 nm FWHM detection bandwidth. The chromophore lifetimes we report here were fit to the sum of two exponential decays using commercial software (Microcal Origin v. 5.0) and are reported as the average of the fits of three decays and the associated standard deviations.

Steady-state optical spectroscopy. The absorbance spectra of oligothiophene chromophores in solution were measured using a Hitachi U-4001 UV-visible spectrophotometer. Spectra were collected with 5 nm resolution. Fluorescence spectra for solutions were measured on a Hitachi F-4500 fluorescence spectrometer. Excitation and emission slits were adjusted according to spectral intensity. Previous Chapters (4,5) that reported on the linear response of oligothiophene monolayers have shown that their steady state spectra are very similar to solution phase spectra.

Optical null ellipsometry. The thicknesses of primed substrates and monolayer samples were determined using a commercial optical null ellipsometer (Rudolph Auto-EL II) operating at 632.8 nm. Data were acquired and reduced using Rudolph software. For both primer and ZP layers, we used a value of the refractive index of $\mathbf{n} = 1.462 + 0i$ for the determination of film thickness.

6.3 Results and Discussion

The focus of this work is on understanding the morphology and structural heterogeneity within a ZP monolayer made with varying concentrations of oligothiophene chromophores. The unusual population decay dynamics of the chromophores in these environments allow for modeling that can shed light on the physical and structural

properties of the monolayers. Because the surface properties extracted from the spectroscopic data depend on the assumptions and approximations made in the modeling, it is important to compare these findings to a direct, physical determination of surface structure and morphology. AFM provides a real space image of surface topography with high resolution. The surface structure and morphology seen with the AFM is in excellent agreement with the information derived spectroscopically. Our findings are significant in and of themselves because it is not clear from first principles that the spectroscopic data are sensitive to the same island properties as the AFM probes. We consider the two bodies of information individually.

Optical Spectroscopy. To appreciate the structural information content of the lifetime data, it is important to consider the result expected for a uniform monolayer first. The systems we report on here, specifically, mixed BDP and DDBPA monolayers, mixed QDP and DDBPA monolayers and mixed BDP, QDP and DDBPA monolayers on oxidized Si(100), all yielded the same non-exponential excited state population relaxation decays (Figure 6.2). We also note that the regressed time constants for these data are independent of chromophore concentration. These two findings place substantial limits on the structural possibilities for these monolayers.

The expected case for a monolayer of chromophore is that Förster energy transfer will dominate the excited state relaxation dynamics. The expected result for a simple monolayer is that the fluorescence lifetime of the donor will decrease monotonically as the concentration of acceptor is increased, due to dipolar donor-acceptor coupling. We synthesized monolayers from 1mM bisphosphonate solutions where the donor BDP is 5% of the total bisphosphonate concentration (0.05 mM) and varying amounts of acceptor

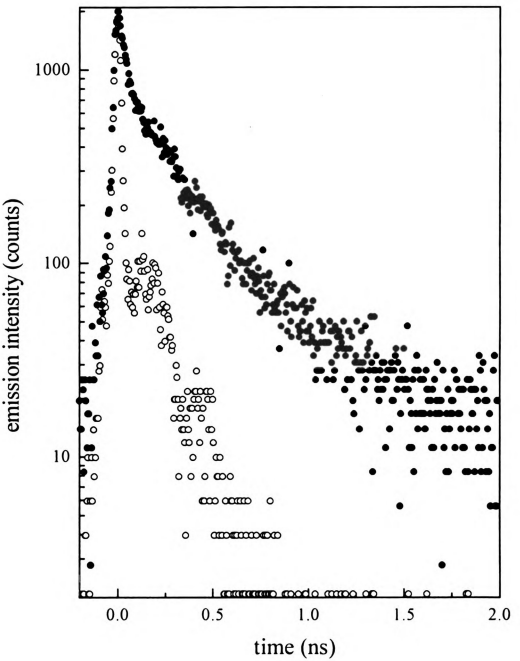

Figure 6.2 Representative instrument response function (O) and excited state population decay for QDP in a monolayer (5%) (●).

QDP (1% - 95%, 0.01 mM - 0.95 mM) are used. The remainder of the monolayer is comprised of an optically inactive component, DDBPA, which, in its all-*trans* conformation, is approximately the same length as the all-*anti* conformation of the acceptor QDP.

In a monolayer where each of the constituents is distributed statistically, the average distance between a donor and the nearest acceptor depends sensitively on the concentration of each. The Förster model predicts that the rate constant for excitation transfer, and therefore the donor radiative lifetime, depends inversely on the D-A spacing to the sixth power.[2,3]

$$k_{D\text{-}A} = \frac{3\kappa^2 R_0^6}{2\tau_D R^6} \qquad [6.1]$$

$$\kappa^2 = \sin\theta_D \sin\theta_A \cos\phi - 2\cos\theta_D \cos\theta_A$$

where $k_{D\text{-}A}$ is the rate constant for donor-acceptor transfer, κ^2 is a geometric factor to account for the projection of the donor transition moment onto the acceptor transition moment, τ_D is the donor lifetime in the absence of acceptor, R is the D-A distance and R_0 is the critical transfer radius. This latter term contains information on the spectral overlap between the donor and acceptor and the cross sections of the relevant transitions. If the Förster model describes excitation transport in the monolayers we report on here, there should be a marked acceptor concentration (*i.e.* R) dependence in the donor lifetime ($k_{D\text{-}A}^{-1}$) data. We present the acceptor concentration dependence of the donor lifetimes for the mixed BDP and QDP system in Figure 6.3. There is no discernible acceptor concentration dependence on the donor lifetimes. For monolayers composed of only one chromophore, it may be reasonable to expect a modest concentration dependence due to

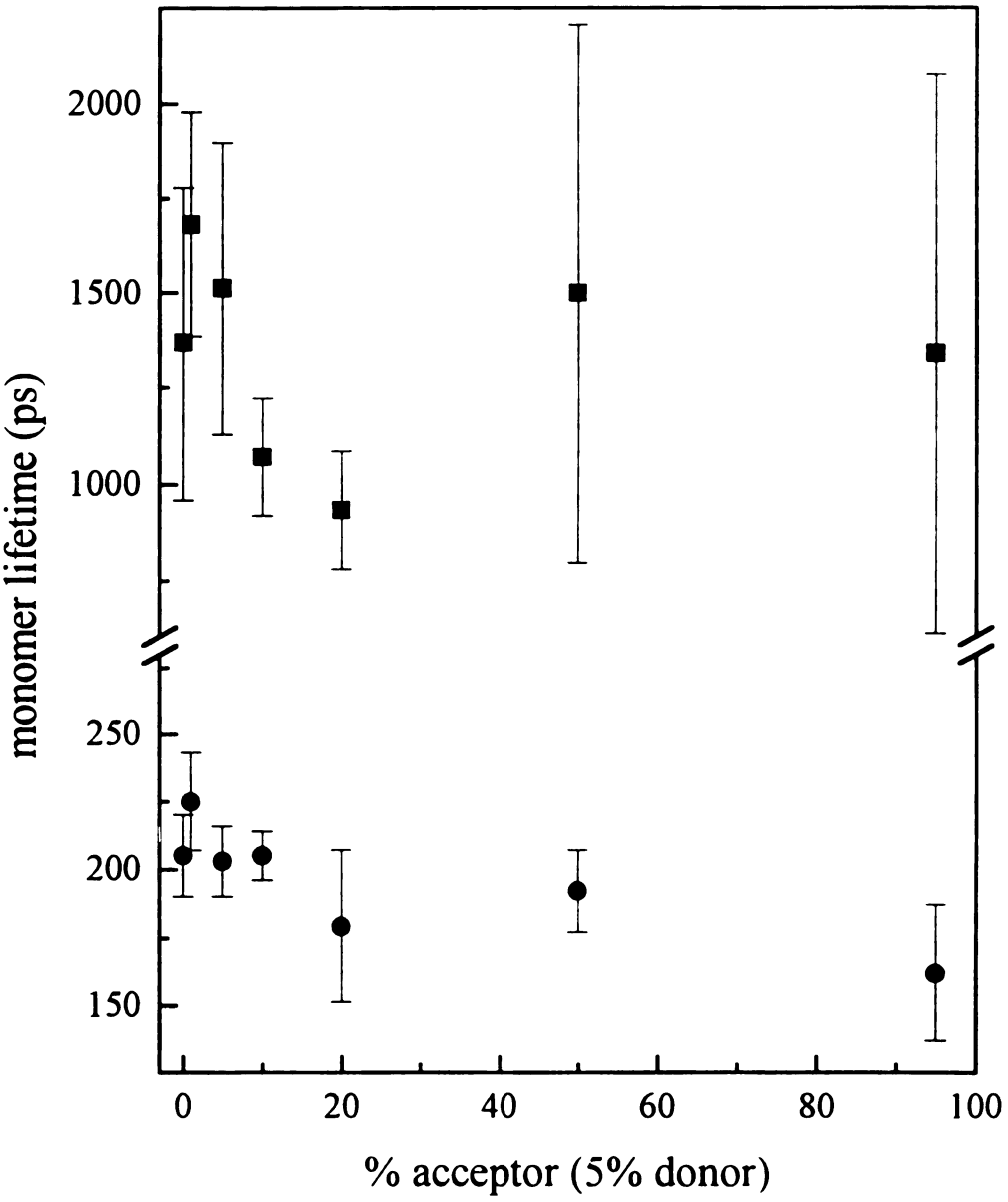

Figure 6.3 Dependence of donor lifetimes on acceptor concentration, for a monolayer containing 5% donor.

the spectral overlap dependence of the Förster critical transfer radius, R_0, and the characteristically large Stokes shifts exhibited by the oligothiophene chromophores (Figure 1.1). For the mixed monolayers, however, we expect to see a measurable donor lifetime dependence on acceptor concentration because of the substantial spectral overlap of the donor emission and acceptor absorption bands, the high fluorescence quantum yield of the donor, and presumably favorable geometry ($\kappa^2 \sim 1$) for dipolar coupling between the donor and acceptor.

There are two possible explanations for our lifetime data. The first is that energy transfer between donor and acceptor may be too fast to resolve with our instrument. If this is true, it would explain the absence of an exponential growth in the acceptor fluorescence time-dependence, but not the absence of the donor lifetime dependence on acceptor concentration. The apparent absence of energy transfer may also be a consequence of the morphology of the monolayers. An underlying assumption of the Förster treatment we described above is the uniformity of the monolayers and that the chromophores behave as individual species. If these assumptions are violated in some manner, it is possible that excitation transport still proceeds but the signature of the process is different than that expected from the Förster treatment. We consider the functional form of the population decays and how these data can be accounted for in a model of excitation transport that takes into account heterogeneous chromophore distribution and aggregation of the chromophores.

To understand the interaction between the donor and acceptor chromophores, we need to understand the functionality of the population decays of the individual chromophores. In Chapters 4 and 5, we reported the presence of two lifetime components

for chromophore monolayers, in contrast to the single exponential decay found for dilute solutions. We recover the same time constants within the uncertainty of our measurements for both chromophores (Table 6.1), and these lifetimes are invariant with respect to concentration of chromophore in the monolayer or the emission wavelength collected.

Table 6.1 Fits of excited state lifetime data and simulated lifetime data to the function $f(t) = A_1\exp(-t/\tau_1) + A_2\exp(-t/\tau_2)$.

	τ_1 (ps)	τ_2 (ps)
BDP on silicon	187 ± 11	1140 ± 377
QDP on silicon	228 ± 45	1254 ± 152
simulated data	197	1230

These data, taken together, suggest that it is not the individual chromophores, but rather the physical or environmental properties of the monolayers that mediate the optical response of the collective system. These results are reminiscent of those seen for the population relaxation of a stilbazolium dye in a Langmuir-Blodgett film.[11] In that work it was found that the chromophores aggregated significantly and the majority of the radiative decay originated from monomer species that were present in more than one environment.

Aggregation is common in conjugated chromophore systems and has been demonstrated in a variety of structural motifs, including monolayers. In a chromophore aggregate, the molecules are spaced closely, (we take this spacing to be ~5 Å for the ZP lattice) so excitation transport can compete effectively with radiative decay. As a consequence, aggregates are typically characterized by a fluorescence quantum yield

significantly lower than that of the corresponding monomer. The dominant optical response of such a system is considered to be from the remaining non-aggregated free monomers. The picture of such a surface is that of aggregate islands of chromophore separated by regions of predominantly non-chromophore (either DDBPA or unreacted surface). The proximity of radiative monomer chromophores to the aggregates can, of course, vary widely, but we consider the two most likely cases for our conditions. Either the monomer is present as a structural defect within an aggregate or it exists near the perimeter of an aggregate. The dielectric response of these two environments will differ significantly and it is therefore reasonable to expect the two types of monomer to be characterized by different lifetimes.[4,5] It is important to determine whether or not the model can account for the population decay behavior we measure experimentally

Song *et al.* have developed a model to describe the excitation dynamics of H-aggregates of stilbazolium dyes in Langmuir-Blodgett layers.[1] In this model, depicted in Figure 6.4, an aggregated island of chromophore molecules, A, is excited by a short pulse of light. The excitation can decay radiatively (a low probability event), or it can execute diffusive excitation transport ("hopping") about the island until it reaches a (radiative) monomer. The radiative monomer could be located within the island (M_1) or in the inter-island interstices (M_2).

A series of coupled differential equations describes the temporal evolution of monomer and aggregate populations as given in Figure 6.4. These equations can be solved numerically to yield the time course of the populations of M_1 and M_2.

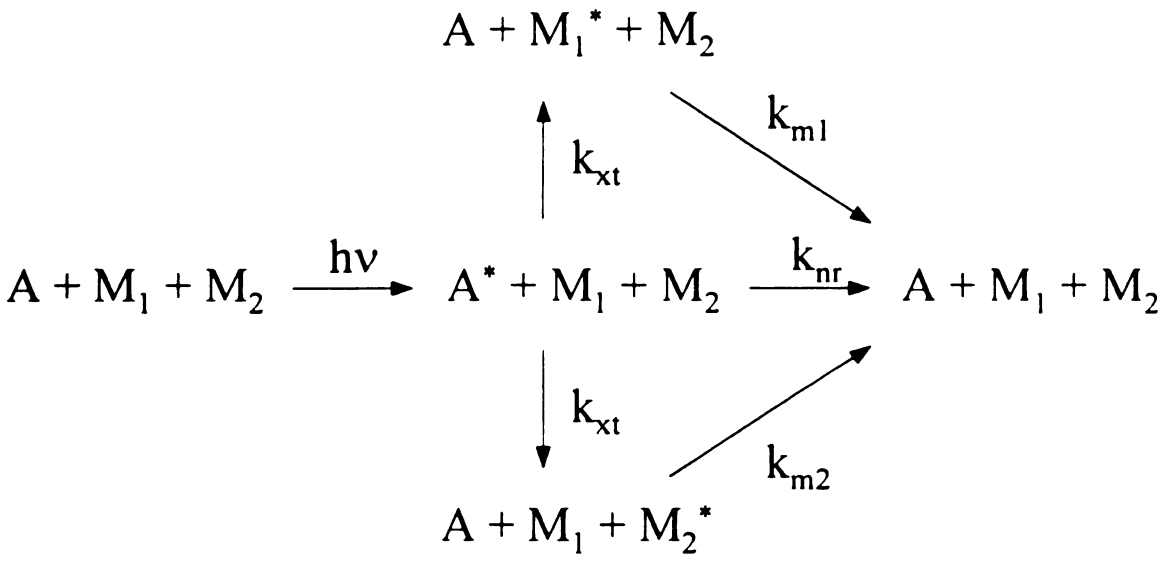

Figure 6.4 Kinetic model proposed for population decay dynamics in donor and acceptor monolayers. A refers to the aggregate species and M_1 and M_2 are monomers in different chemical environments.

$$\frac{d[A^*]}{dt} = -k_{xt}[A^*]([M_1]+[M_2]) - k_{nr}[A^*]$$
$$\frac{d[M_1^*]}{dt} = -k_{M1}[M_1^*] + k_{xt}[A^*][M_1]$$
$$\frac{d[M_2^*]}{dt} = -k_{M2}[M_2^*] + k_{xt}[A^*][M_2] \qquad [6.2]$$
$$\frac{d[M_1]}{dt} = k_{M1}[M_1^*] - k_{xt}[A^*][M_1]$$
$$\frac{d[M_2]}{dt} = k_{M2}[M_2^*] - k_{xt}[A^*][M_2]$$

In the numerical simulations, we assume that the aggregates are excited, with the populations of excited monomers being established by excitation migration. We estimate $k_{xt} = 10^{13}$ s^{-1}, a value consistent with excitation hopping in LB films of stilbazolium dyes. We can place limits on this value, as we discuss below. We estimate the non-radiative decay rate constant $k_{nr} = 10^6$ s^{-1} for the aggregates. While the actual value of k_{nr} may differ somewhat from this estimate, its value does not affect the results of the simulation significantly because k_{nr} will be smaller than k_{xt} for essentially any system where excitation transport is significant. The lifetimes of M_1 and M_2 were varied to produce a decay that closely approximates the experimental population decays. The values used in this simulation (Figure 6.5) were $k_{M1} = 7.0 \times 10^9$ s^{-1} (τ_{M1} = 197 ps by fitting) and $k_{M2} = 1.6 \times 10^9$ (τ_{M2} = 1230 ps). The simulated curve can be fit to a double exponential decay even though four rate constants are used to construct it. While the double exponential fit does not ostensibly account for the dynamics of the chromophores in the monolayer, it provides a useful empirical representation of the relaxation phenomena we measure with the TCSPC experiment. Regression of the experimental data using a double exponential function produces residuals that match those shown for the fit to the model in Figure 6.5.

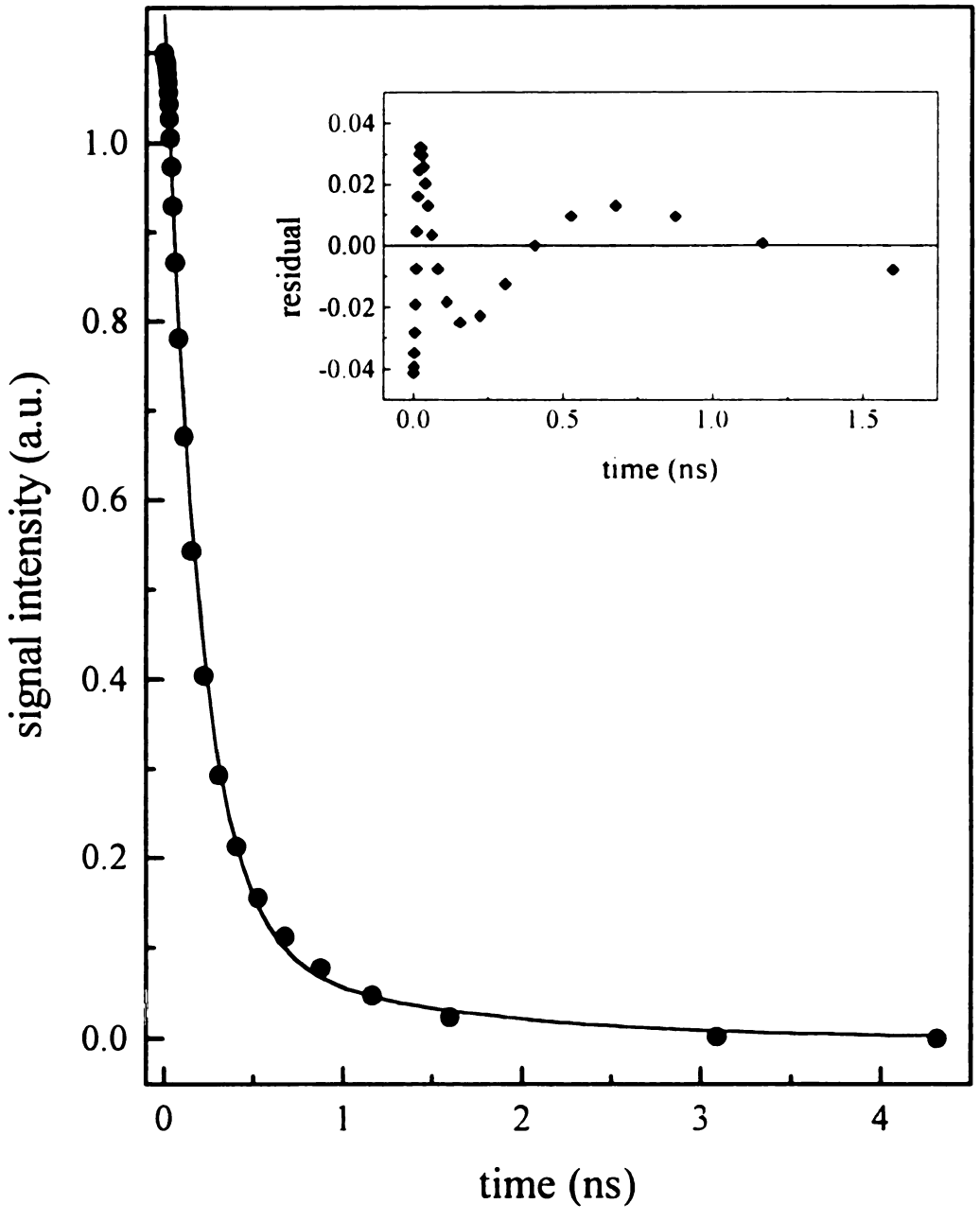

Figure 6.5 Simulated population decay (●) using Equation 6.2 (see text) and fit of data (——) to a double exponential decay of the form $f(t) = A_1\exp(-t/\tau_1) + A_2\exp(-t/\tau_2)$. Inset is a plot of the residuals fit.

Monolayer morphology. The key to understanding the morphology of these systems is relating the experimental data to the sizes of the aggregates. The agreement between model and experiment suggests that the physics of the model are appropriate for our system. There are two system properties that together provide a sensitive measure of aggregate size. These are k_{xt} and the number of excitation transport events, n, required for the aggregate-supported excitation to find a monomer and decay radiatively. The total hopping time ($k_{xt}^{-1}*n$) can be related to average distance traveled by means of a Monte Carlo simulation, as has been reported before.[1] The experimental manifestation of the migration of an excitation to a radiative monomer will be a build-up in our single photon counting signal after time zero. Despite the fact that our instrument response function is short (~35 ps) for this technique, it is longer than the expected build-up time and we do not observe a build-up directly. In an attempt to resolve whether or not there is a build-up in the experimental data at early times, we have attempted deconvolution of the response function from the data. While there is a build-up seen in the deconvoluted data, the actual time constant we recover for the build-up depends sensitively on the initial parameters used in the deconvolution procedure. We therefore do not report a value for this build-up time. Rather, we can place an upper bound of 10 ps on the excitation migration time. From this upper bound, we can place a corresponding upper bound on the size of the aggregate island(s) sensed by the measurement. We consider next the relationship between total excitation migration time and island size.

We need to consider two limiting cases of aggregate-to-monomer transfer because this step can, in principle, affect the estimate of island size. In the first case, the radiative monomers are close in proximity to an island, perhaps even within the island but residing

in a physical position that precludes their participation in the aggregate structure. In this case, the last transfer event, from the aggregate to the monomer, is fast. As detailed above, we cannot quantitate the lifetime of the aggregate excitation, so we use the upper-bound value of $\tau_{xt} \approx 10$ ps. The time constant per excitation transfer event, or hop, is taken to be 0.1 ps, so in 10 ps, an average of 100 hops can occur. Song, *et al.* have published the results of calculations where the dynamics of exciton motion within an H-aggregate were modeled using a random walk approach.[1] This calculation produces a curvilinear relationship ($n^{1/2}$) between mean distance traveled for exciton diffusion and the number of steps taken. For 100 hops, the mean distance traveled is 40 Å. With an approximate 5 Å spacing between lattice sites in the zirconium-phosphonate lattice, the exciton can travel ~8 lattice separations within the aggregate. The actual aggregate shape will, of course, play an important role in determining the island size in this model and it is clear that the results will depend on the aspect ratio of the island. The simplest case for this calculation is a square island, for which we obtain an average aggregate size of 64 molecules. At this point, it is fair to consider the accuracy of our estimation of $\tau_{xt} = 10$ ps. We know from the raw data that it must be significantly faster than ~ 25 ps, and we speculate that it is at least 5 ps. We calculate from these limits that the island size lies in the range of 36 to 144 molecules (Table 6.2).

Table 6.2 Calculated aggregate sizes for selected excitation hopping time constants and total migration times.

τ_{xt} (ps)	τ_{hop} (ps)	excitation diffusion distance (Å)	molecules in aggregate
0.1	5	30	36
	10	40	64
	25	60	144
0.05	5	40	64
	10	55	121
	25	90	324

In addition to uncertainty in the total hopping time, it is possible that our estimate of the hopping time constant is incorrect. If we double k_{xt} and assume a 10 ps time constant for transport, we recover a result that is identical to $k_{xt} = 10^{13}$ s^{-1} and $\tau = 20$ ps. Thus the model still holds. It is unlikely that the hopping rate constant would be slower than 10^{13} s^{-1} because of the proximity of the chromophore molecules to one another.

In the second limiting case, where the radiative monomer is not in direct contact with the aggregate, the last transfer step will not be as efficient, consistent with the Förster R^{-6} dependence (Equation 6.1). To estimate the total time required for excitation transport, we take the critical transfer radius, R_0, to be the lattice spacing, 5 Å. We realize that this is a different estimate than is typical for an organic chromophore. The close proximity and high degree of alignment of neighboring chromophores in this system effectively "screens" an excited chromophore from coupling efficiently to more distant acceptors. Using this critical radius and a radiative lifetime of $\tau_{rad} = 200$ ps, for $\tau_{xt} = 0.1$ ps the maximum D-A spacing is calculated to be $d_{max} = 17.75$ Å. In the simplest model of

the surface, where all the aggregates are spaced evenly, $d_{max} \sim 2.15\sqrt{N}$. Thus N = 68 molecules, in essentially exact agreement with the first case. The location of the radiative monomers relative to the aggregate is thus not a deterministic factor in the estimation of the aggregate size.

To this point, we have postulated the existence of aggregates in these monolayers. The basis for this postulation is the concentration independence and the functionality of the chromophore population relaxation within the monolayer. Within this framework, we have applied an excitation hopping model known to be appropriate for layered assemblies, and we recover an aggregate size of ~65 molecules. Given the uncertainties in estimating the values of some of the model parameters, it is fair to bound our island size estimate to be between 50 and 100 molecules. For a 5 Å inter-site spacing and a square aggregate, we estimate the aggregate size to be on the order of 50 Å x 50 Å. This estimate reflects the domain size sensed by the spectroscopic measurement and it is not clear from first principles the aggregate domain size measured in this manner bears any relationship to the physical size of the aggregate. Indeed, it is reasonable to expect that the density and type of defects within the aggregates will determine the "spectroscopic size", and not the physical size. In addition, the spectroscopic measurements are averaged over all the aggregate domains excited and offer little insight into the distribution of aggregate size and order. We have used AFM to image the local structure and morphology of these monolayers in an effort to compare the spectroscopic data to measurable physical dimensions.

Atomic Force Microscopy Measurements. We have imaged[161] and compared the surfaces of oxidized silicon substrates, APTES-primed substrates, QDP monolayers on the

primed substrates, and monolayers of 5% BDP, 50% QDP and 45% DDBPA on the primed substrates. Example topographic images are shown in Figure 6.6. We found in Chapter 5 that the morphological differences between oxidized silicon and silica substrates mediate the motional freedom of the chromophores in the monolayer while population dynamics are not affected measurably by the substrate identity. As shown in Figure 6.6a, the blank substrate is characterized by grooves in the oxidized surface that are 10 Å - 50 Å deep and ~500 Å apart. The origin of these features is most likely mechanical polishing. Priming alters this morphology substantially. The grooves fill in and islands begin to appear when the substrate is reacted with APTES (Figure 6.6b). The overall surface roughness, 15 Å - 30 Å as determined by the FWHM of a histogram of the topographic images, is very similar for all four types of samples examined. The primer layer has a very distinct surface morphology, in which three-dimensional clusters with lateral dimension 20 Å - 200 Å are clearly visible. A typical nearest neighbor distance between clusters is ~ 100 Å, although the separation between clusters varies from 50 Å to 1000 Å. Higher resolution images (*e.g.* 100 Å x 100 Å) taken at various locations on the surface reveal no long range order or periodicity within an island. Thus the island structure originates from the nature of the initial priming layer chemistry. In contrast to thiol monolayers on gold,[171] we observe no crystalline ordering or structural regularity in these monolayers over length scales of more than a few molecules. We believe that the primer layer island formation is determined by primer polymerization in concert with a non-uniform silanol site distribution for these substrates.

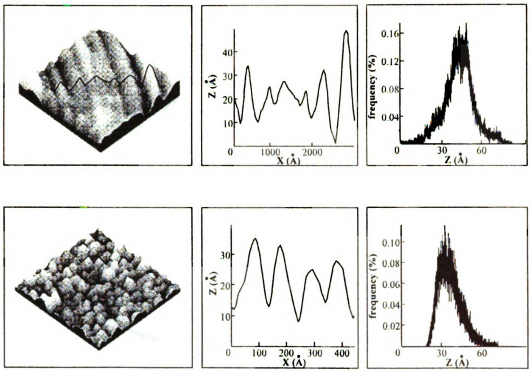

Figure 6.6 Topographic images (left panels) of the surfaces of (a) oxidized silicon (SiO_x) substrate, (b) APTES-primed substrate, primed substrate with QDP adsorbed, and (d) a mixed monolayer of 5% BDP, 50% QDP and 45% DDBPA on a primed substrate. The total scanning area is 1000 Å x 1000 Å except for (a) which is 3000 Å x 3000 Å. The cantilever force constant is 0.1 N/m and the imaging force used here is ~ 0.2 nN. Corresponding cursor profiles and histograms are shown in the middle and right panels, respectively.

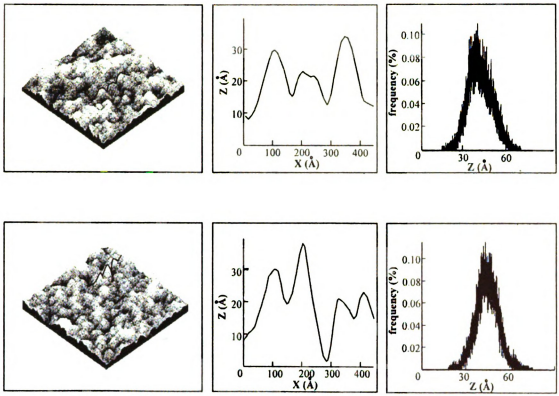

Figure 6.6 (cont'd)

The adsorption of QDP onto a primed and zirconated substrate results in a surface morphology similar to that seen for the primer layer (Figure 6.6c). Despite their outward similarity, there are some subtle differences between the primed and QDP-coated surfaces. Specifically, the QDP-terminated surface has a broader distribution in terms of aggregate lateral dimension, and a narrower distribution in terms of roughness. The typical cluster size is ~ 130 Å, with an average nearest neighbor separation of ~ 200 Å. A large number of small clusters 40 Å to 100 Å in diameter are present in the mixed layer of 5% BDP, 50% QDP and 45% DDBPA, and for this monolayer the typical inter-cluster separation is ~ 130 Å. Because of the change in surface morphology associated with the formation of chromophore layers, we conclude that aggregates form coincident with the growth of these layers. The growth of chromophore layer is thus not simply a decoration of the primed substrate, but aggregation among chromophore molecules also plays an important role. As pointed out earlier, the sizes of most of the aggregates are on the order of hundreds of angstroms. For our sample preparation conditions, we do not see formation of bulkier aggregates or thicker films. The thickness of each film was measured using optical null ellipsometry and AFM. As shown in Figure 6.7, a typical thickness for the three component mixed layer is 40 Å ± 10 Å, with the uncertainty mainly attributed to the roughness of the substrate and the aggregates. QDP films exhibit the same thickness as the mixed layer, as measured by AFM. Considering the fundamentally different nature of the spectroscopic and AFM measurements, the agreement between the two results is both surprising and revealing. For a typical organic chromophore, the Förster critical transfer radius is on the order of 20 Å - 50 Å, so the separation of the aggregate islands on the surface serves to limit excitation migration during the excited state lifetime of the

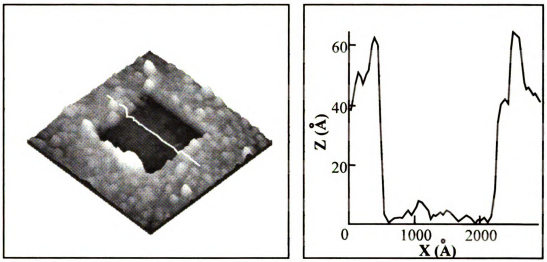

Figure 6.7 Topographic image of a mixed monolayer of 5% BDP, 50% QDP, and 45% DDBPA on a primed substrate. The molecules in the central 2000 Å x 2000 Å area was displaced prior to this image using an AFM tip under a force of 1 nN. The overall scanning area here is 4000 Å x 4000 Å acquired at a reduced imaging force of 0.05 nN. The cursor profile reveals the thickness of the layer to be 40 Å ± 10 Å.

chromophore.

The roles of priming chemistry and substrate heterogeneity. Because the morphology of these layered interfaces depends on both the priming and adsorption chemistries, it is important to understand the reason(s) for the formation of the three-dimensional islands in the first place. In Chapter 5 we reported on the surface relief characteristics of the substrates. That roughness, while important to the motional properties of the chromophores, does not address the basis for the island formation seen in this work.

There are at least three factors contributing to the formation of the islands. The dominant ones are the intrinsic surface roughness and the apparently heterogeneous distribution of active silanol groups on the substrate,[8-10] the nature of the priming chemistry used to form aggregated structures, and the ability of the chromophores to aggregate either before or during the layer formation process.

In an ideal experiment, we could control selected surface properties independent of one another by using different materials. Unfortunately, this level of control is not achievable in materials as complex as silicon oxides. Comparison of mica and SiO_x substrates involves changes in both surface roughness and silanol group density and it is not possible to fully decouple these surface properties. Nonetheless, it is instructive to examine the consequences of the priming chemistry on these two surfaces. We have imaged APTES on mica(001), an atomically flat surface known to possess relatively few hydroxyl groups. The surface of APTES/mica, with a thickness of 7 ± 3 Å as measured by AFM, is much more homogeneous than an APTES/SiO_x surface. In addition, the force required to displace APTES on mica is not as high as it is for APTES on SiO_x, indicating

the importance of surface silanol group density. On the mica surface, scattered three dimensional clusters are seen due to the lower density of silanol anchor sites, where on the APTES/SiO_x surface, relatively dense three-dimensional aggregate structure is characteristic (Figure 6.6).

The primer layer chemistry determines both the stability and the morphology of the primer layer. These properties, in turn, determine the growth behavior of subsequent layers. Priming a SiO_x or oxidized Si surface with APTES is known to produce a cross-linked structure because of the three reactive functionalities present on each primer molecule.[11] In an effort to address the role of the Si-O cross-linking, we have also made monolayers using APDMES. For this primer there is only one ethoxy group per molecule to react with the substrate, eliminating the possibility of cross-linking. Using this chemistry, we observe more homogeneous surface. The non-cross-linked APDMES priming layer is not as stable as the polymerized APTES layer. APDMES can be displaced with 0.1 nN of imaging force, and greater than 1 nN is required to displace APTES. Of key importance is that when a chromophore monolayer is formed on the APDMES-primed substrate, we observe spectroscopic population relaxation dynamics identical to those seen for an APTES-primed monolayer. Aggregates are seen spectroscopically even for monolayers where the potentially complicating role of the priming chemistry has been precluded. This finding provides direct evidence for the importance of chromophore aggregation during the layer formation process.

6.4 Conclusions

The combination of excited state population decay and AFM measurements has afforded substantial insight into the morphology of zirconium-phosphonate monolayers used in this and previous Chapters (4 and 5). The presence of aggregate islands in the layer accounts for the approximately double exponential lifetime behavior we observe. The size and separation of the islands, as resolved by AFM, demonstrates the correspondence between physical and spectroscopic measurements of the interface and explains the apparent absence of Förster energy transfer between donor and acceptor chromophores within the layer. The origin of the island structures in the primer layer of these assemblies appears to lie with the heterogeneous distribution of the active silanol sites on the substrate. The aggregates formed by the chromophores derive their characteristic sizes from both the features of the primer layer and their own propensity for aggregation, either before or during the adsorption process. These findings will be important in evaluating interlayer excitation transport effects in more complex multilayer structures.

6.5 Literature Cited

1. Song, Q.; Bohn, P. W. Blanchard, G. J. *J. Phys. Chem. B* **1997**, *101*, 8865.

2. Förster, T. *Z. Naturforsch* **1949**, *A4*, 321.

3. Förster, T. *Faraday Disc. Chem. Soc.* **1959**, *27*, 7.

4. Girard, C.; Martin, O. J. F.; Dereux, A. *Phys. Rev. Lett.* **1995**, *75*, 3098.

5. Drexhage, K. H. *J. Lumin.* **1970**, *1,2*, 693.

6. We thank Prof. G.-Y. Liu and Y. Huang (Wayne State University) for imaging the samples used in this study.

7. (a) Chidsey, C. E. D.; Liu, G. Y.; Rowntree, P.; Scoles, G. *J. Chem. Phys.* **1989**, *91(7)*, 4421. (b) Poirier, G. E. *Langmuir* **1994**, 13, 2019. (c) McDermott, C. A.; McDermott, M. T.; Green, J. B.; Porter, M. D. *J. Phys. Chem.* **1995**, *99*, 13257. (d) Liu, G. Y., Xu, S., Cruchon-Dupeyrat, S. In *Thin Film: Self-Assembled Monolayers of Thiols;* Ed. A. Ulman, Academic Press, **1998**, *24*, 81.

8. Wang, H.; Harris, J. M. *J. Phys. Chem.* **1995**, *99*, 16999.

9. Lochmuller, C. H.; Colborn, A. S.; Hunnicutt, M. L.; Harris, J. M. *J. Am. Chem. Soc.* **1984**, *106*, 4077.

10. Lochmuller, C. H.; Colborn, A. S.; Hunnicutt, M. L.; Harris, J. M. *Anal. Chem.* **1983**, *55*, 1344.

11. Haller, I. *J. Am. Chem. Soc.* **1978**, *100*, 8050.

Chapter 7

Structural Mediation of Interlayer Excitation Transport in Zirconium Phosphonate Multilayers

Summary

We report on our investigation of interlayer excitation transport in zirconium-phosphonate multilayer structures. We find that dipolar (Förster) excitation transfer between energetically overlapped oligothiophene chromophores in adjacent layers does not play a significant role in determining the relaxation dynamics of these systems. This finding is not consistent with the predictions of the Förster model and we account for this discrepancy by considering the spatial modulation of the dielectric response of the ZP multilayer assemblies. The presence of polarizable Zr-bisphosphonate layers between layers of donor and acceptor chromophores serves to screen dipolar D-A coupling. Intralayer excitation transfer within individual chromophore aggregates dominates population relaxation dynamics in these systems. We also find that spacing the optically active layers away from the primed substrate surface does not eliminate chromophore aggregation. We discuss these data in terms of the dominant factors in the formation of ZP layers.

7.1 Introduction

Both interlayer and intralayer processes must be evaluated to understand the physical limits on the localization of excitations within multilayer assemblies. In Chapter 6 we considered intralayer excitation transport in detail and have found that aggregation and island formation dominates the structural and optical properties of individual layers. With this understanding in place, we next consider the efficiency of excitation transport between layers. To understand and control excitation transport in MP films, we have constructed a series of optically active MP multilayer films where the spatial relationship between donors and acceptors is well controlled.

To study excitation transport within and between molecular layers, chromophores with specific optical properties must be used. In order to facilitate excitation transport and thus place limits on the possible structural motifs appropriate for optical information storage in multilayer systems, the emission band of the donor should overlap the absorption band of the acceptor. The thiophene oligomers 2,2'-bithiophene diylbisphosphonate (BDP) and 2,2':5',5'':2'',2'''-quaterthiophene diylbisphosphonate (QDP) are the donor and acceptor chromophores, respectively, and their structures are shown in Figure 7.1. The emission band of BDP overlaps the absorption band of QDP (Figure 1.1). The thiophene oligomers are not candidates for optical information storage applications because of the facile rotation of individual thiophene rings within the chromophores. This property is beneficial to this work because it precludes significant steric contributions to excitation transport.

In Chapters 4, 5, and 6, we focused on achieving a fundamental understanding of the chromophores both individually and in mixed monolayers. We now know that the

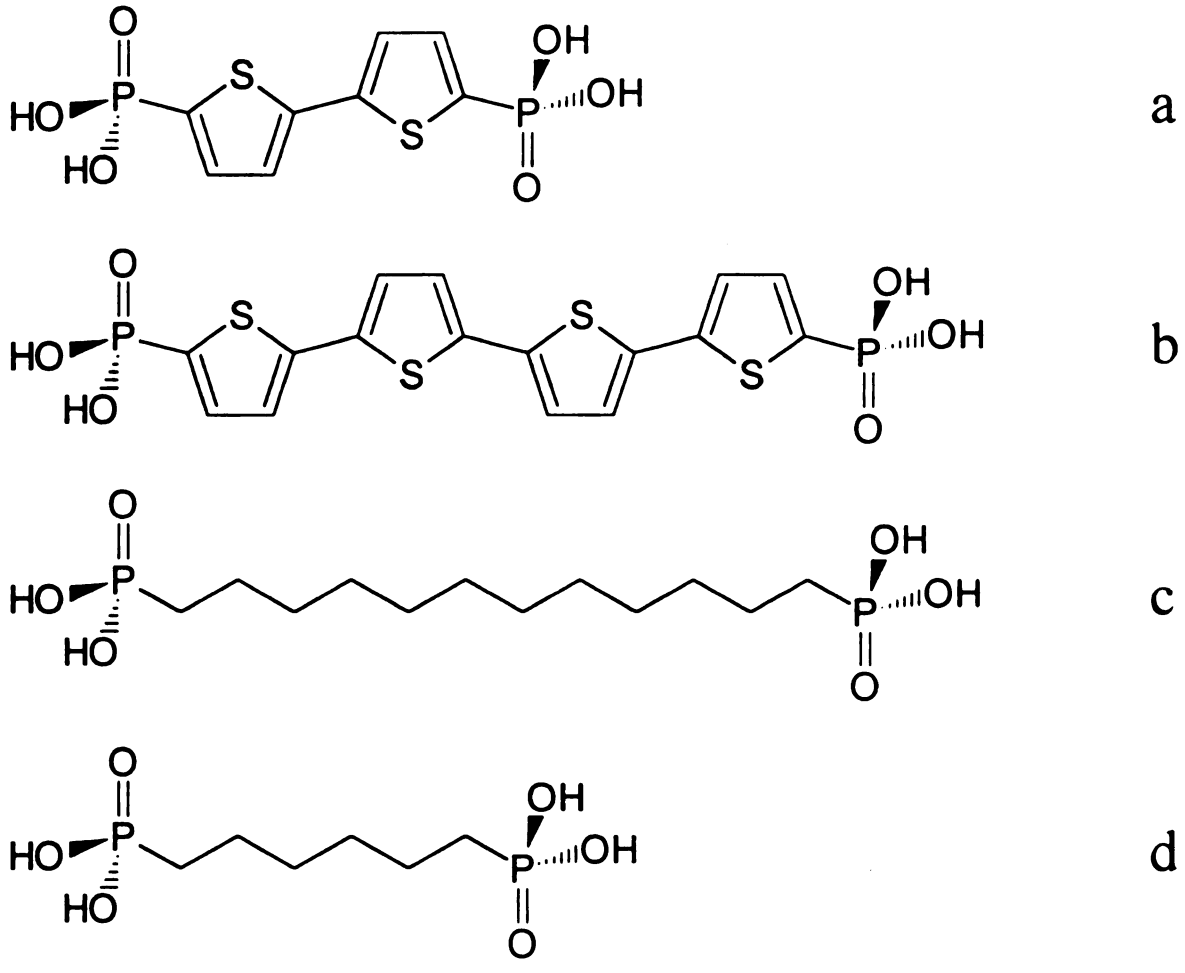

Figure 7.1 Structures of organobisphosphonates used in this work. (a) 2,2'-bithiophene-5,5'-diylbis(phosphonic acid) (BDP); (b) 2,2':5',2":5",2"'-quaterthiophene-5,5"'-diylbis(phosphonic acid) (QDP); (c) 1,12-dodecanediylbis(phosphonic acid) (DDBPA); (d) 1,6-hexanediylbis(phosphonic acid) (HBPA).

properties of the layers are mediated to a substantial extent by the silanol density and distribution on SiO_x and oxidized Si surfaces. Silane-primed SiO_x surfaces are characterized by islands, and the growth of at least the first several organophosphonate layers is templated by the chemically reactive islands. Atomic force microscopy (AFM) images of the primed substrates and of monolayers have confirmed the presence of islands. In addition to the primer island formation, which is mediated by heterogeneity in the distribution of surface silanol sites, we have found that the oligothiophene chromophores aggregate during the deposition process, reinforcing the substrate-mediated island structure. Because of the dominant role of the aggregate islands within these monolayers and the inter-island spacing, intralayer excitation transport over mesoscopic length scales is not efficient.

We are concerned with understanding excitation transport between optically active layers in systems where there is not a statistical distribution of donors and/or acceptors within individual layers. We have synthesized MP multilayer structures with the donor and acceptor chromophores present in varying amounts in different layers. We expect and observe the same island morphology that we have elucidated previously for individual layers. We have found that excitation transport between the donor and acceptor chromophores across different layers is inefficient. We consider the possible reasons for this experimental finding in the context of the orientational and structural properties of these systems.

7.2 Experimental

Multilayer Synthesis. Metal-phosphonate multilayers were synthesized on polished Si(100) substrates (Boston Piezo-Optics) having a native oxide layer of 5-20 Å, as determined by optical null ellipsometry. The substrates were cleaned immediately before use by immersion in piranha solution for 10 minutes (3 H_2SO_4 : 1 H_2O_2) rinsed with flowing distilled water, and dried with a N_2 stream. The surface was primed with a layer of 3-(aminopropyl) dimethylethoxysilane, by immersing overnight in a 0.5% v/v solution in toluene, followed by rinses with toluene, methanol, and water, and drying with N_2. The resulting aminated surface was derivatized to the phosphonate in a solution that is 200 m$\underline{M}$ in both $POCl_3$ and collidine in anhydrous acetonitrile for 10 minutes, then rinsed with acetonitrile and water. A layer of Zr^{4+} was deposited onto the phosphorylated surface using a 5 m$\underline{M}$ $ZrOCl_2$ solution in 60% EtOH(*aq*) for 10 minutes. Multiple layers are synthesized through the alternate deposition of organobisphosphonates (at least four hour deposition time) and Zr^{4+} (ten minute deposition time). The organobisphosphonates were dissolved in 80% DMSO, 20% EtOH solutions with 1 m$\underline{M}$ total concentration ([BDP] + [QDP] + [alkanebisphosphonate] = 1 m$\underline{M}$). The syntheses of BDP, QDP, 1,6-hexane bisphosphonate (HBPA), and 1,12-dodecane bisphosphonate (DDBPA) have been reported in Chapter 2 and their structures are shown in Figure 7.1.

Steady-State Optical Spectroscopy. Spectra of 10^{-5} $\underline{M}$ solutions of each chromophore are shown in Figure 1.1. Absorbance spectra were recorded on a Hitachi U-4001 spectrophotometer with spectral resolution of 5 nm. Emission spectra were measured on a Hitachi F-4500 spectrophotometer. Slits were adjusted according to the emission intensity of the samples.

Fluorescence Lifetime Measurements. Fluorescence lifetimes of chromophore-containing films were measured using time correlated single photon counting (TCSPC). This system has been described in detail in Chapter 3, and we present only the essential details here. The second harmonic of the output of a mode-locked CW Nd:YAG laser (Quantronix 416) is used to pump a cavity-dumped dye laser (Coherent 702-2), operating at 630 nm (Kiton Red, Exciton). The output of the dye laser is frequency doubled ($LiIO_3$ Type I SHG) to excite the multilayer samples at 315 nm. This wavelength is a maximum in BDP absorbance spectrum and, simultaneously a minimum in the QDP absorbance spectrum. The sample surfaces are nearly parallel to the laser table and are held at ~5° with respect to the incident laser beam in two directions: toward the excitation beam and toward the detector. Fluorescence from the sample was imaged through a reflecting microscope objective, and collected in two wavelength ranges with the detection bandwidth being set to 30 nm FWHM in each case. BDP emission was collected at 400 nm and 425 nm, and QDP emission was collected at 525nm and 550 nm. Decays were measured at two wavelengths in each chromophore emission range to test for wavelength dependent dynamics. As we had found in Chapters 4 and 5, the recovered decay time constants were independent of collection wavelength, so the time constants reported for each chromophore are the averages of the lifetimes at both wavelengths in their respective emission range. The typical response function for this spectrometer is ~ 35 ps FWHM, as shown in Figure 7.2. The lifetimes we report are the results of fits of the data to the sum of two exponential decays using commercial software (Microcal Origin v. 5.0)

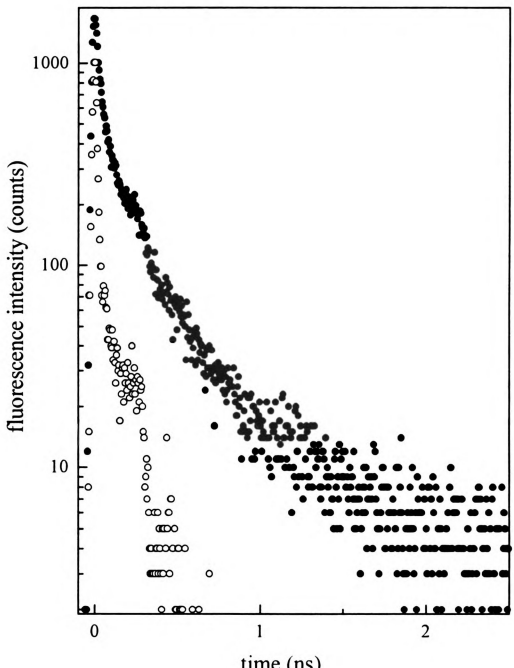

Figure 7.2 Typical instrument response function (O) and excited state population decay (●) (425 nm) for a multilayer with full donor and acceptor layers. The emission at 425 nm is from BDP.

and are reported as the average of the fits of at least 3 sets of experimental data in each wavelength range. The uncertainties represent the standard deviations of the average of the different sets of data.

7.3 Results and Discussion

The goal of this work is to understand the effects of chromophore orientation and layer structure on interlayer excitation transport behavior of oligothiophene chromophores in ZP multilayer structures. In previous studies, we have investigated the role of photonic energy transfer within a single mixed chromophore layer (Chapter 4) and the role of substrate identity in determining the structural freedom available to chromophores within the monolayers (Chapter 5). For a homogeneous monolayer, where the donor and acceptor chromophores are distributed statistically, Förster energy transfer is expected to manifest itself as a decrease in the donor lifetime as the acceptor concentration is increased. For mixed D-A monolayers, we did not observe changes in donor lifetime as a function of changes in acceptor concentration. The absence of the expected response was attributed to structural heterogeneity within the layer. The experimental data are accounted for quantitatively by the model detailed in Chapter 6 for excitation transport where ~100 Å aggregated islands of chromophores are separated by distances sufficiently greater than 50 Å to preclude efficient inter-island excitation transport. With this understanding of intralayer energy transfer processes in MP multilayers, we turn our attention interlayer transport.

The TCSPC measurements yield a nonexponential decay for both donor and acceptor emission that is approximated well using a double exponential decay function.

The short time component is ~ 200 ps, which corresponds to that of radiative oligothiophene monomers, the same as seen in solution, and the long component has a time constant of ~ 1 ns, which we consider to originate from radiative monomers in an aggregated chromophore environment.

The model for radiative dynamics of these layers has been developed by Song, *et al.* for excitation transport in aggregated LB films of stilbazolium dyes [11] The chromophores in a monolayer are present in two forms: most of the chromophores are in aggregates, with a smaller number present as monomers. In this model, the aggregate is excited, and it can either decay radiatively, a low probability event, or its excitation can be transferred to individual molecules in the aggregate. The excitation can "hop" randomly within the aggregate until it reaches a radiative monomer "defect" in the aggregate or one of the radiative, isolated chromophores nearby the aggregate. The different environments of the two radiative chromophores result in the two fluorescence lifetimes, which provide the major contributions to the observed decay dynamics.

We present in Figure 7.3 the kinetic scheme relevant to this system. We reported in Chapter 6 on this scheme for monolayers, where *Layer 1* in Figure 7.3 is the final state. The difference between the monolayer case and that of multilayers lies in the presence of additional final states, containing A_2, M_3 and M_4, where these species reside in layers adjacent to the initially excited layer. The only fundamental difference between the monolayer and multilayer systems is the number of final states. Any measured difference between monolayer and multilayer systems will result from changes in k_{m1}, k_{m2} and k_{nr}. Our signal has significant contributions from each of these rate constants and the Förster model predicts that k_{m1}, k_{m2} and k_{nr} depend sensitively on the presence or absence of

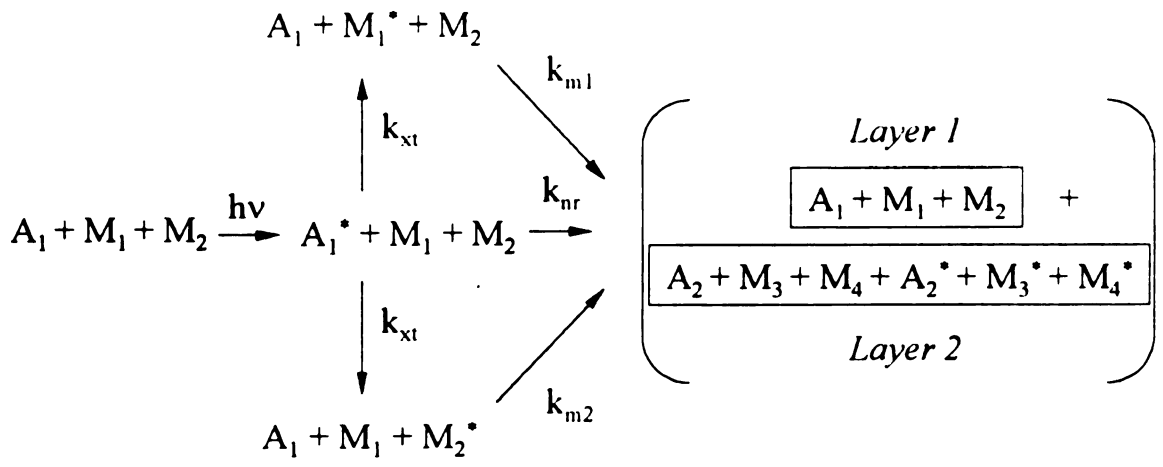

Figure 7.3 Kinetic scheme for population dynamics in layered structures. A_1 is the donor aggregate and A_2 is the acceptor aggregate. M_1 and M_2 refer to radiative donor monomers and M_3 and M_4 refer to radiative acceptor monomers. For a monolayer (Layer 1), only the species A_1, M_1 and M_2 are present in the relaxed system. For a multilayer (both Layer 1 and Layer 2), A_2, M_3 and M_4 are also present in the relaxed system.

Layer 2. The first questions must therefore be the applicability of the Förster model and the size of the expected changes in these rate constants resulting from the presence of acceptor layer(s). Our previous work on monolayers has demonstrated that dipolar energy transfer[2,3] within aggregates and between aggregates and monomers is operative. We therefore expect the same basic mechanism to hold for multilayer systems. The existence of island structures within a given layer precludes efficient energy transfer over large distances within that layer. Because the growth of one layer on top of another requires spatial registration, donor and acceptor chromophores in adjacent layers will be in close spatial proximity to one another. We describe the multilayer structures we have synthesized to evaluate interlayer excitation transport in Table 7.1.

For monolayers, the early time emission dynamics of the radiative monomers are mediated by diffusive excitation transport within the aggregate to the monomer [1] This model provides exact agreement with atomic force microscopy data on the surface morphology of ZP monolayers. (Figure 6.6) This same physical picture holds for each layer in a multilayer assembly based on the form of our spectroscopic data (*vide infra*). The question at hand is to determine whether or not interlayer excitation transport can compete effectively with intralayer transport in ZP multilayers.

Dipolar excitation transport among like chromophores ($D^* \rightarrow D$) as well as between donor and acceptor chromophores ($D^* \rightarrow A$) both proceed within a given layer, as demonstrated in Chapter 6. The depopulation dynamics of D^* are related to the characteristic length scale of structural heterogeneity within the layer. For multilayers, our data point to the donor lifetime being dominated by intralayer ($D^* \rightarrow D$) dipolar excitation transport. Within the framework of the Förster model, this is an unexpected

Table 7.1 Description of layered samples corresponding to the lifetime data presented in Figure 7.4.

	Sample					
layer	1	2	3	4	5	6
8				100% BDP		
7			100% BDP	100% DDBPA	5% BDP; 95% HBPA	100% QDP
6			100% QDP	100% QDP	100% QDP	5% BDP; 95% HBPA
5			100% DDBPA	100% DDBPA	100% DDBPA	100% DDBPA
4			100% DDBPA	100% DDBPA	100% DDBPA	100% DDBPA
3			100% DDBPA	100% DDBPA	100% DDBPA	100% DDBPA
2		100% BDP	100% DDBPA	100% DDBPA	100% DDBPA	100% DDBPA
1	100% BDP	100% QDP	100% DDBPA	100% DDBPA	100% DDBPA	100% DDBPA

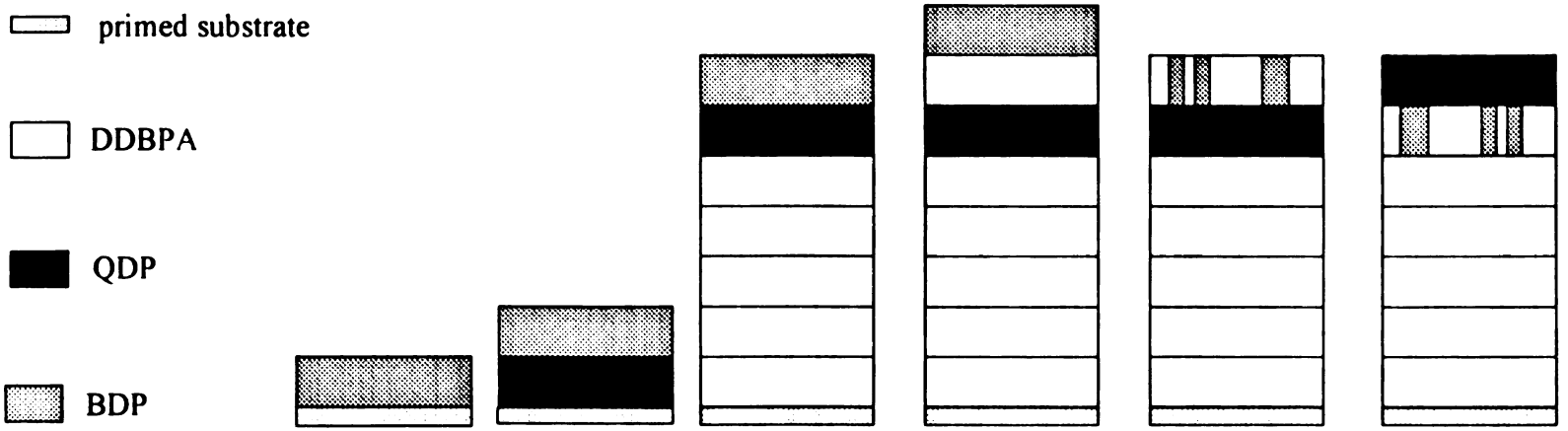

result that reveals the important role of the metal bisphosphonate layers in mediating interlayer excitation transport.

In a heterogeneous ZP monolayer, the aggregate size determines the observed early time dynamics. In a multilayer film, the average distance between layers depends on the thickness of the spacer layers separating the chromophore layers. Both spacing and donor orientation relative to the acceptor will determine the rate constant for energy transfer in the Förster model.[2,3]

$$k_{D-A} = \frac{3\kappa^2 R^6}{2\tau_D R_0^6} \qquad [7.1]$$

The rate constant for energy transfer from donor to acceptor is k_{D-A}, τ_D is the excited donor radiative lifetime, R is the distance between donor and acceptor, and R_0 is the Förster critical radius, a term containing spectroscopic overlap and fluorescence quantum yield information. The term κ^2 is a geometrical factor describing the relative orientation of donor and acceptor transition moments,

$$\kappa = \sin\theta_D \sin\theta_A \cos\phi - 2\cos\theta_D \cos\theta_A \qquad [7.2]$$

where the angles θ_D and θ_A are the angles of the donor and acceptor with respect to the vector connecting them, and ϕ is the azimuthal angle between the transition moments. Angles of $\theta_D = \theta_A = 90°$ and $\phi = 0°$ correspond to a monolayer where the donor and acceptor are parallel to one another. For a multilayer where the donor and acceptor are stacked on top of one another, $\theta_D = \theta_A = 0°$ and the azimuthal angle ϕ becomes coincident with the angles θ. The terms κ^2 and R are the experimental variables pertinent to the interpretation of our data. R_0 and τ_D are constants for the purposes of the experiments we report here. If interlayer transport competes effectively with intralayer

transport, we expect the donor lifetime in a multilayer assembly to be sensitive to the distance between donor and acceptor layers. Experimentally, the lifetimes we measure for multilayers having adjacent donor-acceptor chromophore layers are the same as those we measure for individual chromophore layers (Figure 7.4). We observe that, for the layered oligothiophenes, interlayer Förster energy transfer does not compete efficiently with intralayer relaxation.

We attempt to understand these results in terms of the orientation and proximity of the donor and acceptor chromophore transition moments. The thiophene oligomers are a good choice for the investigation of energy transfer because of their large absorptivities, characteristically high fluorescence quantum yields and substantial spectral overlap of the donor emission and acceptor absorption bands (Figure 1.1). These factors are consistent with a value of $R_0 \sim 25 - 50$ Å for either $D^* \rightarrow A$ or $D^* \rightarrow D$ excitation transport, a range typical for such chromophores. In either case, the intermolecular distance lies within the critical radius, R_0, suggesting efficient interlayer and intralayer excitation transport.

The orientation of the donor and acceptor transition moments can also play an important role in determining the form of the observed data, and this factor is accounted for in the Förster model through the term κ^2. The term κ^2 can vary between 0 and 4 (Equation 7.2 and Figure 7.5) depending on the relative orientation of the donor and acceptor transition moments. For isotropic systems and cases where orientational averaging occurs on a time scale that is fast relative to excitation transport, $\langle\kappa^2\rangle = 2/3$. Within a single ZP layer, $\kappa^2 \sim 1$ because of aggregation and strong interactions that give rise to parallel molecular alignment. We now consider the value of κ^2 for interlayer transport. If chromophores in the donor and acceptor layers are aligned with their

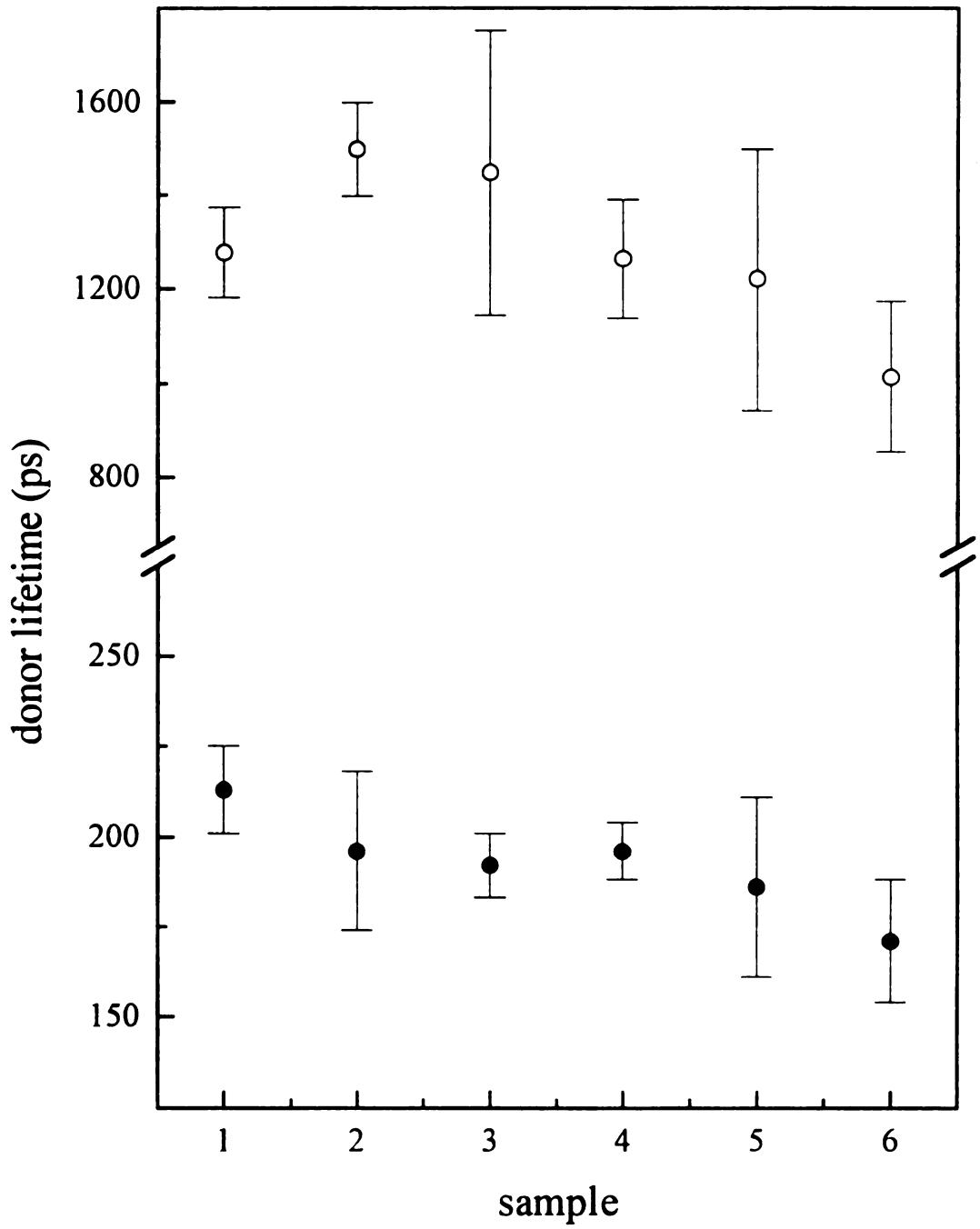

Figure 7.4 Fluorescence lifetimes measured for various layered systems as described in Table 7.1. Decays were fit to the function $f(t) = A_1\exp(-t/\tau_1) + A_2\exp(-t/\tau_2)$.

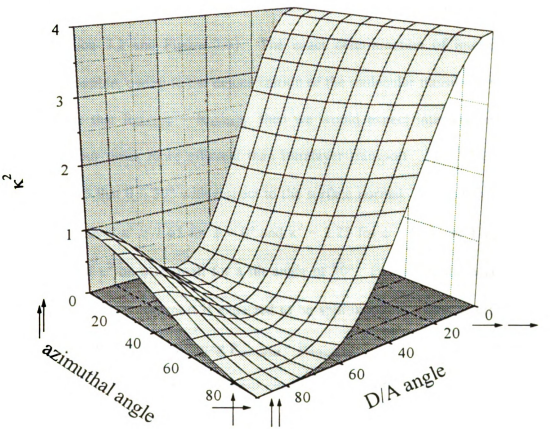

Figure 7.5 Calculated values of κ^2 from Equation 7.2 as a function of donor and acceptor orientation.

transition moments both perpendicular to the layer plane, where θ_D and $\theta_A = 0°$, $\kappa^2 \sim 4$, independent of ϕ. In the limit of θ_D and $\theta_A = 0°$, the angle ϕ becomes coincident with the angles θ (Equation 7.2 and Figure 7.5). The exact determination of intermolecular distance is not possible, owing to the delocalization of the molecular transition moments, but if we assume that $R_{interlayer} \sim R_{intralayer}$, then we would expect interlayer excitation transport to be four times more efficient than intralayer transport. For ZP layers, we found in Chapter 5 that $\theta \sim 30°$ with respect to the surface normal. Using this value for θ_D and θ_A, we recover $\kappa^2 = 1.65$ for $\phi = 0°$ and $\kappa^2 = 2.25$ for $\phi = 90°$ (see Figure 7.5). The dependence of κ^2 on ϕ is small for a tilt angle of 30°. For donor and acceptor tilt angles of ~30°, interlayer transport is expected to be approximately twice as efficient as intralayer transport processes, assuming $R_{interlayer} \sim R_{intralayer}$.

The fact that we observe no interlayer excitation transport stands in sharp contrast to the predictions of the Förster model. This unexpected deviation from Förster behavior can be explained in the context of the structural properties intrinsic to the multilayer assembly. Dipolar excitation transport has been shown to explain our monolayer data quantitatively. We expect the Förster model to hold equally well for multilayers. An important assumption of the Förster treatment is that the dielectric response of the space between donor and acceptor is uniform. For the multilayer assemblies we have constructed, this assumption is not satisfied. Specifically, the layered structure of ZP films produces a spatial modulation of the dielectric response of the system. The presence of the Zr-bisphosphonate layer between donor and acceptor can, in principle, act to screen the oscillating transition dipole moment of the donor from the transition moment of the acceptor. The polarizable phosphonate anions can act as "polarizability

screens", precluding the efficient transfer of excitation between individual layers. Although we are not aware of any direct measurements of the refractive index of bulk $Zr(PO_3R)_2$ compounds where R is a simple substituent such as -H or $-CH_3$, we estimate this value to be $n \sim 1.65$ and for organic constituents, we estimate $n \sim 1.46$. Regardless of the exact values, the modulation of n is sufficient to interfere with direct dipolar coupling of chromophore transition moments in adjacent layers.

While the screening of one transition moment from another is consistent with our experimental data, it is unfortunately not possible to acquire another body of data to evaluate this model directly. The nature of ZP multilayer chemistry does not allow variation of the multilayer structure in such a way as to preclude polarizability screening. Elimination or variation of the MP network will serve to change the chemistry of the system and thus perturb the structural and spectroscopic properties of interest. Further experimentation using different interlayer linking chemistry, where the interlayer connections possess fewer polarizable functionalities, is underway in our laboratory. We do note that no apparent screening effect is seen in multilayer structures where the density and organization of polarizable moieties within the multilayer structure is limited.[4]

In addition to understanding interlayer transport, we can also add to our overall understanding of the morphology of the film as layers are built up. The priming chemistry and the chromophore aggregation give rise to island formation within a monolayer as reported previously, but there is some evidence in the literature that this structure is not preserved with the addition of multiple layers. One possibility for the growth of multiple layers is that one will grow in registration to another, preserving the

initial island structure. This structural motif has been seen by AFM for two C_{16}BPA layers.[5] It is also possible that the layers could "fan out" and grow together to form a more uniform surface with the addition of several layers. There is also some microscopic evidence for this process. To address this question from a spectroscopic point of view, we synthesized films with chromophore layers that were spaced from the surface by five DDBPA layers, in order to probe the local structure further from the substrate. The optical response of the chromophore layers spaced away from the substrate is identical to that of monolayers formed directly above the substrate. This result points to the importance of chromophore aggregation coincident with the formation of the layers. Even if the films do "smooth out" as layers are added, we measure the same time constants for all cases, suggesting that the chromophores aggregate regardless of what type of surface they are deposited on. This finding suggests that the formation of statistically distributed chromophore layers will require a different chemical approach.

Another concern in the synthesis of chromophore-containing films is the effect of the surrounding dielectric environment on the optical properties and dynamic behavior of the chromophores. In a film, a chromophore layer can be adjacent to several possible environments: the primed substrate, another chromophore layer, an alkane layer, or air. As shown in Table 7.1, we have varied both the donor and acceptor environments in the series of films we studied. In Chapter 4, we found that surrounding alkane layers had no effect on the dynamics of a single donor layer. For the multilayer films in this study, we find similar independence of the dynamics of both chromophores on the dielectric environment. This further points to the role of the polarizable ZP network between layers in restricting interlayer interaction in these MP films.

7.4 Conclusions

We have found that excitation transport between layers of oligothiophene chromophores in a ZP multilayer structure does not compete efficiently with intralayer transport, in contrast to the predictions of the Förster model. The absence of interlayer excitation transfer can be accounted for by screening of adjacent chromophore layers by the Zr-bisphosphonate portion of layers. This screening is, in effect, the result of the spatial modulation of the non-resonant dielectric response of the system. These results are important for understanding the morphological, structural, and optical properties that will be useful for the incorporation of layered organic materials in future technologies.

7.5 Literature Cited

1. Song, Q.; Bohn, P. W.; Blanchard, G. J. *J. Phys. Chem. B* **1997**, *101*, 8865.

2. Förster, T. *Z. Naturforsch* **1949**, *A4*, 321.

3. Förster, T. *Faraday Disc. Chem. Soc.* **1959**, *27*, 7.

4. Kaschak, D. M.; Mallouk, T. E. *J. Am. Chem. Soc.* **1996**, *118*, 4222.

5. Byrd, H.; Snover, J. L.; Thompson, M. E. *Langmuir* **1995**, *11*, 4449.

Chapter 8

Conclusions

This dissertation has demonstrated the profound influence of the morphological and dielectric properties of metal-phosphonate films on the energy transfer behavior of the film. In the current MP literature, most of the focus is on the average properties of the films, without any detailed study of how the properties are affected by the morphology of the layers. ZP layers formed on SiO_x substrates are inhomogeneous, characterized by islands, presumably corresponding to high-density areas of silanol active sites. Our transient and steady-state spectroscopic measurements and modeling in Chapters 4 – 6 point to the aggregation of chromophores in a ZP layer, which serves to reinforce the island structure. This aggregation complicates the optical response of the film, as it creates two distinct environments for the chromophore: aggregated and non-aggregated, each with a unique optical response. The separation of the chromophore islands precludes Förster energy transfer from donor to acceptor species, as shown in Chapter 6, but we find that excitation transport *within* the chromophore islands is dominant. The detailed excitation hopping model that corresponds to the observed behavior also was presented in Chapter 6. With the complementary technique of atomic force microscopy (Chapters 5 and 6), we conclude that both substrate and layer morphologies influence the optical properties of the layer.

The segregation of chromophores into microscopic islands appears attractive for optical information storage applications, but there are several drawbacks to this structural motif. The most glaring is our inability to control the island dimensions or placement,

which bears directly on the ability to control the arrangement of "bits" in a storage device. Defects will be associated with any substrate chosen, but different types of defects (e.g. microscopic roughness vs. atomic defects) affect the structural properties of the films in various ways. Metal substrates, especially those that are not susceptible to oxidation, are known to be well-ordered on a microscopic scale. For instance, crystalline Au (111) has dense, uniformly packed active sites, and MP films have been built on gold substrates, using a thiol priming layer.[1-4] Films on metal substrates have found application in certain investigations, such as surface plasmon resonance[3] or QCM[1] studies. Unfortunately, metal substrates are not useful for optical studies of thin films, because of direct dipolar coupling to the metal, which results in lifetime quenching of the chromophores.[5] Future studies of these films should include efforts to identify compatible substrates that do not interfere with the optical response and that have active sites that are more statistically distributed.

Another aspect of the MP films that needs improvement is the priming step. We observed in Chapter 6 that the silane primers smoothed the surface on average, filling in grooves or depressions in the surface of the substrate. Although they seemed to "build up" in the recessed areas, the silanes reacted primarily in regions dense with active sites, forming islands on the surface. The primer we used did not form any extensive network parallel to the surface, as we might expect for trifunctional silanes. Building several subsequent silane layers could serve to smooth out the island structure, but silane chemistry is difficult to control, and unwanted polymerization perpendicular to the surface is likely to interfere.

Problems with aggregation in the layer may be diminished with a different set of chromophores. Lifetimes of the chromophores used in this dissertation averaged 200 ps. If Förster energy transfer was operative in these systems, the lifetimes would approach values that would be too fast to measure easily with our instrumentation. Chromophores that are less rotationally facile would be a benefit to this investigation, because (1) they have stronger tendencies to order within a layer and (2) the excited state fluorescence lifetimes are typically longer,[6] allowing us a larger time window to observe the population dynamics. Identifying chromophores that are less likely to aggregate is also important, for instance, a conjugated molecule derivatized with constituents that prevent the close packing required for aggregation. If the chromophores are sterically unable to aggregate, the constituents of each island could be controlled. Despite island formation, this average signal would approximate a homogeneouly mixed film better than the signal we observe for the films with aggregated chromophore islands. We found that spacing the optically active layers away from the primed substrate surface does not eliminate chromophore aggregation.

In Chapter 7, we examined energy transport between layers in ZP multilayers, having gained an understanding of intralayer behavior in earlier Chapters. Because of the proximity of chromophore layers built directly on top of one another and the favorable alignment of chromophore transition moments, interlayer Förster energy transfer was expected to be operative. However, no energy transfer processes except the intra-island excitation transport were observed. We concluded that the spatial modulation of the dielectric response between the organic and ZP portions of the film in the multilayer

structures caused this behavior. The ZP network seems to act as a polarizability screen of the dipolar oscillations of the chromophores.

It is entirely possible that the screening property of ZP films will find use in optical storage applications, as it prevents optical cross-talk between neighboring chromophore layers. The spacing of the optically active layers with optically inactive layers is another straightforward method of controlling this process, but we were unable to determine this because of the intervening ZP network. Other multilayer chemistries may not have the same screening properties, and it will be important to learn how to control the exchange of photonic energy in these materials. Multilayer chemistries having a lower density of interlayer polarizable groups or a more continuous dielectric response, which won't interfere with the optical response of interest, need to be developed in order to fully determine the feasibility of using molecular assemblies for practical devices.

8.1 Literature Cited

1. Yang, H. C.; Aoki, K.; Hong, H.-G.; Sackett, D. D.; Arendt, M. F.; Yau, S.-L.; Bell, C. M.; Mallouk, T. E. *J. Am. Chem. Soc.* **1993**, *115*, 11855.

2. O'Brien, J. T.; Zeppenfeld, A. C.; Richmond, G. L.; Page, C. J. *Langmuir* **1994**, *10*, 4657.

3. Lee, H.; Kepley, L. J.; Hong, H.-G.; Akhter, S.; Mallouk, T. E. *J. Phys. Chem.* **1988**, *92*, 2597.

4. Frey, B. L.; Hanken, D. G.; Corn, R. M. *Langmuir* **1993**, *9*, 1815.

5. (a) Chance, R. R.; Prock, A.; Sibley, R. *J. Chem. Phys.* **1975**, *62*, 2245. (b) Kurczewska, H.; Bassler, H. *J. Lumin.* **1970**, *1*, 693. (c) Alivatsos, A.; Waldeck, D. H.; Harris, C. B. *J. Chem. Phys.* **1985**, *82*, 541.

6. Karpovich, D. S.; Blanchard, G. J. *J. Phys. Chem.* **1995**, *99*, 3951.